REDOX-RESPONSIVE POLYMER DELIVERY SYSTEMS FOR ANTI-CANCER DRUG AND IMAGING

CHENG WEIREN

B.ENG.(Hons), NUS

A THESIS SUBMITTED FOR THE DEGREE OF DOCTOR OF PHILOSOPHY

NUS GRADUATE SCHOOL FOR INTEGRATIVE SCIENCES AND ENGINEERING

NATIONAL UNIVERSITY OF SINGAPORE

2014

Declaration

I hereby declare that this thesis is my original work and it has been written by me in its entirety. I have duly acknowledged all the sources of information which have been used in the thesis.

This thesis has also not been submitted for any degree in any university previously.

Cheng Weiren

17th April 2014

Acknowledgements

First and foremost, I would like to show my greatest gratitude to my supervisor, Dr. Liu Ye, from Institute of Materials Research and Engineering (IMRE). Despite my slow progression during the first two years, He would continuously show strong belief in my capability and patience in guiding me to overcome major hurdles. He allows me to execute experiments with great freedom and, learn and gaining valuable knowledge and experience through making mistakes. I would also like to express my sincere appreciation to another supervisor, Prof. Zhang Yong for constant instructive guidance and supports.

To my TAC advisors, Prof. Neoh Koon Gee, Prof. Tong Yen Wah and Prof. Li Jun, I would like to thank them for attending all my TAC meetings and giving me precious advices to prepare me in my oral defence.

I would also like to thank my IMRE colleagues of past and present, namely Dr. Wu Decheng, Miss Lay Cheng Leng, Mr Liu Jing, Dr. Kong Kien Voon, Dr. Ping Yuan, Dr. Kumar Jatin Nitin, Dr. Wang Guan, Dr. Pan Xiaoyong and Dr. Connie Liu, in helping me with my work in one way or another. To my SBIC collaborators, Dr. Chuang Kai-Hsiang and Dr. Reshmi Rajendran, thank you for your time and sharing your expertise with me. To my attachment students, thank you for putting in your best effort during your internship.

Lastly, I would like to thank my family members especially my wife and baby son for making my PhD study much less stressful and more meaningful.

Table of Contents

Summary

Cancer is one of the major killers of human. Delivery systems for anti-cancer drugs and imaging agents play important roles in cancer treatment and diagnosis. For development of safe and efficient delivery systems, stimuli-responsive polymers which undergo significant physical or chemical properties change in response to environmental variations including redox-responsive polymers are becoming more and more important. Exploring the much more reductive environment in intracellular compartments compared to extracellular matrixes, redox-responsive polymers are promising to provide high efficacy with low side effects of drugs and imaging agents delivered. In this thesis, a category of redox-responsive poly(amido amine)s is developed with the following works being carried out.

- An optimized condition is identified to prepare linear poly(amido amine)s via Michael Addition polymerization of trifunctional amine, 4-(aminomethyl)piperidine (AMPD), with an equimolar diacrylamide, *N*,*N*-cystaminebisacrylamide (BAC). Poly(ethylene glycol) (PEG) and cholesterol (CE) are conjugated to linear poly(BAC-AMPD) through the reactions with the 2^{o} amino groups in the backbone, respectively, to form poly(BAC-AMPD)-*g*-PEG-*g*-CE. Micelles with PEG shells and hydrophobic cores composed of poly(BAC-AMPD) and CE are formed via self-assembly of poly(BAC-AMPD)-*g*-PEG-*g*-CE in aqueous solution. The anti-cancer drug, doxorubicin (DOX), is loaded into the micelles, and DOX loaded micelles can deliver DOX into the cells and show a higher efficacy in killing cancer cells than free DOX-HCl.

- Vinyl-terminated hyperbranched poly(BAC2-AMPD1) were produced by reacting AMPD with double molar of BAC under optimized condition. Under directed self-assembly, the PEGylated hyperbranched poly(BAC2-AMPD1) were capable of forming micelles and encapsulating DOX with a higher capacity and efficiency than the micelles of poly(BAC-AMPD)-*g*-PEG-*g*-CE. However, its capability to kill cancer cells is slightly poorer or comparable to free DOX-HCl.
- Polydisulfide MRI contrast agent was obtained by grafting diethylenetriaminepentaacetic (DTPA) to disulfide containing poly(amido amine)s-*g*-poly(ethylene glycol) (PEG) and followed by complexation with Gd(III) ions. MRI contrast agent obtained could self-assemble in aqueous solution, forming nanosize micelles with PEG shells and ionic complex cores. Readily redox-induced degradable profiles were observed. Together with a low cytotoxicity and a high r_1 value, poly(BAC-AMPD)-*g*-PEG-*g*-Gd-DTPA is promising to provide better MRI imaging with lower side effects.
- Redox-responsive nanoparticles with aggregation-induced emission (AIE) characteristic for fluorescence imaging were developed by encapsulation of fluorophore with redox- "turn-on" AIE characteristic, TPE-MI, into the micelles of poly(ethylene glycol) (PEG)- and cholesterol (CE)-conjugated disulfide containing poly(amido amine)s. The redox-responsive fluorescence profiles of the nanoparticles were investigated after reaction with glutathione (GSH). The encapsulation of TPE-MI in micelles led to a higher efficiency and red shift in emission, and the fluorescence intensity of the nanoparticles increased with the concentration of GSH. Confocal

microscopy imaging showed that the nanoparticles could provide obvious contrast between the intracellular compartments and the extracellular matrix in MCF-7 and HepG2 cells. Therefore, the nanoparticles with PEG shells and low cytotoxicity are promising to provide fluorescence bioimaging with a high contrast and for differentiation of cellular redox environment.

List of Schemes

List of Figures

List of Tables

List of Symbols

τ_r: rotational correlation time
ACQ: Aggregate caused Quenching
ACS: American Cancer Society
ADR: Adriamycin
AIE: Aggregate-induced Emission
Ala: Alanine
$AlPcS_2$: Aluminium Phthalocyanine Disulfonic acid
AMPD: 4-(aminomethyl)piperidine
BAC: *N*,*N*-cystaminebis(acrylamide)
bis-SorbPC: 1,2-bis[10-(2',4'-hexadienoyloxy)decanoyl]-*sn*-glycero-3-phosphocholine
BSO: Buthionine Sulphoximine
CAP: Cancer-associated Proteases
CE: Cholesterol
CEST: Chemical Exchange Saturation Transfer
CLSM: Confocal Laser Scanning Microscopy
CMC: Critical Micelle Concentration
CT: Computed Tomography
$DC_{8,9}PC$: 1,2-bis (tricosa-10,12-diynoyl)-sn-glycero-3-phosphocholine
DiIC (18)3: Distearoyl Indocarbocynaine
DLS: Dynamic Light Scattering
DOX: Doxorubicin
DPPC: Dipalmitoyl Phosphatidylcholine
DSPC: Distearoyl Phosphatidylcholine
DSPE: Distearoyl Phosphatidylethanolamine
DTT: Dithiothreitol
EPR: Enhanced Permeability and Retention
FITC: Fluorescein Isothiocyanate
Gd(III): Gadolinium ion
Gd-DOTA: Gadolinium-1,4,7,10-Tetraazacyclododecane-1,4,7,10-Tetraacetic acid
Gd-DTPA: Magnevist®, Gadolinium-Diethylenetriaminepentaacetic acid
Gd-DTPA-BMA: Omniscan®, Gadolinium-Diethylenetriaminepentaacetic acid-Bis(methylamide)
Gd-DTPA-DG: Gadolinium-Diethylenetriaminepentaacetic acid-Deoxyglucosamine
Gd-EOB-DTPA: Eovist®, Gadolinium-Ethoxybenzyl Diethylenetriaminepentaacetic acid
Gly: Glycine
GPC: Gel Permeation Chromatography

GSH/GSSG: Glutathione/Glutathione Disulfide
IARC: The International Agency for Research on Cancer
ICP-OES: Inductively Coupled Plasma Optical Emission Spectrometry
LCST: Lower Critical Solution Temperature
MMP: Membrane-type Matrix Metalloproteinase
MRA: Magnetic Resonance Angiography
MRI: Magnetic Resonance Imaging
MSN: Mesoporous Silica Nanosphere
MTT: 3-(4,5-Dimethyliazolyl-2)-2,5-Diphenyl Tetrazolium Bromide
Mw: Molecular Weight
NAC: N-Acetyl-L-Cysteine
NCI: National Cancer Institute
NMR: Nuclear Magnetic Resonance
PAA polymers: Poly(amido amine) polymers
PAMAM dendrimers: Poly(amido amine) dendrimers
PBS: Phosphate Buffered Saline
PCL: Poly(Ɛ-caprolactone)
PDEPT: Polymer-directed Enzyme Prodrug Therapy
PDI: Polydispersity Index
PEG: Poly(ethylene glycol)
PET: Positron-Emission Tomography
PFP: Perfluoropentane
PGA: Poly(glycolide)
PLA: Poly(lactide)
PLGA: Poly(lactide-co-glycolide)
PNIPAAM: Poly(*N*-isopropyl acrylamide)
polyHis: Poly(*L*-histidine)
Pro: Proline
q: Number of water molecules coordinated
r_1: Longitudinal Relaxivity
RES: Reticuloendothelial System
RGD: Arginine-Glycine-Aspartic acid
SPECT: Single Photon-Emission Computed Tomography
T_1: Longitudinal Relaxation Time
T_2: Transverse Relaxation Time
TEM: Transmission Electron Microscope
TMBQ: Trimethyl-locked Benzoquinone
TPE-MI: Tetraphenylethene-Maleimide, thiol specific AIE fluorogen.
uPA: urokinase Plasminogen Activator
Val: Valine
WHO: World Health Organization

List of Publications

1. Redox-Responsive Hyperbranched Poly(amido amine)s with Tertiary Amino Cores for Gene Delivery *Biomacromolecules* **2013**, *14*, 2083-2094.

2. Magnetic Resonance Imaging (MRI) Contrast Agents for Tumor Diagnosis *Journal of Healthcare Engineering* **2013**, *4*, 23-46.

3. pH- and Redox-Responsive Poly(ethylene glycol) and Cholesterol-Conjugated Poly(amido amine)s Based Micelles for Controlled Drug Delivery *Macromolecular Bioscience* **2014**, *14*, 347-358.

4. Redox-Responsive Nanoparticles with Aggregation-Induced Emission (AIE) Characteristic for Fluorescence Imaging *Macromolecular Bioscience* **2014**, *14*, 1059-1066.

5. Stimuli-Responsive Polymers for Anti-Cancer Drugs Delivery *Materials Science and Engineering: C* **2014**, DOI: 10.1016/j.msec.2014.05.050.

6. A Facile Approach to Biodegradable Polydisulfide MRI Contrast Agent *Journal of Materials Chemistry B* **2014**, *2*, 5295-5301.

7. pH- and Redox-Responsive Self-Assembly of Amphiphilic Hyperbranched Poly(amido amine)s for Controlled Doxorubicin Delivery (Manuscript submitted).

Chapter 1

Introduction

1.1. Cancer treatment and diagnosis

Cancer is a disease in which cells do not undergo programmed cell death, apoptosis, and divide uncontrollably to form malignant tumors according to the definition from National Cancer Institute (NCI) and American Cancer Society (ACS). It is stated in "The History of Cancer" published by ACS that cancer was observed as early as 3000 B.C, but , the main causes of cancer are identified only until the 20th century, i.e., chemicals, radiation, viruses and genetics. The World Cancer Report 2014 by The International Agency for Research on Cancer (IARC), the specialized cancer agency of the World Health Organization (WHO), states that there were 14 and 8.2 million of new cancer cases and cancer death per year in 2012, respectively, this set of values are predicted to rise to 22 and 13 million in the next 20 years. It was also indicated that the total annual economic cost of cancer was estimated to be approximately US$1.16 trillion in 2010. Furthermore, cancer has overtaken heart disease as the number one cause of death globally. Therefore, it is motivated and encouraged to search for the elusive cure for cancer worldwide.

To completely eliminate the cancerous cells, patients usually have to undergo a series of treatments including (1) surgical removal of the malignant tumor, (2) chemotherapy which uses drugs to kill the cancerous cells, and (3) radiation therapy which uses high energy electromagnetic waves to kill the cancerous cells. While bulk of the tumor can be successfully removed through surgery and radiation therapy, chemotherapy is still needed to completely eradicate all the cancerous cells..

However, most of anti-cancer drugs used in chemotherapy, e.g., doxorubicin (DOX) and paclitaxel, are highly hydrophobic and insoluble in the circulatory system, thus these drugs tend to aggregate which render the drugs useless and cause serious complications like embolism [1-3]. It is also not effective to use organic solvents and surfactants to improve the drugs' solubility [3]. The free anti-cancer drugs are also very susceptible to clearance from the reticuloendothelial system (RES) due to their hydrophobic nature [4]. Furthermore, free anti-cancer drugs have a very low specificity to cancerous cells [5] so that normal healthy cells are also damaged and killed. As a result, cancer patients have to take in a high dose of drugs in high frequency, which result in high risk of toxicity and side effects like poor body immune system.

The cancer survival rate can be significantly improved if the condition is detected as early as possible and diagnosed accurately. NCI has classified the various screening and diagnosis methods into four different types: (1) physical examination and history – a general health examination and history of past illness, (2) laboratory test – conduct tests on tissue, urine and blood samples, (3) imaging procedures – imaging mainly via computed tomography (CT), and (4) genetic tests – to identify genetic mutations. Of all the four screening and diagnosis methods, only imaging provides the exact location of the tumor which is vital information before surgery and radiation therapy can be conducted. CT scan may be a useful form of imaging technique, however, extensive CT scanning may cause undesirable complications due to the ionizing effects of X-rays. Fortunately, in recent years, magnetic resonance imaging (MRI) and fluorescence imaging have emerged as possible alternatives for cancer screening and diagnosis.

Since cancerous cells have water content similar to surrounding normal healthy cells, it is difficult to differentiate them using MRI scanning. Therefore, the use of contrast agents is necessary for cancer detection. These contrast agents (Magnevist®, Ablavar® and ProHance®) commonly contain heavy metals like gadolinium ions (Gd(III)) to create signal contrast between desired area and its surroundings. However, these contrast agents are unsuitable for cancer detection due to the short retention time, low relaxivity values, and lack intracellular accumulation which is related to the low molecular weight [5-8] and low specificity to cancerous cells [5-10].

Similarly, for fluorescence imaging, agents like organic fluorophores or quantum dots which provide imaging contrast are also needed to highlight the malignant tumor. However, organic fluorophores which are usually highly hydrophobic with low solubility in aqueous environment can create issues like short half-life and embolism alike hydrophobic anti-cancer drugs mentioned above. Furthermore, these fluorophores have low specificity to cancerous cells too [11]. On the other hand, quantum dots have cytotoxicity issues [12].

1.2. Delivery systems of active species for cancer treatment and diagnosis

To address the challenges of cancer treatment and diagnosis, one way is to develop suitable systems to deliver anti-cancer drugs, MRI contrast agents and organic fluorophores to cancer sites with a high specificity.

Generally the delivery systems can be divided into two categories: one is realized via non-covalent encapsulation, and the other is via covalent conjugation of the active species onto the carriers. One of the important approaches to good delivery systems is via self-assembly, which can produce

nano-sized delivery systems, i.e., nanocarriers. Normally nanocarries are composed of hydrophobic cores and hydrophilic shells. The delivery systems can enhance the effectiveness and efficacy and reduce side effects of anti-cancer drugs, MRI contrast agents and fluorophores due to the features below.

- Nanocarriers with hydrophilic shell and hydrophobic core, can hold hydrophobic drugs or organic fluorophores within the cores for secure encapsulation, and also form good dispersion in the aqueous solution [3,13,14-20]. Therefore, the aggregation of the active species can be avoided.
- Nanocarriers with suitable size and hydrophilic shells can effectively evade the RES and increase the circulation time or half-life after administration [4,17,20,21]; or the retention time of the contrast agents significantly [22].
- Nanocarriers can target the active species to the cancerous cells via passive (Enhanced Permeability and Retention (EPR) effect) or active (via conjugation of surface ligands) targeting, thus increasing the efficacy and reducing side effects of chemotherapy and cancer diagnosis [22-24]. Moreover, the contrast agents conjugated nanocarriers can also be modified with stimuli-sensitive moieties that only response to the unique intrinsic conditions of tumors to provide high contrast imaging [25].

However, the challenges as listed below in developing suitable delivery systems for anti-cancer drugs, MRI contrast agents and fluorophores for cancer treatment and diagnosis are still daunting, and these hinder their success in clinical applications.

❖ For anti-cancer drug delivery:

- The payload is released prematurely due to the inherent low stability of the systems and/or uncontrolled release of the payload. An example is Taxol®, formulation of paclitaxel using cremophor, which apply cremophor to enhance the solubility of paclitaxel. However, cremophor has a relatively high critical micelle concentration (CMC) leading to a low stability [26]. Abraxane® may also face stability issue. The 130 nm albumin paclitaxel formulation was reported to break down into 10 nm particles after injected into circulation [27] and this may result in premature paclitaxel release. Similarly, DOXIL®, DaunoXome® and LiPlaCis® which utilize liposomes as nanocarriers, show uncontrolled release behaviours, causing the payloads to be discharged during circulation before reaching the targeted sites [28,29]. On the other end of the spectrum, some delivery systems have such low fluidity that even after reaching the targeted sites, the payloads cannot be released.
- Low specificity of delivery systems result in undesirable distribution and release of payloads, and this can cause detrimental side effects. Taxol® shows higher toxicity than Abraxane®, causing more death in mice which might be contributed by its non-specific nature [30a]. DOXIL® also shows non-specific behaviour leading to cardiotoxicity which is a prevalent concern with DOX delivery systems.

❖ For MRI contrast agent

- In cancer diagnosis, it is possible to produce suitable MRI contrast agents via integrating small molecular Gd(III) chelates with polymers

to form macromolecular MRI contrast agents. This can reduce vascular extravasation [177,179,472-475], improve the tumour targeting capability and T_1 relaxivity [177,472-477]. However, macromolecular MRI contrast agents might lead to a slow and incomplete excretion of Gd(III) ions integrated in these macromolecules, which can result in side effects such as nephrogenic systemic fibrosis (NSF) especially in renal dysfunctional patients [32-34]. Therefore macromolecular MRI contrast agents with suitable degradation rate are needed for feasible excretion of Gd(III) chelates after imaging [478].

- Suitable fluorophores for better cancer diagnosis are needed to provide the features below:
  - To provide high imaging contrast between the cancer tissues and background.
  - To provide indication of the redox status of cancer tissues. Intracellular compartments of cells are much more reductive than the extracellular matrix, and the combined redox state of cellular redox couples, like glutathione/glutathione disulfide (GSH/GSSG) which is often regarded as the major redox buffer, forms the redox environment [43,507]. Oxidative stress is closely linked to the status of cancer [508-510], e.g. a high level of GSH in tumor is related to the resistance to therapies [50].

1.3. Scope of study

A perfect stimuli-responsive polymer delivery system can carry the payloads securely in the absence of certain stimulus, but can release the payloads when the stimulus is present. So suitable stimuli-responsive polymers delivery systems can address the challenges discussed above. It is well recognized that intracellular compartments of cells are much more reductive than the extracellular matrix. The GSH/GSSG couple is regarded as the representative cellular redox couple which plays a critical role in redox homeostasis. The concentration of GSH in intracellular compartments is 100-1000 times higher than in the extracellular matrixes. Hence this thesis focus on developing redox-responsive poly(amido amine)s for anti-cancer drugs, MRI contrast agents and fluorophores to improve the efficacy and reduce side effects.

Redox-responsive polymers were prepared via Michael addition polymerization of trifunctional amines with disulfide-containing bisacrylamide. The polymers obtained were then finely tuned for delivery of anti-cancer drug, MRI contrast agent and fluorophores, respectively.

- For anti-cancer drug delivery: In order to develop delivery systems for anti-cancer drug, DOX, two types of polymers micelles were developed and investigated. The first is from poly(ethylene glycol) (PEG) and cholesterol-conjugated poly(amido amine)s; and the second is from hyperbranched poly(amido amine)s. Beyond redox-response, pH-response also contributes to the improved performance of the delivery systems developed due to the acidic environment of cancer cells. The chemistry of poly(amido amine)s, the structures of delivery systems, release profiles and the efficacy to kill cancer cells were investigated.

- For MRI contrast agent: Macromolecular Gd(III) based MRI contrast agents containing polydisulfide units in the backbone was developed. The chemistry, structure and redox-induced degradation of the polydisulfide MRI contrast agents were characterized and investigated.
- For fluorophore: Delivery system of fluorophores with aggregate-induced emission (AIE) characteristic was developed. The structure and the redox-responsive "turn-on" photoluminescence profiles of system was characterized and investigated.

Chapter 2

Literature Review

2.1. Stimuli-responsive polymers for anti-cancer drug delivery

Cancer is one of the top killers of human. So far, chemotherapy adopting chemical compounds to kill cancer cells is still one of the major therapies of cancer. Most of the chemical compounds investigated for the chemotherapy are water insoluble and cannot be used directly. Suitable formulations are necessary to render the chemical compounds with certain dispersion in aqueous solution, suitable *in vivo* clearance rate and capability to target the cancer site [1-3,5,41]. This requirement applies to new chemical compounds explored for chemotherapy. For anti-cancer drugs already in the market, it is also desirable to develop new formulations with better performances which benefit both the patients and the producers. One of the most important formulations of anti-cancer drugs is to develop suitable drug delivery systems. Organic materials including polymers, lipids, proteins, surfactants are important materials for developing drug delivery systems. Although tremendous efforts have been put to develop suitable drug delivery systems, however, only very few have been in clinic use such as ABRAXANE®, a formulation of paclitaxel using albumin; DOXIL®, a formulation of DOX using PEGylated liposome; DaunoXome, a formulation of daunorubicin using liposome; and LiPlaCis®, a formulation of cisplatin using liposome also [1-3,5,41].

Anti-cancer drugs' high toxicity can lead to serious side effects. One way to reduce the side effects is to deliver the drugs only to the cancer site

without leaking into other organs. This requires the drug delivery systems to provide secure encapsulation of the drugs before reaching the tumor without drug leakage, but be able to release the drugs after entering the cancerous cells. Therefore, the drug delivery systems are required to provide secure encapsulation of the drugs loaded before reaching the cancer site but disassemble after entering the cancerous tissues. To achieve these requirements, stimuli-responsive materials are indispensable. The stimuli-responsive materials can undergo significant changes in physical or chemical properties in response to the variations in the environment. The stimuli-responsive materials are expected to provide secure encapsulation of drugs in the absence of the stimuli, but release the drugs when the stimuli are presented. The stimuli explored can be divided into two categories: endogenous and exogenous stimuli. Endogenous stimuli are the intrinsic conditions of the cancer tissues such as a tough redox environment, an acidic condition, and certain types of enzyme present. The exogenous stimuli can be change in temperature, photo and ultrasound.

One important category of materials for formulation of drug delivery systems is polymers. Here the polymers responsive to the endogenous stimuli including redox, pH and enzyme, and to the exogenous stimuli including change in temperature, photo, and ultrasound are reviewed.

2.1.1. Endogenous stimuli-responsive polymers

2.1.1.1. Redox-responsive polymers

Intracellular compartments of cells are much more reductive than the extracellular matrix, and the GSH/GSSG couple is regarded as the

representative cellular redox couple which plays a critical role in redox homeostasis. The concentration of GSH in intracellular compartments is 100-1000 times higher than in the extracellular matrixes. GSH has significant effects on many cellular functions such as gene expression, protein function, immune responses, cell-cycle regulation and activation of cell death [42-45]. Furthermore, it was also reported that in numerous human diseases like neurodegenerative diseases, liver diseases, stroke, seizure and diabetes, the GSH level is affected [42,46-49]. For example, abnormally high concentration of GSH found in cancerous cells protects the cells against the anti-cancer drugs and free radical generated during radiation therapy, which result in multi-drugs and radiation resistance [42,48,50]. Recently the significant different in the redox environment has been explored for developing redox-responsive drugs delivery systems [43]. One important approach is to incorporate disulfide bonds within the systems via different methods.

Redox-responsive cross-linking is introduced into drug delivery systems via disulfide containing crosslinkers, oxidization of thiol group, and disulfide-thiol exchange reaction. The cross-linking can render good stability to the drug delivery systems such as polymeric micelles [51-53] which have compact structures [51-54], to provide secure encapsulation of drugs in the absence of thiol group. Many types of disulfide containing cross-linker are applied. 3,3'-dithiobis(sulfosuccinimidylpropionate) was used to form cross-linking in poly(L-lysine) shell of micelles from triblock copolymer, PEG-*b*-poly(L-lysine)-*b*-poly(L-phenylalanine). 30% more of docetaxel was released upon treatment with 10 mM GSH than with 2 μM GSH because the cleavage of disulfide bonds within the poly(L-lysine) shell layer facilitated the release

of docetaxel. *in vivo* study showed that docetaxel loaded cross-linked micelles is more effective in inhibiting tumor growth than free docetaxel and its non-cross-linked counterpart [55]. Other redox-sensitive linkers like disulfide-containing dimethyacrylate [56], 2-(2-pent-4-ynoyloxyethyldisulfanyl)ethylpent4-ynoate (bis-alkyne cross-linker with a disulfide bridge) [57] bis(2-azidoethyl) disulfide [58], cystamine [59] were also used.

Oxidation of thiol groups in cysteamine [60] and cysteine [61] conjugated to polymer chains can be achieved by reaction with purged oxygen, which resulted in formation of disulfide bonds containing cross-linking. Also disulfide bonds such as of pyridyldisulfide [62-64] conjugated o polymer chains can form cross-linking by a deficient amount of dithiothreitol (DTT), which led to the formation of thiol and further thiol-disulfide exchange reaction [62,63]. Recently our work showed that thiol-disulfide exchange reaction could occur under a basic condition leading to cross-linked polymers from disulfide-containing hyperbranched poly(amido amine)s [64].

Redox-responsive self-assembly of amphiphilic polymers in the form of micelles or polymersomes were explored for drug delivery [65]. One way is to combine the hydrophobic and hydrophilic segment via disulfide bond. Hydrophobic poly(Ɛ-caprolactone) (PCL) was combined with PEG [66] or dextran [67] via the disulfide bonds. The intracellular release of DOX from redox-responsive micelles is faster than their non-reducible counterparts, which agrees with *in vitro* release profile. The additional advantage that is the detachment of shells upon reduction of the disulfide bonds leads to formation of aggregation and precipitation of the drug delivery systems, which might

prevent the efflux of drugs, one of the causes of cancer drug resistance [68-71]. Amphiphilic polymers can also be obtained by grafting different groups to polymer backbones via the disulfide bond [72-74]. The polymer backbone can be water soluble biopolymer like chitosan [75], hyaluronic acid [76] and chondroitin sulfate [73].

Fully biodegradable polymers were also prepared from disulfide-containing monomers. The polymer backbone can be either linear [77-79] or dendritic [80,81]. In our recent works, linear redox-responsive poly(amido amine)s was obtained from Michael addition polymerization of disulfide containing *N*,*N*-cystaminebis(acrylamide) (BAC) and trifunctional amine, 4-(aminomethyl)piperidine (AMPD), due to the different reactivity of the three types of amines [82,83]. Then PEG and cholesterol were conjugated to the polymer backbone. Upon reduction, the redox-responsive micelles released 13% and 15% more DOX in 24 h and 72 h respectively. The redox-responsive DOX loaded micelles also exhibited a higher cytotoxicity than free DOX in both MCF-7 and HepG2 cell lines [77]. Another type of amphiphilic graft copolymer with disulfide bonds along the polymer backbone also form micelles which released DOX in the presence of DTT [78]. Dendritic amphiphilic hyperbranched multiarm copolyphosphate (HPHSEP-*star*-PEP$_x$) with disulfide bonds in the backbone could be loaded with DOX and the *in vitro* cytotoxicity of the DOX loaded micelles is higher when a higher GSH level is present [80].

Also redox-responsive polymer-drug conjugates or polymer prodrugs were prepared [84]. Linear redox-responsive polymer-drug conjugate was reported to release less than 20% of drugs in the absence of reducing agents

even after a long period of time [85-87]. Dendritic polymers were also explored [81,87,88]. N-Acetyl-L-cysteine (NAC), an antioxidant and anti-inflammatory agent, was conjugated to either amine or carboxyl terminal PAMAM dendrimer. Around 18 of the 64 terminal groups of the dendrimers could be conjugated with NAC via disulfide linkages. When the NAC conjugated dendrimers were subjected to 2 μM of GSH to mimic the extracellular GSH concentration, only less than 1% of NAC was released within 1 h. However, more than 50 times greater of NAC was released in the same length of time when intracellular (10 mM) GSH concentration was used [88]. Sometimes, the conjugation of drugs to polymer can be challenging especially when the drugs have limited reactive functional groups like camptothecin with just one hydroxyl group [87,89,90]. On the other hand, drugs like DOX with more functional groups allow more variation in the conjugation process which might affect the drug functions [85,91].

Beyond applying disulfide linkage, recently trimethyl-locked benzoquinone (TMBQ), which can be reduced into lactone, was used to form redox-responsive drug delivery systems [92]. The polymers were synthesized by reacting TMBQ serinol monomer with adipoyl chloride which can self-assemble and encapsulate paclitaxel within the nanoparticles. After reaction with reducing agent sodium dithionite, the conversion of TMBQ to lactone destabilized the nanoparticles leading to the release of drugs. However, TMBQ is commonly known to undergo intracellular enzymatic reduction and might not to react with thiols like GSH [93.94]. Therefore, more work has to be done to further improve this system.

2.1.1.2. pH-responsive polymers

To meet the high demand for energy to maintain rapid cell divisions, cancerous cells adopt the metabolism of glycolysis instead of normal oxidative phosphorylation, an phenomenon known as the Warburg effect. As a result, lactic acid, the product of glycolysis, accumulates around the tumors in high concentration which lowers the pH of the extracellular environment [95]. Furthermore, the lower pH found in endosomes (5-6) and lysosomes (4-5) have also been explored for developing pH-responsive drug delivery systems, which are designed to only release their loaded drugs after endocytosis [96].

One category of the responsive polymers which contains amino or carboxylic acid groups undergoes protonation-induced change in polymer hydrophobicity [77,97,98]. When pH was dropped from 10 to 4, the diameter of micelles of PEG-*b*-poly(*L*-lysine)-*b*-poly(*L*-phenylalanine) increased from 15 nm to 60 nm facilitating the release of drug loaded. Reversibly, hydrogels with carboxylic acid groups swell when the pH of the aqueous medium is raised [99-101]. A higher degree of ionization of carboxylic acid increases electrostatic repulsion among the polymer chains leading to higher solubility in aqueous solution [102,103]. If the ratio of carboxylic group within the hydrogels is raised, a greater extend of swelling can be expected [99]. Due to the swelling, these systems release drugs faster at a high pH condition [104,105]. This effect is particularly useful for oral delivery route. As the drug delivery systems pass through the stomach usually with a pH of ca. 2, the condensed systems can protect the drugs. However the drugs are released for absorption into the body after reaching the intestine usually with a neutral pH [99,100]. For polyelectrolyte complex based drug delivery systems, structural

transformation occurs when the charge balance is disrupted with pH [106,107]. PAMAM dendrimers were complexed with diblock copolymer of poly(methacryloyl sufladimethoxin)-PEG modified by lactose (LA-PEG-*b*-PSD) [106]. The complexes have hydrodynamic size of ca. 50 nm at pH 7.4 and the drugs loaded within the complexes were released much slower than PAMAM dendrimers due to the presence of LA-PEG-*b*-PSD. However, when the pH was reduced to 6.5, the complexes were disintegrated, leading to fast release of the drug similar to PAMAM dendrimers.

Poly(*L*-histidine) (polyHis) was also explored for preparation of pH-responsive drug delivery systems. PolyHis was used to form the core of polymer micelles, the ionization of polyHis disrupts the hydrophobic interaction within the core to release the drugs [108-110]. It was shown that a higher content of polyHis in the diblock copolymer caused a faster release of DOX at both pH 7.4 and 5.5 [108]. Besides inducing structural deformation, polyHis was used in micelles to expose TAT peptides for membrane penetration [111,112]. At physiological pH, due to hydrophobic interaction of the TAT peptide and polyHis, the TAT peptides are shielded within the PEG shells. However, when the polyHis are ionized at low pH, the freed TAT peptides protrude out of the PEG shell making the micelles more susceptible for cellular uptake. To demonstrate this idea, MCF-7 cells were incubated with the micelles at different pH. The result showed that at pH 7.4, the uptake by MCF-7 is minimal, but at pH 7.0 and 6.8, the uptake is increased by 30 and 70 times respectively. This indicates that cellular uptake of the micelles can be significantly improved with more TAT peptide protruding out at a low pH [111].

pH-responsive polymer prodrugs were also developed. Hydrazone linkage which undergo acid catalyze hydrolysis, is extensively studied by Younsoo and coworkers. A variety of block copolymers were conjugated to different drugs like adriamycin (ADR) [113-115], DOX [116-118], dexamethasone [119] and others [120,121]. ADR was conjugated to PEG-*b*-poly(aspartate) via the hydrazone bonds and the micelles formed showed pH dependent release of the drugs with the fastest release rate being observed at pH 3. Both *in vitro* and *in vivo* studies of these micelles showed that the micelles can inhibit growth of the cancer cells. Furthermore, the studies also revealed that the toxicity of the micelles loaded with ADR is lower, the circulation of the drugs in the blood is extended, and a higher concentration of ADR is found in the tumor. To improve the cellular uptake of these micelles, the PEG-*b*-poly(Asp-Hyd-ADR) was further functionalized with folate which has corresponding binding protein overexpressed on the cancer cell membrane. *in vitro* results showed that the folate enhanced the uptake leading to a higher toxicity. Another pH-responsive linkage is the acetal bond with its hydrolytic rate being tuneable by varying the alcohol derivatives [122]. pH-responsive bonds are also frequently used in the pH induced degradation of drug delivery systems [123-126]. The degradation and dissociation of the drug delivery systems under acidic condition facilitate the release of drugs.

2.1.1.3. Enzyme-responsive polymers

Enzymes are a group of proteins which play vital roles in many biological functions, and one unique feature of enzymes is their specific activities based on the lock and key mechanism. For example, different enzymes were used to

cleave alanine-valine (Ala-Val) and glycine-proline (Gly-Pro) peptide sequence. While thermolysin and proline endopeptidase can readily break down Ala-Val and Gly-Pro peptides respectively, thermolysin cannot cleave Gly-Pro and proline endopeptidase cannot break Ala-Val [127]. Furthermore, it has been observed that there are upregulated expression of certain enzymes in some pathological conditions like cancer and inflammation. Therefore, these features can be exploited for developing enzyme-responsive materials for drug delivery systems. There are six groups of enzymes, i.e., oxidases, transferases, hydrolases, lyases, isomerases and ligases. However, hydrolases, which catalyses the hydrolysis reaction, is widely investigated.

A well-documented class of hydrolase is the cancer-associated proteases (CAP) which include urokinase plasminogen activator (uPA), membrane-type matrix metalloproteinase (MMP), and these enzymes have been used to design protease sensitive biomaterials for controlled drug delivery. Self-assembled matrix with uPA sensitive motif connecting two peptide β-sheets was developed. In the presence of uPA, the matrix disassembled and released the drugs with the degradation being uPA concentration dependent. Moreover, when the sequence of uPA sensitive motif was scrambled, the degradation was impeded [128]. Other uPA responsive drug delivery systems including polymer caged liposomes with uPA sensitive crosslinker [129] and albumin conjugated DOX prodrug with uPA sensitive linker [130] were also reported. MMP- responsive cisplatin hydrogel delivery system was developed by forming hydrogel of PEG diacrylate matrix conjugated with cisplatin via MMP sensitive linker. It was observed that only hydrogel with high molecular weight PEG diacrylate showed MMP sensitivity

due to the larger mesh size of the hydrogel allows free diffusion of MMPs to cleave the linker [131,132]. Cathepsin is primarily an intracellular enzyme related to upregulation in cancer [133]. *N*-(2-hydroxypropyl)methacrylamide copolymers were conjugated to DOX via cathepsin sensitive linker, and this prodrug showed cathepsin sensitivity [134]. Furthermore, the effectiveness of this prodrug can be enhanced by applying the polymer-directed enzyme prodrug therapy (PDEPT) which is a two-steps approach. The prodrug is administrated followed by the polymer-cathepsin B conjugate. The second dose of polymer-enzyme conjugate will cleave the cathepsin sensitive linker of the prodrugs that are already accumulated in the tumor to release the DOX. i*n vivo* study demonstrated that the concentration of DOX detected in the tumor is much higher using PDEPT than the one-step approach with the DOX level in the liver and heart being comparable [135].

2.1.2. Exogenous stimuli-responsive polymers

Unlike endogenous stimuli, exogenous stimuli are exposed via an external treatment. Although this additional step seems unappealing, exogenous stimuli-responsive drug delivery systems might be more encouraging and favourable because endogenous stimuli vary due to the heterogeneous physiological conditions of human population [136].

2.1.2.1. Thermoresponsive polymers

Thermoresponsive polymers undergo phase transition when subjected to temperature change. The temperature change can be realized via heat treatment directly, applying light or magnetic field on gold particles-

containing systems or iron oxide-containing systems respectively. A prime thermoresponsive polymer is the poly(*N*-isopropyl acrylamide) (PNIPAAM) [137-140]. PNIPAAM has a lower critical solution temperature (LCST) of around 31-32 ^{o}C. PNIPAAM polymer chains become water soluble or insoluble when the temperature is below or above LCST, respectively [141]. The LCST of PNIPAAM can also be raised by copolymerization or conjugation with other hydrophilic polymers and vice versa [142]. Thermoresponsive polymer formed by grafting chitosan to PNIPAAM, can self-assemble to encapsulate curcumin forming nanoparticles (TRC-NP) [143]. Depending on the ratio of chitosan to PNIPAAM, the TRC-NP has a LCST ranging from 38 to 44 ^{o}C. Moreover, the *in vitro* drug release profiles showed that the TRC-NP released 5% and 100% of the drugs loaded when incubated at temperature below and above its LCST respectively. Thermoresponsive block copolymers composed of the poly(NIPAAM-*co*-N,N-dimethylacrylamide) and poly(D,L-lactide), PCL or poly(D,L-lactide-*co*-ε-caprolactone) were also reported [144]. A longer poly(D,L-lactide) or poly(D,L-lactide-*co*-ε-caprolactone) hydrophobic block results in a lower LCST, and the block copolymers also display temperature dependent drug release behaviour. PNIPAAM has a non-biodegradable polyacrylate backbone so the biocompatibility might be an issue, so biodegradable PNIPAAM with adjustable LCST was reported by conjugating NIPAAM to poly(amino ester)s. The resulting thermoresponsive and pH-responsive polymer is capable of self-assembly [145].

Another thermoresponsive system consists of dipalmitoyl phosphatidylcholine (DPPC) and distearoyl phosphatidylcholine (DSPC). As

heat is applied, the increase in passive permeability of the lipid bilayer during the gel to liquid crystalline phase transition period, allows the entrapped drugs to diffuse out at a faster rate [146]. The ratio of DPPC and DSPC also determines the temperature of the phase transition and permeability of the liposomes. A higher content of DPPC results in a lower transition temperature and a more permeable liposomes [147,148]. These thermoresponsive liposomes have been explored for the formulations of drugs including cisplatin [149,150] and methotrexate [151,152]. Gold nanoparticles were also used as localized heat sources [147,153]. The gold nanoparticles were either embedded within the lipid bilayer, the inner and outer surface of the lipid layer or loaded within the core of the liposomes. The results showed the presence of gold nanoparticles in the liposomes affected the structural integrity of lipid bilayer and cause calcein to leak slightly even without light activation regardless of position. However, upon UV irradiation, only the gold nanoparticles embedded/loaded liposomes were able to release calcein readily, with the release more pronounced in liposomes that had gold nanoparticles embedded in the lipid bilayer. The gold nanoparticles were able to absorb energy from the UV irradiation and transfer the heat to the lipid molecules more efficiently when it is in contact with the molecules. Furthermore, it was proven that the gold nanoparticles were indeed acting as localized heat source heating the neighbouring environment. If the UV irradiation lasts 30 s or more, the DPPC undergo phase transition from lamellar gel phase to ripple phase then further to fluid lamellar phase.

Also magnetically induced thermoresponsive drug delivery systems were investigated. Magnetic materials, usually iron oxide nanoparticles, are

applied to convert magnetic energy to heat under the influence of alternating magnetic field. An additional advantage of magnetically induced thermoresponsive drug delivery systems is target guiding by permanent magnetic field. Using Fe_3O_4 coated with PNIPAAM microgel under alternating magnetic field, the LCST of NIPAAM was determined [154]. Furthermore, under the alternating magnetic field, mitoxantrone loaded PNIPAAM-SA-Fe_3O_4 microgel could get heated up from 298 to 323 K in 4 minutes and displayed temperature dependent drug release. Thermoresponsive liposomes loaded with DOX and magnetic nanoparticles were functionalized with folate targeting group (MagFolDox) [155]. Under the influence of permanent magnetic field, the cytotoxicity of MagFolDox was higher than liposomes without the magnetic nanoparticles. In other work where Fe_3O_4 was also used, similar drug release behaviour was observed. Only when alternating magnetic field was applied, drugs were released [156,157].

2.1.2.2. Photo and ultrasound- responsive polymers

Irradiation energy can be used to directly trigger the drug release. A photo-responsive liposome, consisting of PEG_{2000}-dioleoylPE, cholesterol,dioleoylPC, and 1,2-bis[10-(2',4'-hexadienoyloxy)decanoyl]-*sn*-glycero-3-phosphocholine(bis-SorbPC) which disassemble upon UV irradiation was reported [158]. These sterically stabilized liposomes release 220 times more water soluble fluorescence markers (ANTS) than non-irradiated liposomes. Moreover, the irradiation led to the release of the bis-SorbPC monomer from the lipid bilayer. It was suggested that the photo-induced polymerization of bis-SorbPC created disorder along the lipid bilayer

and increase its permeability. Also a photosensitizer, distearoyl indocarbocynaine (DiIC (18)3), was added into a similar photo-sensitive liposomes which still contain bis-SorbPC to enable visible light stimulation [159]. The photoactivation of DiIC (18)3 generates oxygen radicals which initiate the polymerization of bis-SorbPC to increase the lipid's permeability. Photopolymerizable lipid, (1,2-bis (tricosa-10,12-diynoyl)-sn-glycero-3-phosphocholine) ($DC_{8,9}PC$) was also applied. A higher ratio of $DC_{8,9}PC$ increases the sensitivity of the liposomes to irradiation, releasing calcein more rapidly. No change in the size distribution of the liposomes after UV irradiation indicates that the release of calcein is not due to rupture of the lipid bilayer but the formation of pores [160,161]. Besides photopolymerization, other reactions like photooxidation and photodeprotonation can also affect the permeability of the lipid bilayer [162].

For liposomes which lipids are non-photo sensitive, it is still possible to achieve photo triggered release by introducing this photosensitizer, aluminium phthalocyanine disulfonic acid ($AlPcS_2$) in the lipid bilayer [163]. This photo-release mechanism is based on the photodynamic action of $AlPcS_2$. Upon irradiation by red light, oxygen radical generated by $AlPcS_2$ reacts with the unsaturated fatty acids thus increasing lipid bilayer permeability and cause 10 times faster release of 5-carboxyfluorescein.

Acoustic cavitation of surfactant stabilized microbubbles can temporarily change the permeability of cell membrane to enhance drug uptake which is known as the sonoporation [164,165]. It was shown that the cellular uptake of DOX was enhanced and more cell apoptosis was induced using the combination of DOX treatment and microbubbles with ultrasound [166].

However, this method of co-injecting the free DOX and DOX loaded delivery systems can lead to accumulation in undesirable areas [167]. Therefore, a connecting system of microbubbles and drug loaded liposomes was developed. DOX loaded liposomes are conjugated to the surface perfluorobutane gas microbubbles stabilized by lipid. The *in vitro* cytotoxicity studies demonstrated that the cytotoxicity of these DOX-liposomes-microbubbles under the influence of ultrasound is much higher than that of DOX-liposomes with or without ultrasound, and DOX-liposomes-microbubbles without ultrasound [168,169].

Although the sonoporation technique seems like a favourable method to increase the effectiveness of drugs, it does not achieve controlled release. Therefore, polymer coated microbubbles are exploited as ultrasound-responsive drug delivery. One of such systems is the nanodroplets of perfluoropentane (PFP) coated by PEG-co-PLA or PEG-co-PCL [170]. When ultrasound is applied to these block copolymer stabilized nanodroplets, the PFP vaporizes and microbubbles are formed. This ultrasound-induced droplet-to-bubble transition is known as the acoustic droplet vaporization. If drugs are loaded into the polymer coating, during the ultrasound transition, a significant increase in the volume and surface area of the microbubbles may facilitate the release of the drugs. *in vivo* studies, paclitaxel loaded nanodroplets can effectively inhibit the growth of ovarian, breast and pancreatic tumor grafted onto mice. Another similar work, using PFP nanodroplet, showed that the cellular uptake of DOX is highest with fully vaporized droplets as compared to non-vaporized or partial vaporized nanodroplets [171]. Besides microbubbles, liposomes can also be acoustic sensitive. It was found that

distearoylphosphatidylethanolamine (DSPE) based liposomes are ultrasound responsive and the sensitivity increases with the content of DSPE in the liposomes [172]. Upon ultrasound exposure, there is an increase in the mean size of the liposomes, and the DOX release is seven times faster than DSPC based liposomes. It was suggest that the enhanced in permeability may be due to the induction of local defect or polymorphic phase transition in the lipid bilayer during ultrasound exposure. The temperature effect like those observed in thermoresponsive liposomes as the cause of the leakage was ruled out. *in vivo* experiment on the DSPE-based liposomes showed that together with ultrasound, the DSPE-based liposomes can effectively inhibit the growth of tumor grafted on mice [173].

2.2. T_1 MRI contrast agents

In comparison with other diagnosis techniques such as X-ray CT, positron-emission tomography (PET), single photon-emission computed tomography (SPECT) and ultrasound, MRI is non-invasive and can provide tomographic information of whole animals with a high spatial resolution and soft tissue contrast [174,175]. There are many types of MRI technique, including the longitudinal relaxation time (T_1)-weighted imaging with a hyper-intense signal and the transverse relaxation time (T_2)-weighted imaging with a hypo-intense signal. The key challenge in MRI technique is its low diagnosis sensitivity. Currently, 40-50% of MRI scans use contrast agents that contain magnetic metal ions to enhance the intensity of signal [174,176]. The contrast agents for T_1-weighted MRI (i.e., T_1 contrast agent) usually contain lanthanide or

transitional metal ion (Gd(III) or Mn(II)) that is chelated to reduce serious side effects [177-179].

Since nuclear magnetic resonance was explored for diagnosis of disease in 1971 [2], MRI has been well developed for diagnosis of various diseases. For tumor diagnosis, MRI contrast agents are useful to obtain good contrasts for differentiating tumor from healthy tissues, and indicating tumor malignant status and the treatment efficacy. There are many seminal reviews on MRI contrast agents, most of which are generally about MRI contrast agents for diagnosis of various diseases [177-179]. In this review, we focus on contrast agents for tumor diagnosis based on T_1-weighted MRI. The contrast agents used in clinical tumor diagnosis are described first, followed by an update of the progress in developing T_1 MRI contrast agents through exploring new chelates and combining low molecular weight T_1 MRI contrast agents with various types of carriers. The approaches to improving targeting capability of both T_1 MRI contrast agents via either passive targeting or active targeting are covered.

2.2.1. T_1 MRI contrast agents for clinical tumor diagnosis

Several types of T_1 MRI contrast agents, i.e., Gd-DTPA (Magnevist®), Gd-EOB-DTPA (Eovist®) and Gd-DTPA-BMA (Omniscan®), have been employed for clinical tumor diagnosis. Petterssonet al. showed that Gd-DTPA enhanced only the richly vascularized parts and the surrounding of the soft tissue tumors in 10-15 minutes after injection [180]. For the detection of mediastinal lymph nodes, Gd-DTPA-enhanced MRI could provide a diagnosis with a sensitivity of 100%, an accuracy of 97% and a specificity of 91% as

compared to 62%, 74% and 100% for non-enhanced MRI, respectively [181]. However, Gd-DTPA might not be helpful in screening other types of cancer. Hawnaur et al. demonstrated that it is complicated to identify tumor in bladder using Gd-DTPA-enhanced MRI due to the excretion of Gd-DTPA in urine and changes in bladder volume, which could affect the interpretation of results; it was also not reliable in determining the effectiveness of the radiotherapy due to structural changes in the bladder after radiotherapy [182].

Gd-EOB-DTPA is suitable for liver tumor diagnosis due to its good liver-specificity [183]. Vander et al. reported that Gd-EOB-DTPA was taken preferably by an excised and perfused rat liver than Gd-DTPA [184]. Shimada et al. showed that Gd-EOB-DTPA-enhanced MRI was more accurate and sensitive in detecting small hepatic metastases of a diameter smaller than 2 cm than diffusion-weighted MRI [185]. Gd-EOB-DTPA induced a much better tumor enhancement of solid hepatocellular carcinoma lesion of rats than Gd-DTPA and Mn-DPDP. The Gd-EOB-DTPA almost disappeared in 24 hours while a high concentration of Mn-DPDP still remained in the liver [186].

Recently, USFDA approved clinical use of MS-325 in magnetic resonance angiography (MRA). MS-325 can form complex with endogenous serum albumin via hydrophobic interaction without covalent linkages [187-189], and provide longitudinal relaxivity (r_1) of a value 10 times higher and a longer vascular residence time than non-protein-binding contrast agents. The reversible bonding between albumin and MS-325 could facilitate the excretion of MS-325 and avoided poor clearance. MS-325 was also used in the assessment of capillary permeability in rat breast tumor [190].

Although several types of T_1 MRI contrast agents have been employed for clinical tumor diagnosis, their sensitivities still need to be improved in terms of higher r_1 value and/or capability to target tumor.

2.2.2. New T_1 MRI contrast agents for tumor diagnosis under investigation

Two approaches are discussed below regarding development of T_1 MRI contrast agents for tumor diagnosis with improved sensitivity, i.e., low molecular weight Gd(III) complex composed of suitable chelates and targeting ligands, and low molecular weight T_1 MRI contrast agents combined with various carriers.

2.2.2.1. Low molecular weight T_1 MRI contrast agents

One of the most promising chelates for preparing T_1 MRI contrast agents for tumor diagnosis is porphyrin-based compounds with possible multi-functionality. Porphyrin could function as a ligand and was potentially applicable for cancer photodynamic therapy [191]. As the ring of porphyrin is too small to accommodate Gd(III) ions securely *in vivo* [192], porphyrin-like synthetic macrocycle, texaphyrin, was explored as a chelate of Gd(III) instead, which could provide a longer MRI contrast enhancement of the V2 carcinoma than Gd-DTPA [193]. Another type of contrast agent obtained from texaphyrin, Motexafin-Gd, could provide MRI contrast enhancement of brain tumor and killed the cancer cells via redox cycling simultaneously [194, 195].

Enhanced targeting of MRI contrast agents to tumor sites can improve the sensitivity significantly. Various types of ligands have been explored to

improve the tumor specificity of low molecular weight T_1 MRI contrast agents. Arginine-glycine-aspartic acid (RGD) peptide is well known for its high and specific affinity for $\alpha_v\beta_3$-integrins which are over-expressed in endothelial cells during angiogenesis of tumors. Parket al. reported a liver specific contrast agent, cyclic RGD conjugated gadolinium-1,4,7,10-tetraazacyclododecane-1,4,7,10-tetraacetic acid(Gd-DOTA) (Gd-DOTA-RGD) [196]. Gd-DOTA-RGD could produce a high signal intensity of the tumor, but almost lost this enhancement when the $\alpha_v\beta_3$-integrins were blocked [196]. Deoxyglucosamine conjugated Gd-DTPA (Gd-DTPA-DG) was developed to target the hypermetabolic cancer cells because deoxyglucosamine was rapidly taken up by tumor due to the over-expressed glucose transporters [197]. Gd-DTPA-DG could provide a higher MRI enhancement of A549 tumor than Gd-DTPA and a higher retention rate because the metabolism pathway was blocked by the deoxyglucosamine analogy [197]. MRI contrast agents were also developed to target the overexpression of estrogen and estrogen related progesterone receptors in breast and ovarian cancers. Sukerkar et al. conjugated progesterone to Gd-DO3A to improve the cellular uptake by around 3 times higher in two breast cancer cell lines and provided a higher contrast enhancement of the xenograft tumors in nude mice [198]. Pais et al. developed another type of breast cancer specific MRI contrast agent, EPTA-Gd, by conjugating 17b-estradiol to pyridinetetra-acetate-Gd (PTA-Gd) for differentiating estrogen receptors-transfected PR(+) from wild-type PR(-) human breast cancer cells[199].

2.2.2.2. Low molecular weight T_1 MRI contrast agents combined with carriers

Combination of low molecular weight T_1 MRI contrast agents with carriers including polymers and nanomaterials can produce contrast agents with a high payload of chelated Gd(III), normally a higher r_1 value, and enhanced tumor targeting capability. One factor contributing to the enhanced targeting capability is the EPR effect owing to accumulation of complexes of carriers and low molecular weight T_1 contrast agents, which are larger, in tumors with loosely vascular structures [23]. However, the possible release of free Gd(III)was observed from some liposome loaded with low molecular weight T_1 MRI contrast agent, which showed a long retention time [200]. Therefore, the safety issues of the complex of carriers and low molecular weight T_1 contrast agent should be taken into account as well.

2.2.2.2.1. Water-soluble polymer as carriers

Many types of water soluble polymers, including linear polymers, dendrimers, and proteins, have been explored for carrying low molecular weight T_1 MRI contrast agents. Generally, such conjugation limits the rotation and motion of the chelated Gd(III) leading to a higher r_1 value [201-204].

Gd-DTPA conjugated polylysine was able to accumulate in grafted tumor in rat models and therefore provided an enhanced imaging for several days [205]. Gd-DTPA conjugated polyaspartamide demonstrated a preferential uptake and therefore an enhanced MRI contrast in hepatoma in mouse models [206]. A high molecular weight polyglutamic acid based MRI contrast agent exhibited an improved tumor accumulation [207]. Low molecular weight T_1

MRI contrast agents were also conjugated with polysaccharides including dextran, starch, inulin and oligoglucoamines. Conjugates of Gd-DTPA with dextran or oligopolyglucoamines were investigated for delineation of tumor in rabbits [208], while Gd-DO3A conjugated carboxymethyl hydroxyethyl starch showed the ability to image leaky vasculature of tumor [209]. Galatose units targeting the lectin asialoglycoprotein receptor (ASGPR) expressed on liver hepatocytes [210] were explore for imaging of hepatocyte carcinoma through combination with either DOTA [211] or DTPA [210,212].

In comparison with linear polymers, dendrimers have well-defined, rigid dendritic structures together with abundant terminal groups. The conjugation to the terminal groups produces dense peripheral layers of low molecular weight T_1 MRI contrast agents which can induce high r_1 values. For example, the r_1 of G6-(C-DOTA-Gd)115, prepared using a preligation technique, could reach 89.1 $mM^{-1}s^{-1}$ as compared to 4.2 $mM^{-1}s^{-1}$ for DOTA-Gd [201]. It was also found that G6 or G7 dendrimers provided the highest r_1 values, while protonation of amines [213,214] and formation of adducts [215,216] could further improve the values by forming more rigid and open structures with a lower internal motion. Therefore, a higher level of contrast enhancement of tumors could be obtained using a lower amount of PAMAM [217-220] and polylysine dendrimer [221] conjugated with low molecular weight T_1 MRI contrast agents. PEGylated and non-PEGylated Gd labelled dendrimers had a r_1 value higher than 20 $mM^{-1}s^{-1}$ together with a longer retention time [222-224]. Targeting ligands, e.g., OST7 [225], murine monoclonal IgG1, folic acid which targets folate receptor (hFR) [226-229], and cyclic RGD as an angiogenesis marker [230], were applied to improve

active targeting of the conjugates of PAMAM and low molecular weight T_1 MRI contrast agents. Also, dendrimer nanoclusters with folic acid as ligand were developed with a high payload of low molecular weight T_1 MRI contrast agents [231]. In order to improve biocompatibility, biodegradable esteramide dendrimer was combined with low molecular weight T_1 MRI contrast agents [202] which showed a low toxicity similar to Gd-DTPA [232,233].

Low molecular weight T_1 MRI contrast agents were also combined with proteins such as albumin [234,235], IgG and fibrinogen [236] and could increase r_1 by 3 folds. Albumin-Gd-DTPA was employed to monitor the histological profile of tumor and abnormal capillary permeability in cancer models [36-40]. The changes in capillary permeability could estimate angiogenic activity and the effects of pharmacological stress [237], radiation and toxins. The combination with certain types of proteins could improve the tumor targeting capability. Through the interaction between biotin and avidin, Gd(III)-labelled avidin was used to image the dynamic response of tumors to etoposide treatment in mice [238] and breast cancer [239]. Antibody was also explored to deliver MRI contrast agents to tumor specifically. It was shown that antibody labelled Gd-DTPA could visualize melanoma [240,241], human rectal carcinoma [242] and human gastrointestinal cancer. However, many results have shown that conjugation could destroy the immune reactivity of antibodies; therefore, the targeting capability of these MRI contrast agents was limited [243,244].

2.2.2.2.2. Nanomaterials as carriers

With the advancement in nanotechnology, many types of nanomaterials have been developed, such as polymer micelles and vesicles, liposomes and lipid particles, viral particles, carbon nanotubes and fullerenes, gold nanoparticles, and silica particles; most of them have been explored as carriers of Gd(III) as MRI contrast agents for tumor diagnosis.

Ratzinger et al. reported Gd-DTPA and Gd-DOTA labelled PLGA nanoparticles with an r_1 of 17.5 $mM^{-1}s^{-1}$ [245]. In another work, Gd-DOTA was conjugated to PEG-polylysine which could form micelles [246]. Micelles containing low molecular weight T_1 contrast agents could also be obtained by mixing Gd-DTPA conjugated PEG-b-poly(aspartic acid) with polyallylamine/protamine or Gd-DOTA conjugated PEG-polylysine with poly(methacrylic acid) [10,247] via forming polyelectrolyte complex. The r_1 of the polyelectrolytes micelles containing Gd-DTPA was reduced to 2.1 and 3.6 $mM^{-1}s^{-1}$ but was increased to 10 and 11 $mM^{-1}s^{-1}$, respectively, once the micelles were dissociated [10,247]. All these micelles containing low molecular weight T_1 contrast agents showed a preferential accumulation in tumors [216,246]. Gd-DTPA loaded into PEG-b-poly(glutamic acid)/bis(nitrato) (trans-l-1,2-diaminocyclohexane) platinum(II) micelle complex resulted in an increase in r_1 value by 24 times[248]. Theranostic systems such as Gd-DOTA conjugated to unimolecular micelles which composed of fourth generation hyperbranched polyester (*Boltorn H40*) cores, hydrophobic PCL inner layers and hydrophilic poly(oligo(ethylene glycol) shells coated with folic acid. Paclitaxel, an anti-cancer drug, was encapsulated in the hydrophobic PCL layers with a drug loading capacity of 6.67%. That

system showed an r_1 value of 18.14 $mM^{-1}s^{-1}$ and a long retention time of up to 20 hours [249]. Other theranostic systems with higher r_1 values have also been reported with FA as targeting moiety and DOX as drug [6,250,251].

Bui et al. incorporated Gd-DTPA into PEG-coated phospholipid nanoparticles (LNP), which showed a very high r_1 value of 134.8 $mM^{-1}s^{-1}$; the Gd-DTPA loaded LNP was excreted from the body through the biliary system instead of the renal system due to its lipid nature [252]. Low molecular weight T_1 MRI contrast agents were loaded into liposomes in several ways [179,253]. For example, ensomes with reduced r_1 values and memsomes with higher r_1 values were formed when low molecular weight T_1 MRI contrast agents were trapped in the inner parts and the membranes of liposomes, respectively. These systems demonstrated an enhanced passive targeting of tumor such as liver tumor [254]. For active targeting, RGD was employed to label PEGylated liposomes encapsulated with Gd-DTPA and provided a higher MRI contrast enhancement of human lung cancer in xenograft mice [255]. Transferrin, which is over-expressed in many cancerous cells, was used to label liposomes loaded with Gd-DTPA to image the detailed pathway of the liposomes in the human prostate cancer cells inoculated in nude mice [256]. These liposomes entered the peripheral region of the tumor reflected by higher signal intensity observed in 10 minutes after injection of the contrast agent, and then entered the cells via endocytosis where Gd-DTPA was released. Finally liposomes and the released Gd-DTPA were pumped out by the cancer cells and were then accumulated in the necrotic area due to the lack of washout mechanism indicated by the significant increase in signal intensity in 60 minutes after injection [256]. Moreover MRI based on chemical exchange

saturation transfer (CEST) has a high potential to provide better imaging [179,253,257]. MRI contrast agents for this technology can be obtained by loading low molecular weight T_1 MRI contrast agents into non-spherical liposomes to form LipoCEST agents.

Nanosize silica has been explored for loading low molecular weight T_1 MRI contrast agents. Gd-DTPA was conjugated to PEG functionalized mesoporous silica nanospheres (MSN) with anisamide as a targeting ligand via cleavable disulfide linkage, and provided an r_1 value up to 25.7 $mM^{-1}s^{-1}$ [258]. Such nanospheres could be taken up by AsPC-1 pancreatic cancer cells, and the *in vivo* results indicated that Gd-DTPA was cut from MSN in 15 minutes after injection, reflected by a strong imaging enhancement of the bladder, due to rapid reduction of the disulfide linkage by plasma thiols [258]. The biocompatibility of silica nanoparticles was investigated using Gd_2O_3 doped mesoporous silica nanocomposite, which indicated that silica particles showed a low toxicity in cell lines and no potential immunotoxicity [259]. Silica nanoparticles coated with $Gd_2(CO_3)_3$ were also prepared and exhibited a low r_1 value of 1.6 $mM^{-1}s^{-1}$ [260].

Low molecular weight T_1 MRI contrast agents were also conjugated with other types of nanomateirals. Conjugation with viral capsids could significantly improve r_1 values [261]. Anchoring low molecular weight T_1 MRI contrast agent onto Au nanoparticles could improve r_1 value by several times [262,263]. Furthermore, these Gd conjugated Au nanoparticles help to achieve desirable and detectable contrast enhancement at only μM Gd(III) incubation concentration indicating favorable cellular uptake of the nanoparticles [263]. With the use of Au nanoparticles, the fluorescence tagged

Gd conjugated Au nanoparticles can achieve multimodal cell imaging (CT, MRI and fluorescence) which is not possible with polymer based MRI contrast agents developed earlier on by the same group [264]. When Gd was loaded into fullerenes, gadofullerene formed with either PEG shells or succinic acid shells provided r_1 50 to 60 times higher than Gd-DTPA, and the gadofullerene was tested for imaging of brain tumor in rat models [265,266].

2.3. Biodegradable polymers

It is preferred to use biodegradable polymers for preparation of delivery systems, which are biocompatible and safe [267, 268]. Any materials which are not intended to be in contact with living system for long period of time like those used in permanent joint implants should be eliminated to avoid accumulate in the body [269]. These polymers being biodegradable not only facilitate glomerular clearance of non-toxic degradation products, their degradation behaviours can also modulate the release profile of payload (if any is loaded) [270]. The degradation of polymers is realized via the reactions of the species in the biological systems with certain units of polymers. The biological species can be water which can lead to hydrolysis of units including ester, thiol which cut disulfide unit, enzymes which can cut certain units specifically. Biodegradable polymers based on the water-induced hydrolysis are the most common polymers investigated for bio-related applications, among which polyesters and polyanhydrides are the most important.

2.3.1. Poly(ester)s

2.3.1.1.Poly(lactide)s

Poly(lactide)s (PLAs) is one of the most prominent biodegradable synthetic polymers. Similar to all other poly(ester)s, the presence of ester groups in PLAs allows the polymers to readily undergo bulk hydrolysis in hydrated environment like in human tissues. There are mainly two different synthesis routes for PLAs. First, via the condensation polymerization, lactic acid monomers are polymerized under high temperature and vacuum, without or with catalyst to yield low to intermediate molecular weight PLAs [271]. On the other hand, using the ring opening polymerization of lactides which are cyclic intermediate dimer of lactic acids with catalysts, PLAs with controlled molecular weight can be yielded [271]. Besides being biodegradable, PLAs also has low cytotoxicity and immunogenicity which are favourable for biomaterials [272]. Typically, PEG which promotes membrane penetration [273-278], prevents nonspecific proteins adsorption, provides long-circulation time in blood stream [279-284] and facilitates endocytosis[285], is attached to the free carboxylic end group of PLAs to form diblock copolymer which can self-assemble to form nanocarriers. Therefore, due to these encouraging properties, PLA-*b*-PEG has been studied in the area of drug and protein delivery [286-288]. Among them, some studies have achieved controlled release through the degradation of PLAs [287,289,290].

2.3.1.2. Poly(glycolide)s

Poly(glycolide)s (PGAs) is also another poly(ester) which is a well-known biodegradable synthetic polymer. Similar to PLAs, PGAs can be synthesized

either by condensation polymerization or ring opening polymerization [291]. However, due to the formation of water during condensation polymerization which leads to lower molecular weight polymer, the ring opening polymerization is usually preferred. The ability of PGAs to biodegrade *in vitro* and *in vivo* and biocompatibility are well demonstrated in resorbable sulture, Dexon®, which is used since the 1970s [292-294]. In comparison to degradation rate of the homopolymers of PLAs and PGAs, the copolymer, poly(lactide-co-glycolide)s (PLGAs), degrades at a faster speed which is dependent on the composition ratio. 75% PLA : 25% PGA and 75% PGA : 25% PLA have similar *in vivo* degradation half-life of 0.6 months while 50% PLA : 50% PGA has 1 week *in vivo* degradation half-life [295]. The increase in degradation rate of PLGA is due to the decrease in crystallinity, amorphous regions of the polymers are more susceptible to hydrolysis of the ester bonds [296]. Therefore with well-controlled and documented degradation rate and profile, PLGAs are used in a wide range of biomedical applications like controlled release and imaging [245,297-300].

2.3.1.3. Poly(Ɛ-caprolactone)s

PCLs, another synthetic biodegradable poly(ester)s, is also extensively studied and investigated. Likewise, the synthesis of PCLs is generally via the ring-opening polymerization and among the different reaction mechanisms (divided by initiator), coordination-insertion ring-opening polymerization is preferred since well-defined PCLs may be yielded by living polymerization [301,302]. Although PCLs degrade much slowly than PLAs, PGAs or PLGAs, like all other poly(ester)s, PCLs tend to undergo bulk hydrolysis unless the size of the

polymer is larger than 10^{-1} m [303]. According to a model drawn to predict the mode of degradation; surface or bulk, if the degradation of the polymer is more rapid than the diffuse of water into the polymer bulk, the polymer is likely to undergo surface degradation. On the other hand, if the diffusion is faster than degradation, the polymer is expected to go through bulk degradation [303]. PCLs, PLAs, PGAs and PLGAs all also exhibit a characteristic autocatalytic degradation. The trapped carboxyl groups produced after the hydrolysis of ester bonds further catalyse the remaining ester bonds, resulting in the acceleration of internal degradation compared to the surface [304,305]. Likewise, when PCLs are PEGylated, the polymers demonstrated minimal *in vitro* and *in vivo* cytotoxicity [306,307] and are reported in vast range of biomedical applications [308-311]. Similarly, some of these studies have indicated the degradation of PCLs has affected the release behaviours [287,312,313].

2.3.2. Polyanhydrides

If poly(ester)s are classical examples of bulk degradation polymer, then the representative polymer for surface degradation is polyanhydrides which can be synthesized by a whole range of techniques, melt condensation, ring-opening polymerization, interfacial condensation, dehydrochlorination and dehydrative coupling agents [314]. Due to its hydrophobicity which restricts the penetration of water into the bulk, hydrolysis of highly water labile anhydride bonds only happens on the surface. Moreover, by altering the type of monomer and their ratio, the rate of degradation can be controlled [270,315]. Polyanhydrides have also shown good *in vitro* and *in vivo* tissue compatibility

[316-318]. Unlike bulk degrading polymers, polyanhydrides are able to release their payload at a constant rate which is directly proportional to their degradation rate, as a result, polyanhydrides have gained lots of interest in the area of controlled delivery [319-322]. One of such polyanhydrides worth mentioning is the P(CPP-SA) which the FDA has approved for brain cancer treatment. The degradation studies done on this polyanhydrides clearly indicates the ability to alter degradation rate of the polymer by varying the hydrophobicity [323]. Furthermore, their results also shows that the degradation profile of P(CPP-SA) matched the drug release profile and controlled release was achieved [323].

2.4. Poly(amido amine)s

For different bio-related applications, the requirements are different so various types of polymers are also explored. Poly(amido amine)s is a category of polymers promising for different applications including drug delivery, gene delivery, protein delivery, MRI imaging and fluorescent imaging.

2.4.1. Poly(amido amine) dendrimers

Poly(amido amine)s, a versatile class of synthetic polymers, are extensively studied for use as biomaterials and polymer therapeutics and a well-known form of these polymers is the poly(amido amine) (PAMAM) dendrimers which are also commercially known as the first family of the Starburst® dendrimers. These PAMAM dendrimers consist of concentric amidoamine shells around a central initiator core such as ammonia and ethylenediamine [324,325] and are synthesized via either the divergent or convergent methods

[326]. The resulting poly(amido amine)s with dendritic architecture have very well-defined three-dimensional structures, very low polydispersity and high functionality [326].

With numerous intramolecular voids within each PAMAM dendrimer to aid in the solubilization of small organic molecules and affect their release rates [327,328], PAMAM dendrimers are thus promising drug carriers. However, concerns on the cytotoxicity and haemolytic issues of PAMAM dendrimers are widespread [326,329,330]. The *in vitro* cytotoxicity of PAMAM dendrimers is dose and generation dependent and high generation PAMAM dendrimers are highly capable of damaging and creating leakage in cell membranes [331-333]. Furthermore, 4th generation PAMAM dendrimers have shown to exhibit significant haemolytic toxicity [334,335]. Fortunately, although PAMAM dendrimers can induce intracellular reactive oxygen species generation and cytokine production which may lead to cell death in macrophages [336], they are concluded to have weak immunogenicity [329,331]. There are limited reports on the *in vivo* toxicity of PAMAM dendrimers and for those which did observed that PAMAM dendrimers are rapidly cleared from circulation [337] and the results are unlikely to deter future development of PAMAM dendrimers in biomedical applications [331]. Since the cytotoxicity is strongly influenced by the cationic surface amino groups of PAMAM dendrimers [336,337], surface modification may be the key in abating the cytotoxicity. Many reports have demonstrated surface modification like PEGylation [335,338], acetylation [339,340], with anionic groups [337,338,341], etc. can considerably reduce the cytotoxicity of PAMAM dendrimers. With the safety issues tentatively resolved, the

development of PAMAM dendrimers in the area of biomedical applications like gene delivery [340,342-344], drug delivery [345-348], MRI contrast agents [349-351], etc can flourish.

2.4.2. Linear poly(amido amine)s

Unlike the PAMAM dendrimer, the linear poly(amido amine)s (PAAs) especially the amphoteric ones have raised lesser concern on cytotoxic [352]. The synthesis of these linear PAAs via Michael addition specifically aza-Michael addition is usually the stepwise polyaddition of primary or secondary aliphatic amines to an activated bisacrylamide [352-354]. Typically, a Michael addition reaction is performed in protic solvent to expedite proton transfer [352,355] and catalysed by a base. However in aza-Michael addition reaction, the amine monomer itself functions as the catalyst and its basicity affects the rate of reaction [353,82]. To facilitate further functionalization of the resulting linear PAAs, functional groups which do not participate in the polymerization like hydroxyl, ether, etc but not groups which can react with activated double bonds like SH and NH_2, can be introduced by using properly functionalized monomers [352]. Linear PAAs which contain amide group can undergo hydrolytic degradation in aqueous buffer solution [356,357] and the degradation rate is affected by pH but not in the presence of lysosomal enzymes [358]. Furthermore, the introduction of disulfide bonds which can be reduced by intracellular thiols and enzymes along the PAAs background can hasten the rate of degradation [359]. Similarly, linear PAAs are also explored in tissue engineering [360], gene [361-363] and controlled drug delivery [364,365].

2.4.3. Poly(amido amine)s derived with trifunctional amines

Linear PAAs are usually yielded using bifunctional amine monomers with the third functional amine (if present) protected from the reaction. However, a handful of publications on Michael addition polymerization with trifunctional amines have surfaced in the recent decade. In 2003, Liu.et al first reported the use of trifunctional amines, 1-(2-aminoethyl)piperazine, and equimolar diacrylate to synthesize linear poly(amino ester) via Michael addition polymerization. Their result clearly showed that the yielded polymers are linear and potential biodegradable DNA carriers [83]. Subsequently, the same group examined the polymerization mechanism in detail and confirmed the reactivity sequence of the three types of amines in the trifunctional amines as such: 2^o amine (original) > 1^o amine >> 2^o amine (formed) in poly(amino ester)s [82], PAAs [366] and poly(sulfone amine)s [367]. Furthermore, using similar monomers and polymerization techniques, several PAAs based polymers are studied in the area of controlled gene and drug delivery [77,368,369].

Due to ease of synthesis, hyperbranched polymers which have comparable three-dimensional structure as dendrimer are gaining popularity. A comprehensive study on the polymerization mechanism with trifunctional amines to form hyperbranched polymer was first reported by Wu. et al [370]. They observed *in situ* that during the one-pot Michael addition polymerization of trifunctional amines and double molar diacrylates, hyperbranched poly(amino ester)s were formed from the B''A_2-type intermediates which were in turn from the B'B''A-type intermediate. Although the resulting hyperbranched polymers compared to dendrimers are more polydispersed,

they contain negligible linear portion which is akin to the well-defined structure of dendrimers. Almost immediately, Wang et al. also reported similar results with hyperbranched PAMAM derived from trifunctional amines in a one-pot Michael addition polymerization [371]. Ever since, a few hyperbranched PAMAM based polymers were explored in controlled gene and drug delivery [372-376]. Interestingly, as amino-containing polymers fluoresce [377], several hyperbranched PAMAMs are also investigated for fluorescent imaging [376,378-381].

Chapter 3

Characterization Instruments and Assay

3.1. Nuclear magnetic resonance spectroscopy

Nuclear magnetic resonance (NMR) spectroscopy is a technique which uses the NMR phenomenon to study physical, chemical and biological properties of materials. When atom with non-zero nuclear spin is placed in an external static magnetic field, spin polarization which is the alignment of the nuclear spin with the external magnetic field occurs. Then, subsequent irradiation with radio frequency signal of proper frequency on the atom can induce a transition or flip between spin states. Once the radio frequency signal is removed, the relaxation of the spin to lower state generates a detectable amount of radio frequency signal which is related to the spin flip [382].

Very often, to determine the chemical structure of organic molecules using NMR spectroscopy, the analysis of NMR spectrum (usually ^{1}H or ^{13}C) which is a plot of the absorption of radio frequency energy against the external field is necessary. The shift in frequency or chemical shift in the NMR spectrum is characteristic to atom or molecules in their given environment and the area under the signal in the NMR spectrum is proportional to the number of nucleus in the atom group. Using this information, the chemical structure of the organic molecules measured can be determined.

In our work, ^{1}H NMR and ^{13}C NMR spectra were obtained using a Bruker DPX 400 MHz NMR spectrometer. The polymers were dissolved in suitable deuterated solvent in a concentration of ~5 % for ^{1}H NMR or 20-25 % for ^{13}C NMR in specific sample tube.

3.2. Gel permeation chromatography

Gel permeation chromatography (GPC) is a chromatographic technique which characterizes the molecular weight distribution of polymers. The separation of the polymers is based on the size of the polymers in solution and not molecular weight, therefore for accurate measurement, suitable solvent is essential. The general concept of GPC is macromolecular polymers have lower tendency to penetrate the well-controlled pores of cross-linked gel bead and thus are wash away with the elute more rapidly. On the other hand, smaller polymers can enter these pores more easily and be retained for a longer period of time before eluting. To determine the molecular weight distribution of the sample polymer, usually polystyrene or polyethylene oxide with narrow molecular weight distribution is used as standards [383].

The distribution coefficient (K) in GPC is defined as

$$K = V_{si}/V_s \qquad \text{(E3.1)}$$

where V_{si} is the pore volume of the bead accessible to permeation by the *i*th polymer with a specific molecular size and V_s is the volume of the stationary phase.

The GPC chromatograph is a plot of detector signal against retention volume. In this graph, the peak height of the signal is proportional to the value of N_iM_i, where N_i is the number of molecules of the *i*th kind with molecular weight M_i. With calibration, these values can be easily obtained to calculate M_n, M_w and the polydispersity, M_w/M_n.

$$M_n=\sum N_iM_i / \sum N_i \qquad \text{(E3.2)}$$

$$M_w=\sum N_iM_i^2 / \sum N_iM_i \qquad \text{(E3.3)}$$

In this report, the Waters 2690 apparatus with two columns in series (Waters Ultrahydrogel 250 and 200) and a Waters 410 refractive index detector were used anda mixture of 0.5 M acetic acid/0.5 M sodium acetate was used as eluent. The polymer concentration is ~ 5 mg/mL.

3.3. Dynamic and static light scattering

Dynamic light scattering (DLS), also known as photon correlation spectroscopy, is a popular technique to determine the size of particles in the sub-micron range. By shining laser onto a solution of particles, the changes in the scattered light such as frequency, angular distribution, polarization and intensity fluctuation by the particles are related the diffusion coefficient and size of the particles. This technique is also based 2 assumptions which the particles are in Brownian motion and the particles are assumed to be spherical. Most of the commercial "particle sizing" systems can only operate at one angle (90^o), use red light (675 nm) and are usually no dependent on the sample concentration [384].

On the other hand, static light scattering (SLS) is a technique to measure the intensity of scattered light to obtain molecular weight of macromolecules. By measuring the intensity of scattered light at various angles in different sample concentrations and plot the data in a Zimm plot, the radius of gyration, second virial coefficient and molecular weight can be obtained.

In my study, the Brookhaven BIS200 laser light scattering system was used for both the DLS and SLS measurements. The sample solutions are typically filtered before measurement to yield reliable readings. For DLS, the

scattering angle was fixed at 90^{o} for the measurement of hydrodynamic radius (*R*h) and the *R*h values were obtained using CONTIN and NNLS algorithm. As for SLS, the measurements were done at various scattering angles with different sample concentrations.

3.4. Transmission electron microscopy

Transmission electron microscopy (TEM) is an advanced microscopy technique which utilizes the same basic principle of optical microscopy. In TEM, instead of light, powerful electron beam is used to irradiate the sample to obtain images of resolution thousand times higher than normal optical microscope. Using electromagnetic lenses to focus the electrons into very fine beam, the TEM images are obtained from electrons which transmit through the sample unscattered and hit onto a fluorescent screen [385].

The TEM used in this report is the high resolution Philips CM300 transmission electron microscope (FEGTEM) at 300 kV, and the samples were prepared by dropping micelles suspension onto a copper grid cover with carbon followed by drying in a desiccator. Then, the dried grid was left in 1% osmium oxide in heptane for 2 hours.

3.5. Fluorescence spectroscopy

Fluorescence spectroscopy is a technique which detects the fluorescence emitted by excited samples. At room temperature, most molecules are at the lowest vibrational level of the ground electronic states and upon absorption of light, the electrons are excited to higher vibrational sub-level which corresponds to the wavelength of the incident light. Then, the excited electrons

rapidly fall back to the original ground states and emit a lower energy radiation which is collected by the machine [386]. Very often, the use of fluorescence spectroscopy is accompanied by the application of the Beer-Lambert Law which states that absorption is directly proportional to the concentration of the sample.

In our work, the fluorescence emission spectra were recorded on a Perkin–Elmer LS55 Fluorescence Spectroscopy instrument fitted with a R928-sensitive sample photomultiplier.

3.6. MTT assay

MTT (3-(4,5-dimethythiazol-2-yl)-2,5-diphenyl tetrazolium bromide) assay is a colorimetric assay for assessing cell viability. First described in 1983 by T. Mosmann [387], the MTT cytotoxicity assay is based on the mitochondrial activity of viable cells to convert yellow MTT to dark blue formazan by mitochondrial dehydrogenases and therefore, the amount of formazan generated is directly proportional to viable cell number. Then, the formazan which is solubilized in organic solvent and released from the cells can be spectrophotometrically measured to determine its quantity.

The detailed MTT assay protocol used in this report is presented as following. The cells were seeded in 96-well plates with a typical seeding density of 10,000 cells/well and were cultured in DMEM supplemented with 10% FBS and 1% penicillin-streptomycin solution in an incubator at 37 ^{o}C, 5% CO_2, and 95% relative humidity. The cells were allowed to adhere to the well bottom upon overnight incubation. Then the medium was replaced with the sample solutions of different concentrations. Meanwhile, wells containing

only cell culture medium were prepared as untreated controls. After predetermined time, the medium containing samples was aspirated and the wells were washed with 1 ×PBS solution for two times to removed non-internalized sample. Then 100 μL of DMEM and 10 μL of MTT solution (5 mg/mL in 1 ×PBS solution) were added to the wells. After incubation for 4 h at 37 ^{o}C, the solution was removed and the formazan precipitate was dissolved in 100 μL of DMSO. The absorbance intensity of the solution was then quantified spectrophotometrically using a microplate reader (TECAN SpectraFluor Plus) at 570 nm. Cell viability was expressed by the following equation:

Cell viability (%) = Abssample / Abscontroll × 100%

where Abssample was the absorbance for cells treated with samples, while Abscontroll was the absorbance for untreated control cells. All the tests were performed in multiples.

3.7. Confocal laser scanning microscopy

Confocal laser scanning microscopy (CLSM) is form of optical microscopy which can obtain high resolution images with depth selectivity [388]. With shallow depth of field, the CLSM image obtained has high z-resolution and reduced out-of-focus blur, thus making the image clearer. However, as the image is acquired point-by-point and reconstructed by computer, the imaging process is more time-consuming.

In my study, confocal imaging of either living or fixed cells was done with Olympus Fluoview FV1000 with excitation wavelength of 405 nm.

3.8. Flow cytometry

Flow cytometry is a laser-based technique which can be used for cell counting, cell sorting and biomarker detection. Basically in this machine, the cell suspension is forced into a narrow column through the flow chamber by the sheath fluid, thus allowing the cells to pass through the laser focal point singly. In the case of biomarker detection, the emitted fluorescence is collected and amplified by the photodiode detector and then processed into useful readings like the fluorescence intensity of the biomarker in each individual cell [389].

The flow cytometer used here is the BD LSR Fortessa Flow Cytometry Analyser. The cell suspensions were passed through 80 μm filter before they were analysed.

Chapter 4

pH- and Redox-Responsive Poly(ethylene glycol) and Cholesterol-Conjugated Poly(amido amine)s Based Micelles for Controlled Drug Delivery

4.1. Introduction

Nanomedicine technology can overcome some limitations of cancer chemotherapy such as a short half-life and a low specificity [5,41]. Several products including Taxol®, Doxil® and Abraxane® are already in clinical applications [390,391]. In order to further reduce the side effects and improve the efficacy of anti-cancer drugs, stimuli-responsive nanocarriers are being pursued which can ensure secure drug encapsulation before reaching cancer sites and be triggered to release the drugs after entering the cells [142,392-394]. The release of drugs from these stimuli-responsive nanocarriers can be realized using external triggers such as thermal treatment; however, it is preferred to explore the intrinsic conditions in malignant tumor as internal triggers [144,395].

Among the internal triggers, pH- and redox-stimuli are generating more and more interest. As malignant tumor generates most of its energy through glycolysis instead of the normal oxidative phosphorylation, the Warburg effect results in a lower pH environment [396]. pH-responsive drug carriers can be realized either via the hydrolysis of pH sensitive bonds [113,114,397-399], or the swelling and dissociation of protonatable groups [97,106,400-402]. Meanwhile the concentration of GSH, which acts as

antioxidant in the body and plays many roles in cell metabolisms, is significantly higher in the intracellular compartments (2-10 mM) than in the extracellular matrix (2-20 μM) [403]. Moreover, it was also reported that malignant tumor contains an elevated level of GSH than normal healthy tissues, with a few studies reporting as much as a 10 times difference [42,47,48,404]. Therefore, redox-responsive drug delivery systems can encapsulate cancer drugs securely and release drugs once within the cells. Redox-responsive drug carriers have been developed by integrating disulfide groups in various ways such as into backbones of polymers [364,405], as linkages between polymer blocks or hydrophilic/hydrophobic segments [67,69,74,,364,406,407] or gates of silica based carriers [408], and forming cross-linker [53,55,59,61,409-413].

Poly(amido amine)s, a versatile class of polymers, are promising biomaterials due to the low hemolytic activity and peptide-mimicking properties and have been explored for preparation of drug and gene delivery systems [64,359,364,405,414-417]. One type of poly(amido amine)s for pH- and redox-responsive drug delivery was prepared by Michael Addition polymerization of disulfide containing diacrylamide with two primary amines with different functional groups [364].

Our previous works have demonstrated that the Michael Addition polymerization of trifunctional amines with an equimolar diacrylic monomer can produce linear poly(amino ester)s and poly(amido amine)s containing secondary amines in the backbone [83,370,418], and the secondary amines in the polymer backbone can be further conjugated with functional species [145,366,]. Here we report one novel type of pH- and redox-responsive

amphiphilic poly(amido amine)s based drug delivery systems as shown in Scheme 4.1. First linear disulfide- and secondary amine-containing poly(amido amine)s, poly(BAC-AMPD), was obtained via Michael Addition polymerization of trifunctional amine, AMPD, with an equimolar diacrylamide, BAC, under an optimized condition. Then the secondary amines in the backbone of poly(BAC-AMPD) were further conjugated with PEG and cholesterol (CE), respectively, to form poly(BAC-AMPD)-*g*-PEG-*g*-CE. Micelles were formed via self-assembly of poly(BAC-AMPD)-*g*-PEG-*g*-CE in aqueous solution. Anti-cancer drug, DOX, could be loaded into the micelles. The DOX loaded micelles showed pH- and redox-responsive release of DOX and redox-induced formation of aggregates. The DOX loaded micelles could deliver drugs into the cancer cells and showed a higher efficacy in killing cancer cells than free drug.

Scheme 4.1. Synthesis of poly(BAC-AMPD)-*g*-PEG-*g*-CE.

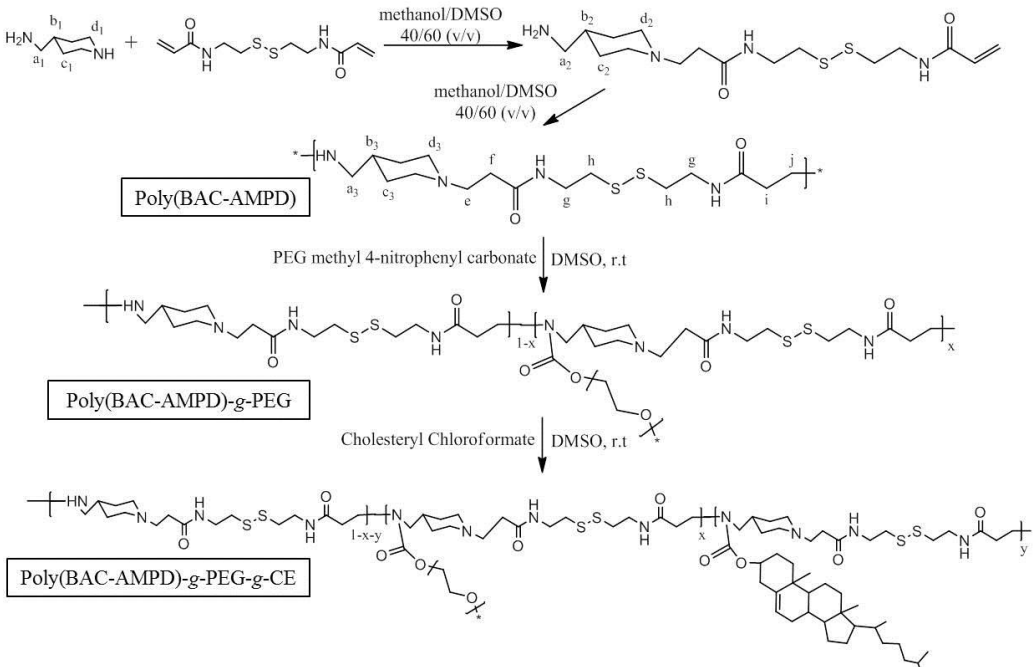

4.2. Experimental section

4.2.1. Materials

N,*N*-cystaminebis(acrylamide) (BAC) from Polysciences, 4-(aminomethyl)piperidine (AMPD) from Alfa Aesar, cholesteryl chloroformate and doxorubicin hydrochloride (DOX-HCl) from Fluka Analytical, and L-dithiothreitol (DTT) from Sigma Aldrich were used as received. Monomethyl poly(ethylene glycol) (PEG) (~2000 g/mol) 4-nitrophenyl carbonate was prepared as in our previous report [419]. Methanol, dimethylsulfoxide (DMSO), and other solvents used in this study were purchased from Tedia and used as received.

MCF-7 (human breast adenocarcinoma) cells and HepG2 (human hepatoma) cells were obtained from American Type Culture Collection (ATCC, Rockville, MD). They were maintained in Dulbecco's modified eagle medium (DMEM, invitrogen) with 10% fetal bovine serum (FBS), 2 mM glutamine, 100 units/ml penicillin and 100 µg/ml streptomycin at 37 °C in an incubator with 5% CO_2 atmosphere.

4.2.2. Synthesis of poly(BAC-AMPD)

In a typical experiment, 6.96 g (26.7 mmol) of BAC was added into 3.10 g (26.8 mmol) of AMPD in a mixture of 16 ml of anhydrous methanol and 24 ml of anhydrous DMSO under stirring at 50 ^{o}C with argon. After 25 days, 1% of AMPD was added to the solution. 24 h later, some of the solution was taken for GPC measurements and the rest was dialyzed using dialysis membrane with a molecular weight cutting-off of 3500 in methanol. Also the polymerization was monitored *in situ* using NMR by performing the

polymerization in NMR tube using methanol-d_4 and DMSO-d_6 instead. The total monomer concentrations were kept around 20% (w/v), and ^{13}C NMR spectra were measured using a power-gated decoupling program (PD) with 200 times scan taking ca.10 minutes.

In order to investigate the effects of solvent, a mixture of anhydrous methanol and DMSO with various contents of methanol, i.e., 90% (v/v), 70% (v/v), 40% (v/v), 20% (v/v), were adopted.

4.2.3. Synthesis of poly(BAC-AMPD)-*g*-PEG-*g*-CE

In a typical experiment, 5.31 g (2.35 mmol) of monomethyl PEG(~2000 g/mol) 4-nitrophenyl carbonate was added to 3.98 g (10.6 mmol) of poly(BAC-AMPD) in 50 mL of anhydrous DMSO. The solution was stirred for 5 days at room temperature under argon, and then was dialyzed using membrane with a molecular weight cutting-off of 3500 in methanol. In a typical experiment for conjugation of CE, 2.28 g (5.1 mmol) of cholesteryl chloroformate and 1.84 mL (13.2 mmol) of TEA were added into 2.86 g (0.27 mmol) of poly(BAC-AMPD)-*g*-PEG in 25 mL of anhydrous DMSO under stirring at room temperature with argon. After 5 days, the solution was precipitated in diethyl ether and the solid obtained was dried under vacuum at 40^{o}C overnight.

4.2.4. Formation and characterization of micelles of poly(BAC-AMPD)-*g*-PEG-*g*-CE

40.5 mL of deionized water was added at a rate of 0.25 mL/h using a syringe pump to 45 mg of poly(BAC-AMPD)-*g*-PEG-*g*-CE in 4.5 mL of DMSO

under a rapid stirring. Then the solution was dialyzed using membrane with a molecular weight cutting-off of 1000 in deionized water to remove DMSO.

4.2.5. Degradation of micelles

10 mL of micelles solution was incubated with 2 mM of DTT at 37 ^{o}C under stirring. 5 days later, precipitate in the solution was lyophilized. ^{1}H NMR spectrum of the dried solid sample in chloroform-d was obtained.

4.2.6. Preparation of DOX loaded micelles

22.5 mL of deionized water was added at a rate of 0.25 mL/h using a syringe pump to 2.5 mL of DMSO containing 25 mg of poly(BAC-AMPD)-*g*-PEG-*g*-CE (25 mg), 5 mg of DOX-HCl and 2.5 μL of triethylamine (TEA) under rapid stirring. Then the solution was dialyzed using membrane with a molecular weight cutting-offof 1000 in deionized water to remove the DMSO and DOX. After dialysis, aggregates of unloaded DOX were removed by filtration through a filter with a pore diameter of 0.45 μm.

4.2.7. *in vitro* DOX release of DOX loaded micelles

2 mL of the DOX loaded micelle solution in dialysis membrane with a molecular weight cutting-off of 10 000 was submerged in 40 mL of phosphate buffered saline(PBS) at 37 ^{o}C with various conditions, i.e., pH 7, pH 5, pH 7 with 2 mM of DTT, pH 5 with 2 mM of DTT, respectively. At fixed intervals, 4 mL of dialysis solution (PBS) was collected and 4 mL of fresh PBS was added. The fluorescence intensity of the solutions at 590 nm was measured

with an excitation of 440 nm, and the concentration of DOX was determined based on a calibration curve.

4.2.8. DOX loading capacity

The DOX loaded micelles solution was lyophilized, and a certain amount of dried DOX loaded micelles was dissolved in DMSO. The solution was dialyzed using membrane with a molecular weight cutting-off of 2000 in DMSO. The concentration of DOX in the dialysis solution was measured as above. The loading capacity and the loading efficiency were calculated:

Loading capacity = Mass of DOX loaded / Mass of DOX loaded micelles × 100%

Loading efficiency = Mass of DOX loaded / Mass of DOX added × 100 %

4.2.9. Cellular imaging

MCF-7 and HepG2 cell lines were seeded in 8 chamber borosilicate coverglass with a cell density of 5,000 cells/chamber and were cultured in DMEM supplemented with 10% FBS and 1% penicillin-streptomycin solution in an incubator at 37^{o}C, 5% CO_2, and 95% relative humidity. The cells were allowed to adhere to the chamber bottom upon overnight incubation. Then the medium was replaced with DOX loaded micelles solution in DMEM. At a designed time interval, the medium was removed and the wells washed with 500 µL of PBS once followed by adding 250 µL of 90 % (v/v) cold ethanol to fix the cells in dark for 10 minutes. After the ethanol was aspired, the wells were washed with 500 µL of PBS, and 200 µL of 4',6-diamidino-2-phenylindole (DAPI) (10µg/mL) was added to stain the nuclei of the cells. 5

minutes later, DAPI was removed, and the wells were washed with 500 µL of PBS twice followed by adding 150 µL of PBS to prevent the cells from drying up. The cells were imaged under a confocal laser scanning microscope (CLSM) (FV1000, Olympus, Japan).

4.2.10. *in vitro* cytotoxicity evaluation of samples

Cytotoxicity of micelles of poly(BAC-AMPD)-*g*-PEG-*g*-CE, DOX-HCl, and DOX loaded micelles of poly(BAC-AMPD)-*g*-PEG-*g*-CE were evaluated in MCF-7 and HepG2 cell lines. Viability of the cells was assessed by the standard thiazolyl blue [3-(4,5-dimethyliazolyl-2)-2,5-diphenyl tetrazolium bromide] (MTT) assay. This colorimetric assay allows determination of the number of viable cells through the metabolic activity of the cells.

The cancer cells were seeded in 96-well plates with a seeding density of 10,000 cells/well and were cultured in DMEM supplemented with 10% FBS and 1% penicillin-streptomycin solution in an incubator at 37 ^{o}C, 5% CO_2, and 95% relative humidity. The cells were allowed to adhere to the well bottom upon overnight incubation. Then the medium was replaced with the sample solutions of different concentrations. Meanwhile, wells containing only cell culture medium were prepared as untreated controls. At the predetermined time, the medium containing samples was aspirated and the wells were washed with 1 ×PBS solution for two times to removed non-internalized sample. Then 100 µL of DMEM and 10 µL of MTT solution (5 mg/mL in 1 ×PBS solution) were added to the wells. After incubation for 4 h at 37 ^{o}C, the solution was removed and the formazan precipitate was dissolved in 100 µL of dimethyl sulfoxide (DMSO). The absorbance intensity of the

solution was then quantified spectrophotometrically using a microplate reader (TECAN SpectraFluor Plus) at 570 nm. Cell viability was expressed by the following equation:

Cell viability (%) = Abssample / Abscontroll × 100%

where Abssample was the absorbance for cells treated with samples, while Abscontroll was the absorbance for untreated control cells. All the tests were performed in multiples.

4.2.11. Measurements

Gel permeation chromatography (GPC) was performed on a Waters 2690 apparatus with two columns in series (Waters Ultrahydrogel 250 and 200) and a Waters 410 refractive index detector. A mixture of 0.5 M acetic acid/0.5 M sodium acetate was used as eluent, and poly(ethylene oxide) standards were used. Nuclear magnetic resonance (NMR) spectra were obtained on a Bruker DPX 400 MHz NMR spectrometer. A Brookhaven BIS200 laser light scattering system was used for dynamic light scattering (DLS) measurements. The light source is a power adjustable vertically polarized 35 mW argon ion laser with a wavelength of 633 nm. The scattering angle was fixed at 90^{o} for measuring the hydrodynamic radius (*R*h) and the average scattering intensity. *R*h values were obtained using a CONTIN analysis. TEM images were obtained using a high resolution Philips CM300 transmission electron microscope (FEGTEM) at 300 kV, and the samples were prepared by dropping micelles solution onto a copper grid cover with carbon followed by drying in a desiccator. Then, the dried grid was left in 1% osmium oxide in heptane for 2 hours.Fluorescence excitation and emission spectra were

recorded on a Perkin–Elmer LS55 Fluorescence Spectroscopy instrument fitted with a R928-sensitive sample photomultiplier. Confocal imaging was done with Olympus Fluoview FV1000 with excitation wavelength of 405 nm.

4.3. Results and discussion

4.3.1. Synthesis of linear poly(BAC-AMPD)

Disulfide- and 2^o amine- containing linear poly(BAC-AMPD) was prepared via Michael Addition polymerization of AMPD with an equimolar BAC in methanol. According to the previous reports [83,368,369,418], linear poly(BAC-AMPD) should be produced due to the reactivity sequence of the three type of amines in AMPD, i.e., 2^o amine (original) > 1^o amine >> 2^o amine (formed), with the 2^o amine (formed) being kept intact when trifunctional amine was polymerized with an equimolar diacryl monomer. However, poly(BAC-AMPD) synthesized in methanol was found containing branching units as indicated by the appearance of peak at ca. 50.2 ppm in the ^{13}C NMR spectrum as shown in Figure 4.1a, and the degree of branching was determined to be ca. ~20% via equation E4.1.

$$\text{Degree of branching} = I_{50.2} / I_{46.5} \times 100\% \qquad \text{(E4.1)}$$

Where $I_{50.2}$ and $I_{46.5}$ are the integral intensity of the peaks at 50.2 ppm and 46.6 ppm, respectively.

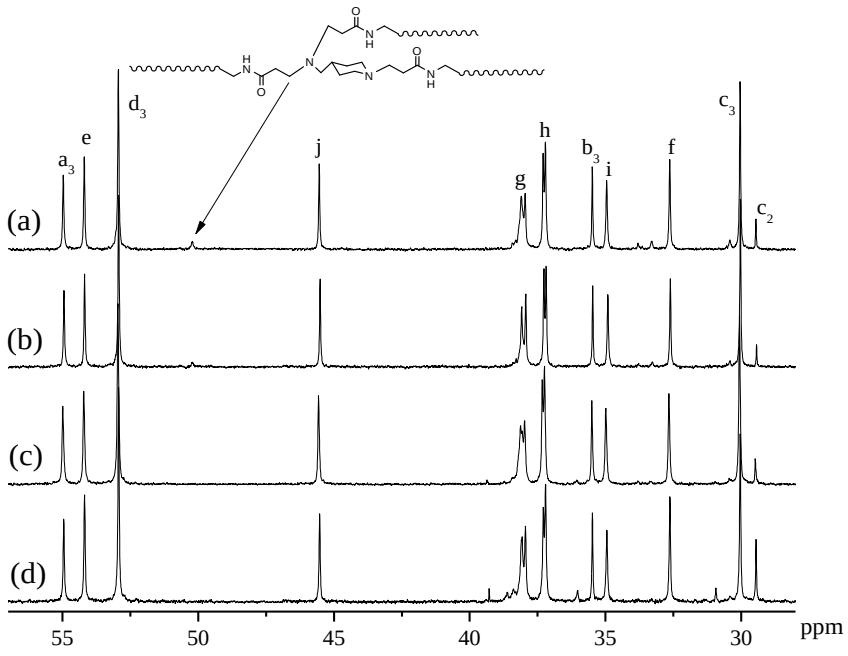

Figure 4.1. ^{13}C NMR spectra of poly(BAC-AMPD) synthesized and measured in a) methanol-d_4; b) mixture of methanol-d_4/DMSO-d_6 (70/30); c) mixture of methanol-d_4/DMSO-d_6 (40/60); d)DMSO-d_6. The peaks attribution is listed in Scheme 4.1.

Considering that the branched structure might affect the self-assembly behaviour of poly(BAC-AMPD)-*g*-PEG-*g*-CE and lead to loss and instable aggregates with a poor and insecure drug encapsulation, linear poly(BAC-AMPD) was pursued [420,421]. The formation of branching unit was due to the narrow reactivity difference among the three types of amines in AMPD, i.e., 2^o amine (original), 1^o amine and 2^o amine (formed), in methanol which led to the participation of 2^o amine (formed) in the reaction. So the reactivity of 2^o amine (formed) in AMPD should be reduced in order to produce linear poly(BAC-AMPD). Here the Michael Addition reaction is a base-catalyzed nucleophilic addition of amine to α,β-unsaturated carbonyl [353]. The amine also functions as the base catalyst, and its basicity determines the polymerization rate and the reactivity of its functional amine moieties

[353,418]. Many of poly(amido amine)s were prepared in methanol or methanol/water mixture [368,422,423], as protic methanol can facilitate hydrogen transfer and thus increase the reactivity of the amines. In order to reduce the reactivity of the 2^{o} amine (formed) in AMPD, aprotic DMSO was explored as the polymerization solvent [355]. No peak attributed to the branching unit can be observed in ^{13}C NMR spectrum of poly(BAC-AMPD) produced in polymerization performed in DMSO as shown in Figure 4.1d. However, the polymerization rate was so slow that the peaks attributing to the carbon double bonds in BAC in ^{1}H NMR spectrum disappeared only after 68 days. Therefore, a mixture of methanol and DMSO was used as polymerization solvent. ^{13}C NMR spectra of the polymers produced in a mixture of solvent of methanol and DMSO with different compositions are shown in Figure 4.1. Table 4.1 summarizes the effects of the solvent composition on the degree of branching in the polymer produced. The results reflect that the methanol content should be kept below 40% (v/v) to produce linear poly(BCA-AMPD). Thus a mixture of 40 % (v/v) methanol and 60% (v/v) DMSO was chosen to produce linear poly(BAC-AMPD). Figure 4.1c shows ^{13}C NMR spectrum of poly(BAC-AMPD) obtained from polymerization of AMPD with an equimolar BAC in 40% methanol (v/v) and 60% DMSO (v/v) at 50 ^{o}C for 25 days, and it is obvious that no peak attributed to the branching units can be observed. The polymerization in the mixture of methanol/DMSO (40/60 in v/v) was also monitored using ^{13}C NMR, and the results shown in Figure 4.2 indicates that the polymerization mechanism is the same as the Michael Addition polymerization forming linear poly(amino ester)s [83]. First the 2^{o} amine (original) reacts with BAC

to form the intermediate as shown in Scheme 4.1, and then the 1^{o} amine joins in the reaction to form linear poly(BAC-AMPD). The weight average molecular weight (*Mw)* and the molecular weight polydispersity index (PDI) of linear poly(BAC-AMPD) produced were determined to be 7175 g/mol and 2.20, respectively, using GPC. Linear poly(BAC-AMPD) obtained is insoluble in water but soluble in methanol and DMSO.

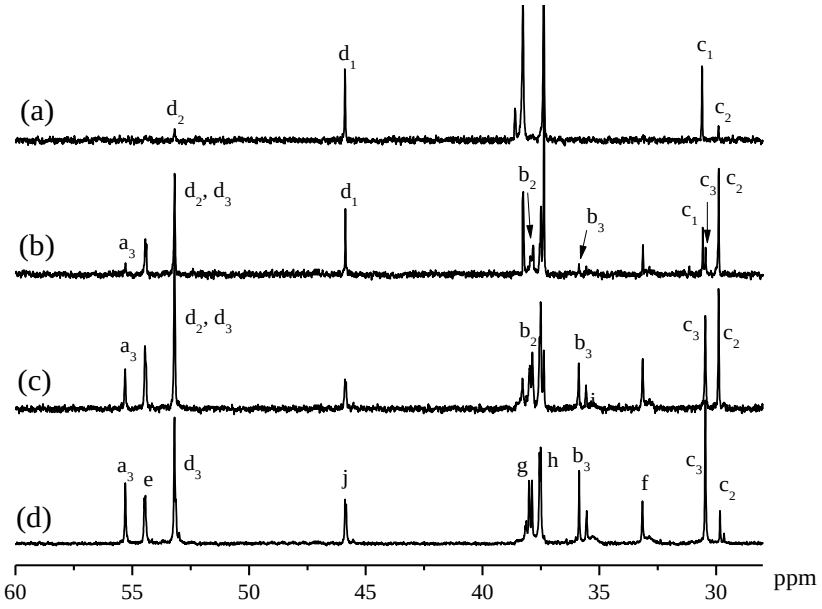

Figure 4.2. Comparison of ^{13}C NMR spectra recorded for the polymerization of AMPD with an equimolar BAC in 40% methanol-d_4 / 60% DMSO-d_6 (v/v) with a monomer concentration of 20% (w/v) at 50 ^{o}C for a) 0.75 h; b) 4.5 h; c) 24.5 h; d) 25 days. The attribution of the peaks is listed in Scheme 4.1.

Table 4.1. Structures of poly(BAC-AMPD) synthesized in a mixture of methanol and DMSO of different compositions.

Solvent Composition (v/v)		**Polymerization**	***Mw***	**PDI**	**Degree of**
Methanol	**DMSO**	**Time at 50^{o}C (day)**	**[g/mol]**		**Branching (%)**
100	**0**	4	12521	2.73	20
90	**10**	7	12516	2.77	11
70	**30**	12	11631	2.60	9
40	**60**	25	7175	2.20	Negligible
20	**80**	38	4217	1.69	Negligible
0	**100**	68	3397	1.56	Negligible

4.3.2. Synthesis of poly(BAC-AMPD)-*g*-PEG-*g*-CE

PEG was grafted onto poly(BAC-AMPD) to improve water solubility and introduce other performances such as minimizing non-specific adsorption of proteins and increasing circulation time in bloodstream [279,424]. As shown in Scheme 4.1, PEG was grafted via urethane groups formed by the reaction of 2^o amines in the backbone of poly(BAC-AMPD) with monomethyl PEG 4-nitrophenyl carbonate. In order to control the grafting degree, the feeding molar ratio of PEG to 2^o amine in poly(BAC-AMPD) was kept at 1 : 4.5. Figure 4.3b shows ^{1}H NMR spectrum of poly(BAC-AMPD)-*g*-PEG, and the peaks attributed to the protons of the carbon in PEG adjacent to the urethane groups can be observed at ca. 4.17 ppm. The molar ratio of the grafted PEG to the BAC-AMPD unit was determined to be ca. 1: 4.3 on the basis of equation E4.2:

$$\text{Molar ratio of PEG/BAC-AMPD} = I_{4.20} / I_{1.29} \qquad \text{(E4.2)}$$

Where $I_{4.20}$ and $I_{1.29}$ are the integral intensity of the peaks at 4.20 ppm and 1.29 ppm, respectively.

Poly(BAC-AMPD)-*g*-PEG obtained is soluble in water, methanol and DMSO. Then CE was also conjugated onto poly(BAC-AMPD)-*g*-PEG through urethane bonds formed via the reaction of the remaining 2^o amines in the backbone of poly(BAC-AMPD) with cholesteryl chloroformate. Figure 4.3c is ^{1}H NMR spectrum of poly(BAC-AMPD)-*g*-PEG-*g*-CE, and the grafting of CE is confirmed by the appearance of peaks attributed to CE such as the peak at ca. 4.43 ppm which is attributed to protons of the double bond in CE. The molar ratio of the grafted CE and PEG unit was determined to be 1.8 : 1 using equation E4.3:

Molar ratio of CE /PEG = $2 \times I_{4.43} / I_{4.20}$ (E4.3)

Where $I_{4.43}$ and $I_{4.20}$ are the integral intensity of the peaks at 4.43 ppm and 4.20 ppm, respectively.

Although a great excess of cholesteryl chloroformate was added in the reaction, only 1.8 of 3.3 free 2^o amines were conjugated. This is probably due to steric hindrance or the low solubility of cholesteryl chloroformate in DMSO.

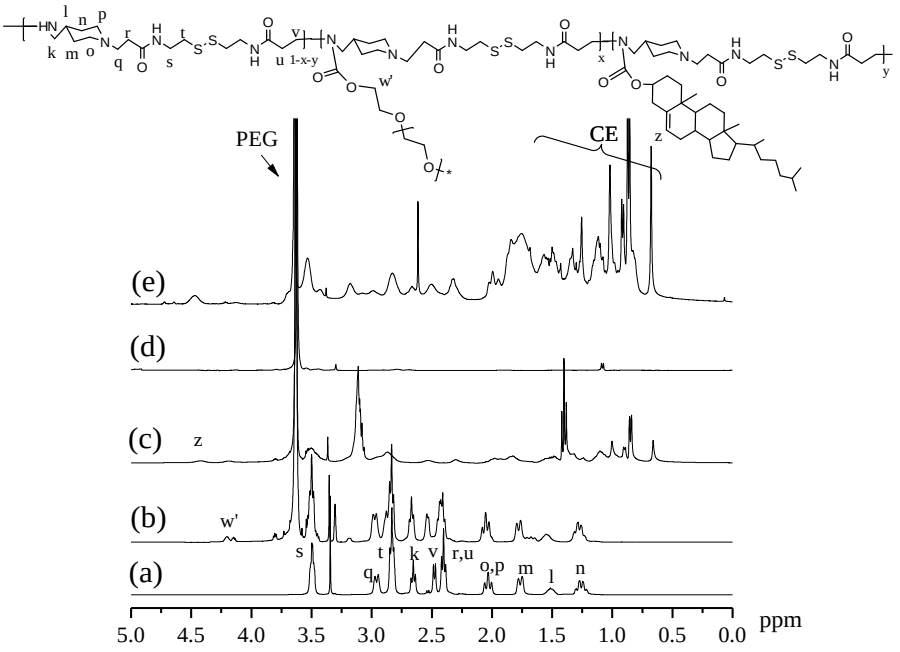

Figure 4.3. ^{1}H NMR spectra of a) poly(BAC-AMPD) in methanol-d_4; b)poly(BAC-AMPD)-*g*-PEG in methanol-d_4; c) poly(BAC-AMPD)-*g*-PEG-*g*-CE in chloroform-d; d) poly(BAC-AMPD)-*g*-PEG-*g*-CE in D_2O; e) precipitate of aqueous micelles solution of poly(BAC-AMPD)-*g*-PEG-*g*-CE after treated with 2 mM DTT for 5 days in chloroform-d.

4.3.3. Self-assembly of poly(BAC-AMPD)-*g*-PEG-*g*-CE

Micelles were formed from self-assembly of poly(BAC-AMPD)-*g*-PEG-*g*-CE in aqueous solution. Figure 4.4a presents the TEM images of the micelles of poly(BAC-AMPD)-*g*-PEG-*g*-CE, and the average diameter of the micelles is determined to be ca. 100 nm. DLS measurement illustrated that the micelles

have an average hydrodynamic diameter of 135.7 ± 13.6 nm, which is larger than the micelles in a dry state observed in TEM due to the micelles' tendency to swell in aqeuous solution.Since only the protons of polymer segments with a high solution mobility can be observed in solution ^{1}H NMR spectrum [425-427], solution ^{1}H NMR spectra were used to get more information of the micelles formed. Figure 4.3d shows the ^{1}H NMR spectrum of poly(BAC-AMPD)-*g*-PEG-*g*-CE in D_2O. Comparing with the ^{1}H NMR spectrum of poly(BAC-AMPD)-*g*-PEG-*g*-CE in chloroform-d as shown in Figure 4.3c, it is obvious that the peaks attributed to CE and poly(BAC-AMPD) almost disappear, meanwhile the peaks attributed to PEG still can be observed as shown in Figure 4.3d. These reflect that the micelles formed contain hydrophobic cores composed of CE and poly(BAC-AMPD),which are inaccessbile to water, and PEG shells soluble in water. The CMC of the micelles of poly(BAC-AMPD)-*g*-PEG-*g*-CE were determined via the relationship between the average light scattering intensity and the concentration of polymers shown in Figure 4.5 [428], and CMC of the micelles of poly(BAC-AMPD)-*g*-PEG-*g*-CE is determined to be ca. 9.8 μg/mL.

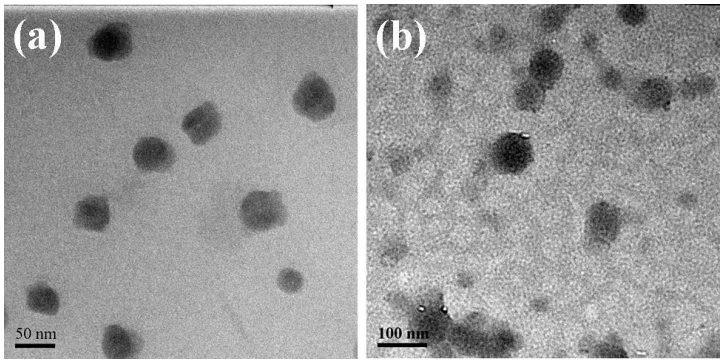

Figure 4.4. TEM images of a) micelles of poly(BAC-AMPD)-*g*-PEG-*g*-CE stained with osmium oxide; b) DOX loaded micelles stained with osmium oxide.

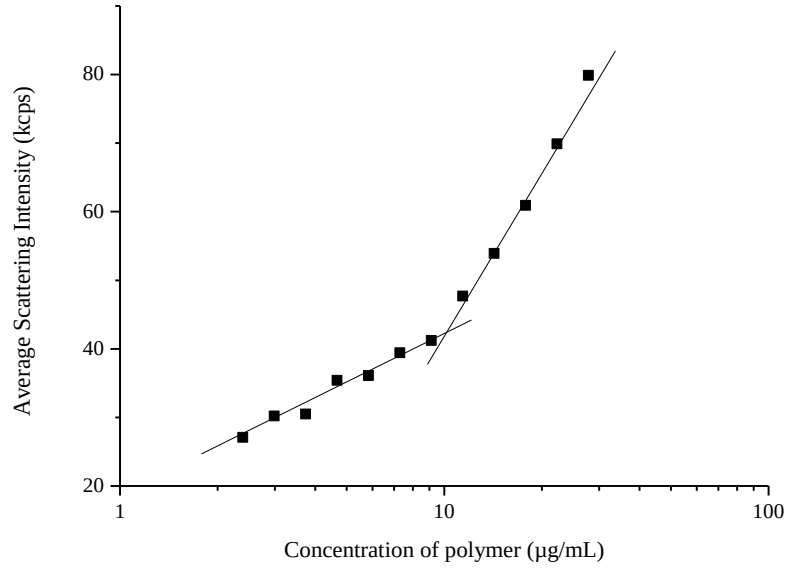

Figure 4.5. Relationship between the average scattering intensity from DLS measurements and the concentration of poly(BAC-AMPD)-*g*-PEG-*g*-CE (μg/mL) in deionized water.

Redox-induced degradation of the micelles of poly(BAC-AMPD)-*g*-PEG-*g*-CE were investigated using a model compound, DTT. After incubation with 2 mM DTT for 5 days, some precipitation was formed in the micelles solution of poly(BAC-AMPD)-*g*-PEG-*g*-CE. The precipitate was collected and lyophilized, and ^{1}H NMR spectrum of the precipitate in chloroform-d was

obtained as shown in Figure 4.3e. From Figure 4.3e, the molar ratio of CE to PEG in the precipitate could be measured using equation E4.3. It was found that the molar ratio of CE to PEG in the precipitate is 8 times higher than that of poly(BAC-AMPD)-*g*-PEG-*g*-CE. So it could be concluded that the segments containing hydrophobic CE precipitated and those containing PEG remained soluble in the solution after DTT-induced degradation. Furthermore, the formation of precipitate upon DTT-induced degradation also illustrates non-uniform degradation of the amphiphilic polymers. The polymer sections grafted to PEG which is more hydrophilic tends to degrade more rapidly than parts conjugated to CE which is more hydrophobic. As a result, after shedding the PEG shells, the hydrophobic cores aggregate to form the precipitate.

The cytotoxicity of micelles of poly(BAC-AMPD)-*g*-PEG-*g*-CE was evaluted in MCF-7 and HepG2 cell lines using the MTT assay, and the results are shown in Figure 4.6. In both MCF-7 and HepG2 cell lines, the micelles of poly(BAC-AMPD)-*g*-PEG-*g*-CE show limited cytotoxicity. Around 80% and 90% of MCF-7 cells and HepG2 cells are still viable, respectively, when polymer concentration reaches 68 μg/mL

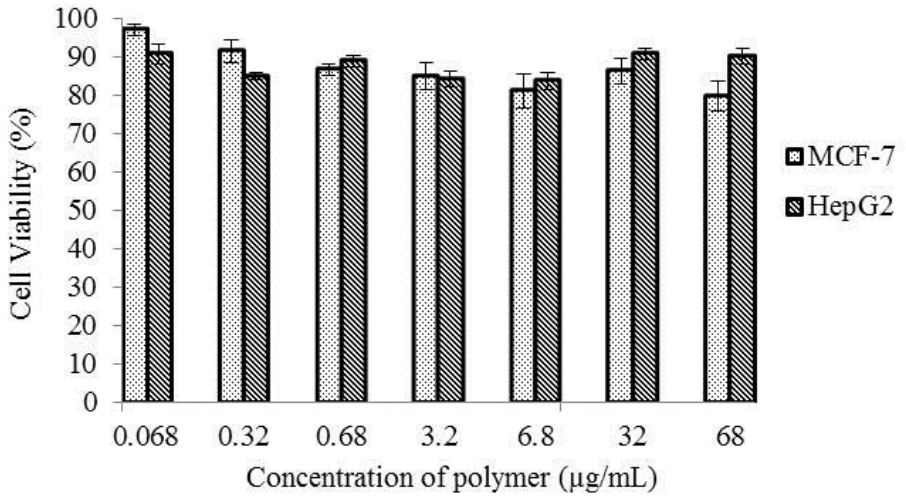

Figure 4.6. *in vitro* cytotoxicity of polymer in MCF-7 cells and HepG2 cells. All data represent mean ± SD (n = 6).

4.3.4. DOX loaded micelles

DOX loading was performed by dropwise addition of water into DMSO solution of poly(BAC-AMPD)-*g*-PEG-*g*-CE and DOX followed by dialysis. The loading capacity and efficiency of DOX loaded micelles were measured to be 5.4 ± 1.7 % and ~ 27.1 ± 8.9 %, respectively. Figure 4.4b shows TEM images of DOX loaded micelles, and the diameter was determined to be ca. 100 nm. DLS measurement showed that the diameter of the micelles in aqueous solution was ca. 131 nm. Thus the loading of DOX did not increase the micelle size significantly.

The drug release profiles of DOX loaded micelles were investigated in PBS buffer under pH 7 and pH 5 with and without DTT (2 mM) at 37 ^{o}C, respectively, and the results are presented in Figure 4.7. Figure 4.7 shows that the release profiles of DOX are similar at pH 7 and pH 5 without DTT in the first 10 h with ca. 24% and 27% of DOX being released respectively.

However, ca. 29% and 50% of DOX are released at pH 7 and pH 5 in 72 h, respectively. These might reflect that ca. 24% - 27% of DOX was loaded near the surface of the hydrophobic cores and possibly in the PEG shells of the micelles which were released in the early period regardless of pH environment. So similar release profiles are observed at pH 7 and pH 5 in first 10 h. Then the remaining DOX, which were probably encapsulated deep in the hydrophobic core, exhibited a release profile at pH 7 different from that at pH 5.At pH 7, the integrity of the hydrophobic cores were maintained well, so only 5% more of the encapsulated DOX was released from 10 h to 72 h. In comparison, at pH 5, the protonated amines in the backbone of poly(BAC-AMPD)-*g*-PEG-*g*-CE formed at pH 5 caused swelling of the cores resulting in the release of more DOX in 72 h [97]; also the protonated DOX formed at pH 5 with a high solubility in aqueous solution could also lead to release of more DOX. Figure 4.7 shows that DOX is released faster in the presence of DTT at both pH 7 and pH 5. At pH 7 and pH 5, ca. 37% and 38% of DOX are released in 10 h, and ca. 44% and 54% of DOX are released in 72 h, respectively. So DTT-induced degradation of hydrophobic cores resulted in a fast release of more DOX although the degradation resulted in obvious precipitation in aqueous solution of DOX loaded micelles as shown in Figure 4.8.

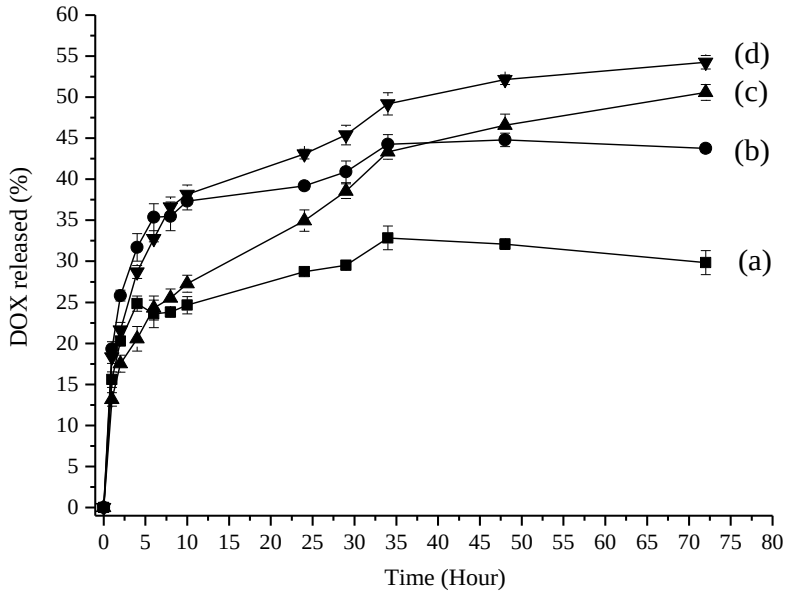

Figure 4.7. DOX release profiles of DOX loaded micelles of poly(BAC-AMPD)-*g*-PEG-*g*-CE at (a) pH 7; (b) pH 7 with 2 mM DTT; (c) pH 5; (d) pH 5 with 2 mM DTT. All data represent mean ± SD (n = 5).

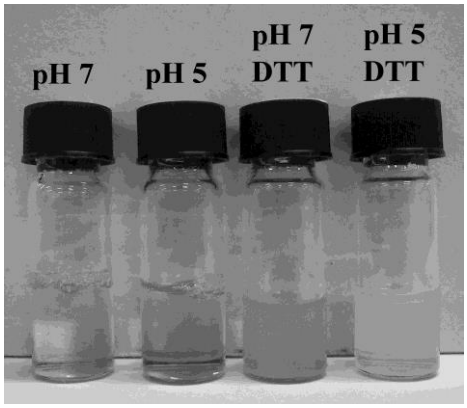

Figure 4.8. Photograph of DOX loaded micelles aqueous solution at pH 7 and pH 5 with and without DTT.

4.3.5. Cellular uptake of DOX loaded micelles and intracellular distribution of DOX

Confocal laser scanning microscopy (CLSM) was applied to investigate the cellular uptake of DOX loaded micelles and the intracellular distribution of DOX. The micelles were incubated with MCF-7 and HepG2 cell lines which contain a high level of GSH intracellularly [373]. The concentration of DOX

used was kept at 0.8 µg/mL to minimize cytotoxicity but allow sufficient uptake for visualization using confocal microscopy. Due to the low concentration of DOX applied, very weak DOX fluorescence in the cells could be observed after an incubation of 24 h. However, obvious DOX fluorescence could be observed in both MCF-7 cells and HepG2 cells after an incubation of 48 h as shown in Figure 4.9. After an incubation of 48 h, the majority of DOX is found in the cytoplasm together with some located around the nuclei of MCF-7 cells and HepG2 cells as shown in Figure 4.9. However, more DOX can be observed in the cytoplasm and around the nuclei after an incubation of 72 h. These results reflect that the DOX loaded micelles of poly(BAC-AMPD)-*g*-PEG-*g*-CE can deliver DOX into cancer cells and also probably to the nuclei of the cells.

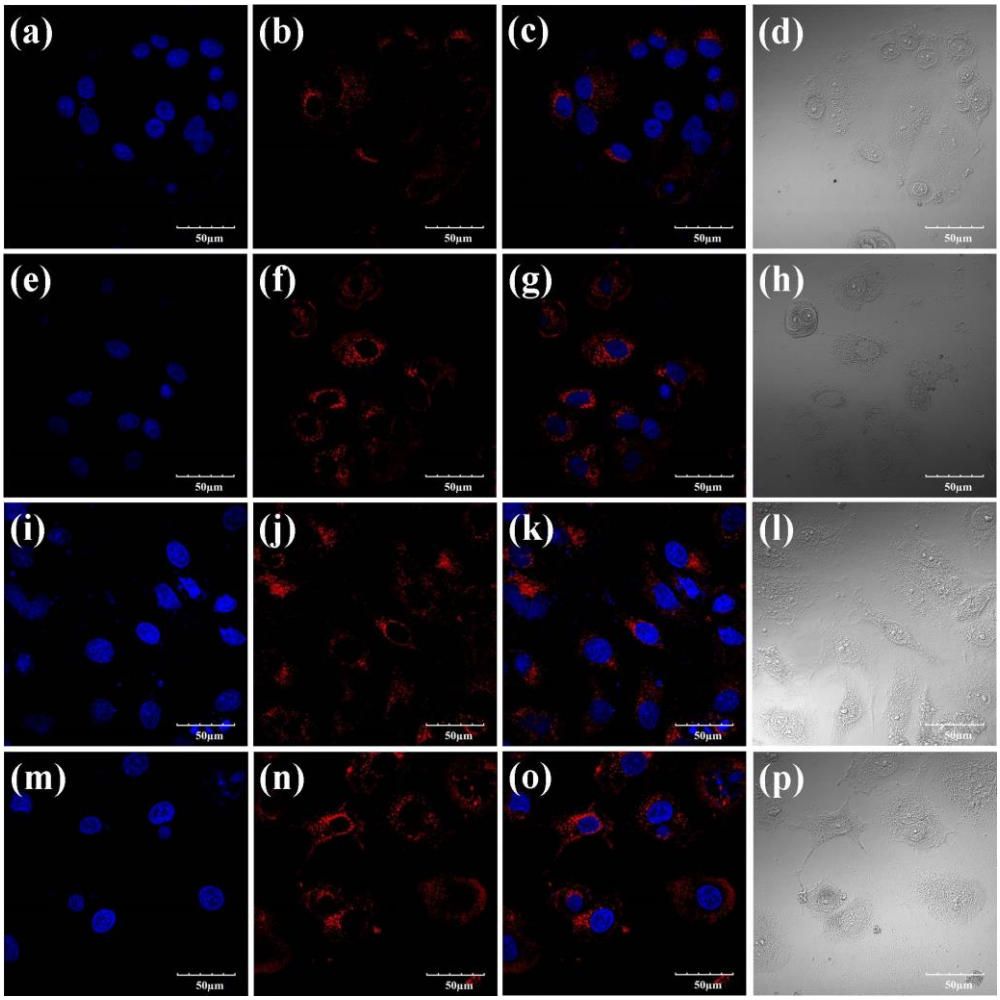

Figure 4.9. Confocal microscopy images of cells after incubation with DOX loaded micelles of poly(BAC-AMPD)-*g*-PEG-*g*-CE: 1st row and 2nd row: MCF-7 cells after an incubation of 48 h and 72 h respectively; 3rd row and 4th row: HepG2 cells after an incubation of 48 h and 72 h, respectively. For each panel, images from left to right show a,e,i,m) cells with nuclear staining with DAPI; b,f,j,n) cells with DOX fluorescence; c.g,k,o) overlays of cells with nuclear staining with DAPI and DOX fluorescence; d.h,l,p) under bright field.

4.3.6. Efficacy of DOX loaded micelles in killing cancer cells

The cytotoxicity of DOX loaded micelles of poly(BAC-AMPD)-*g*-PEG-*g*-CE was evaluated in MCF-7 and HepG2 cell lines using the MTT assay. As shown in Figure 4.10, the DOX loaded micelles display a higher efficacy in killing both MCF-7 cells and HepG2 cells than free drug after an incubation of 72 h. As listed in Table 4.2, the IC_{50} values of DOX loaded micelles are

several times lower than those of free DOX in MCF-7 cells and HepG2 cells, respectively. There are several factors which might have contributed to the higher efficacy of DOX loaded micelles of poly(BAC-AMPD)-*g*-PEG-*g*-CE. The DOX loaded micelles can enter the cells via endocytosis as other drug loaded delivery systems [429], which can avoid the efflux of drug out of cancerous cells by P-glycoprotein [430].Furthermore, the high intracellular GSH concentration can result in the formation of aggregates of the DOX loaded micelle cores, which remain in the cells favourably and at the same time continue to release more DOX into the cytoplasm [431]. Hence more DOX can get into the nuclei of cancer cells to stop DNA replication, inhibit macromolecular synthesis, and ultimately kill the cancer cells [432].

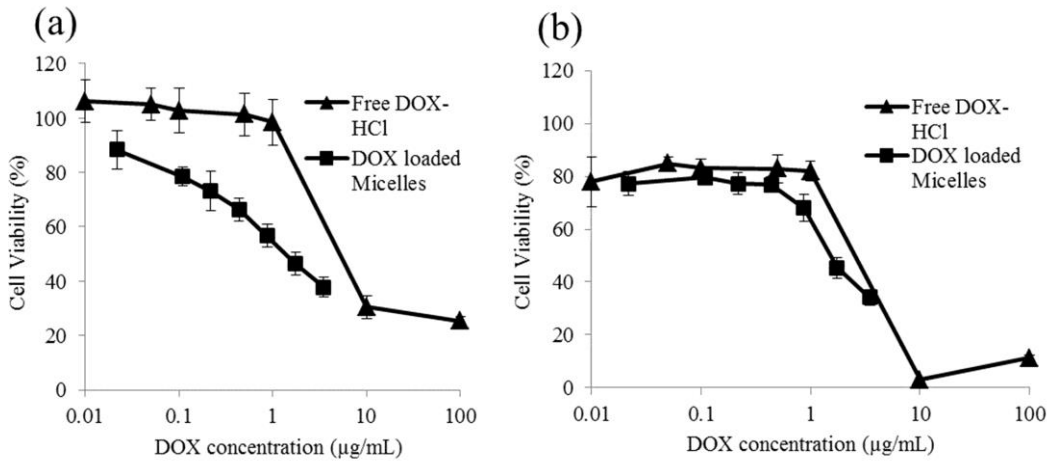

Figure 4.10. *in vitro* cytotoxicity of DOX loaded micelles and free DOX in a) MCF-7 cells; b) HepG2 cells. All data represent mean ± SD (n = 12).

Table 4.2. IC_{50} of DOX loaded micelles in MCF-7 cells and HepG2 cells.

IC_{50} (μg/mL)	**MCF-7**	**HepG2**
DOX loaded micelles	1.44	1.57
Free DOX-HCl	7.42	4.64

4.4. Conclusions

Linear poly(BAC-AMPD) was produced by applying a mixture of 40% methanol and 60% DMSO (v/v) as a solvent for Michael Addition polymerization of trifunctional amine, AMPD, with an equimolar diacrylamide, BAC. Amphiphilic poly(BAC-AMPD)-*g*-PEG-*g*-CE was obtained by conjugating PEG and cholesterol onto the linear poly(BAC-AMPD) through reactions with the 2^{o} amine groups. Self-assembly of poly(BAC-AMPD)-*g*-PEG-*g*-CE in aqueous solution formed micelles with PEG shells and cores composed of poly(BAC-AMPD) and CE. DOX could be loaded into the micelles, and DOX loaded micelles showed pH- and redox-responsive drug release of DOX and could form redox-induced aggregates. These factors contribute to the higher efficacy of the DOX loaded micelles of poly(BAC-AMPD)-*g*-PEG-*g*-CE in killing cancer cells than free drug. The biodegradability and high efficacy of DOX loaded micelles in killing cancer cells render poly(BAC-AMPD)-*g*-PEG-*g*-CE promising for preparation of drug delivery system for safe and efficient cancer chemotherapy.

Chapter 5

pH- and redox-responsive micelles of hyperbranched poly(amido amine)s for controlled drug delivery

5.1. Introduction

Dendritic polymers mainly include dendrimers and hyperbranched polymers and a classical example is poly(amido amine)s dendimer, Starburst®. Although hyperbranched polymers may not have structure and polydispersity as well-defined and uniform as dendrimers respectively, they also possess numerous surface functionality and similar three dimensional structures. However, one main feature which makes hyperbranched polymers distinctly superior than dendrimers, is their ease of synthesis. While hyperbranched polymers can usually be fabricated in an one-pot synthesis [370-373,433], dendrimers regardless of synthesis method (divergent or convergent) require multiple steps and extensive purifications to yield perfect dendrimer structure [326]. So hyperbranched polymers are attracting more interest for various applications.

With high surface functionality, hyperbranched polymers are exceptionally favorable for preparation of prodrugs or drug conjugates with drugs being conjugated to the polymers. With this mode of delivery, the drugs can remain inactive during delivery and only become potent upon cleavage at target sites. As a result of these advantageous features, many drugs like DOX [434-436], chlorambucil [437], ibuprofen [438], methyl prednisolone [439], methotrexate [434,440] and paclitaxel [441] have been conjugated to

hyperbranched polymers and demonstrated their feasibility as drug delivery systems.

However, compared to drug conjugation, physical encapsulation of drugs is a more preferred mode of drug delivery. This is because many polymers and drugs do not possess reactive functional groups and without chemical modification, pharmacological effectiveness of the drug is maintained [442]. When dendritic polymers are applied for encapsulation and delivery of drugs, the drugs can be encapsulated within either the hyperbranched polymers or the core of the micelles formed. It has been reported that ibuprofen, DOX, chlorambucil have been successfully encapsulated within hyperbranched polyesters [443,444], hyperbranched poly(amine ester)s [445,446] and poly(amido amine)s [447], respectively. In some cases, the hyperbranched polymers are modified to yield either amphiphilic or double hydrophilic hyperbranched polymers which can serve as unimolecular micelles. Typically, the hyperbranched polymers are functionalized with PEG to facilitate unimicellar formation. Besides commonly employing PEG, numerous works have been carried out with hyperbranched aliphatic polyester Boltorn® H40 due to its biodegradability, three dimensional structure and chain end functionalities [448-450]. The most basic form of such amphiphilic hyperbranched polymer is the PEGylated Boltorn® H40 which has been shown to enhance the solubility of paclitaxel by more than 35 times [451]. Then, another two groups independently fabricated a similar amphiphilic hyperbranched copolymer with H40 core, PLA inner shell and PEG outer shells. Disulfide linkages were also introduced as redox-responsive linkage between PLA and PEG to achieve controlled drug delivery

[452]. On the other hand, the unimicelles are functionalized with folate to afford targeted drug delivery [453]. Alternatively, drugs can also be encapsulated within the core of the micelles formed by the hyperbranched polymers [454-458], with stimuli-responsive micelle systems being particularly interesting [436,459].

Low drug loading capacity and efficiency is a major hurdle in the development of polymeric micelles for drug delivery [460]. There are several factors which can affect the loading capacity of the polymeric micelles. One is the affinity of the loaded drugs to the core polymer. For example, due to increase in electrostatic interaction, in the form of hydrogen bonds, a higher PCL / poly(ethylene oxide) ratio results in a higher loading capacities of cucurbitacin B and cucurbitacin I in diblock copolymer micelles [461]. Another factor which influences drug loading capacity is the volume of hydrophobic core. A higher core volume can hold more drugs. Other factors such as solubility and molecular volume of drugs can also have an effect on the loading capacity and efficiency [460,462,463].

In this chapter, we report a novel pH- and redox-responsive hyperbranched poly(amido amine)s for controlled drug delivery as shown in Scheme 5.1.Michael addition polymerization AMPD with double molar of BAC was performed to produce vinyl-terminated hyperbranched poly(BAC-AMPD).Then terminal vinyl groups of hyperbranched poly(BAC-AMPD) is changed to amine group via reaction with excess AMPD. PEG was conjugated to form amphiphilic hyperbranched poly(BAC-AMPD)-PEG to impair hydrophilicity. Via self-assembly in aqueous solution, pH- and redox-responsive micelles can be formed and anti-cancer drug, DOX, can be

encapsulated within the core. The self-assembly and drug loading capacity of the micelles were investigated, and pH- and redox-responsive DOX releases profiles of the micelles was indicated. Using fluorescence technique, the endocytosis of micelles and DOX loaded micelles of hyperbranched poly(BAC-AMPD)-PEG by HepG2 and MCF-7 cell lines was imaged and quantified with CLSM and flow cytometry analysis, respectively, with GSH level being changed. *in vitro* cytotoxicity study of the micelles in HepG2 and MCF-7 cell lines were carried out.

Scheme 5.1. Synthesis of hyperbranched poly(BAC-AMPD)-PEG

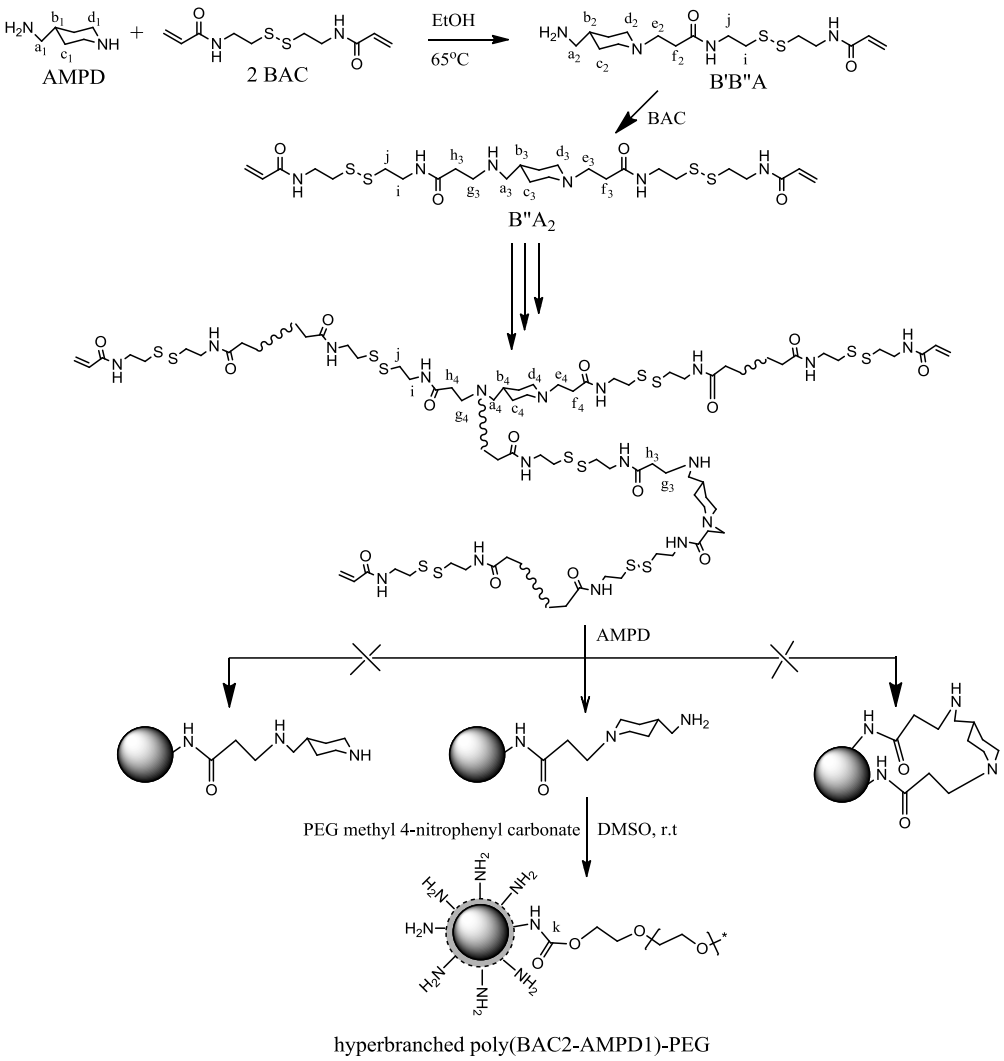

5.2. Experimental section

5.2.1. Materials

N,*N*-cystaminebis(acrylamide) (BAC) from Polysciences, 4-(aminomethyl)piperidine (AMPD) from Alfa Aesar, doxorubicin hydrochloride (DOX-HCl) from Fluka Analytical, and L-glutathione reduced (GSH), fluorescein isothiocyanate (FITC) and buthionine sulphoximine (BSO) from Sigma Aldrich were used as received. Monomethyl poly(ethylene glycol) (PEG) (~2000 g/mol) 4-nitrophenyl carbonate was prepared as in our previous report [419]. Methanol, ethanol, dimethylsulfoxide (DMSO), and other solvents used in this study were purchased from Tedia and used as received.

MCF-7 (human breast adenocarcinoma) cells and HepG2 (human hepatoma) cells were obtained from American Type Culture Collection (ATCC, Rockville, MD). They were maintained in Dulbecco's modified eagle medium (DMEM, invitrogen) with 10% fetal bovine serum (FBS), 2 mM glutamine, 100 units/ml penicillin and 100 µg/ml streptomycin at 37 °C in an incubator with 5% CO_2 atmosphere.

5.2.2. Synthesis of hyperbranched poly(BAC2-AMPD1)

In a typical procedure, 2.36 g (20.4mmol) of AMPD in 10 mL of ethanol was added dropwise to 10.58g (40.6mmol) of BAC in 50 ml of ethanol at 65 ^{o}C under argon. After 14 days, the reaction solution was added dropwise into 11.79 g (101.9 mmol) of AMPD in 60 mL of anhydrous DMSO at room temperature under argon. 24 h later, the solution was dialyzed using dialysis membrane with a molecular weight cut-off of 3500 in methanol. To monitor the polymerization, a small amount of the reaction solution was dried and then

dissolved in methanol-d_4 for ^{13}C NMR experiments with the total monomer concentrations being kept at ca. 25% (w/v). ^{13}C NMR spectra were obtained using a power-gated decoupling program (PD) with 200 times scan taking ca.10 minutes.

5.2.3. Synthesis of amphiphilic hyperbranched poly(BAC2-AMPD1)-PEG

In a typical experiment, 3.93 g (1.7mmol) of monomethyl PEG(~2000 g/mol) 4-nitrophenyl carbonate was added to 6.86 g (18.3mmol) of hyperbranched poly(BAC2-AMPD1) in 55 mL of anhydrous DMSO. The solution was stirred for 5 days at room temperature under argon followed by dialysis using membrane with a molecular weight cut-off of 10 000 in methanol.

5.2.4. Formation and characterization of micelles of hyperbranched poly(BAC2-AMPD1)-PEG

9 mL of deionized water was added at a rate of 0.5 mL/h using a syringe pump to 20 mg of hyperbranched poly(BAC2-AMPD1)-PEG in 1 mL of DMSO under a rapid stirring. Then the solution was dialyzed using membrane with a molecular weight cut-off of 1000 in deionized water to remove DMSO. In order to investigate pH- and redox-responsive properties, 2 mL of micelle solution was treated using 10 mM hydrochloride or sodium hydroxide solution to designed pH or incubated with 10 mM of GSH at 37 ^{o}C under stirring, and the change in the size of the micelles was monitored with dynamic light scattering (DLS).

5.2.5. Preparation of DOX loaded micelles

22.5 mL of deionized water was added at a rate of 0.5 mL/h using a syringe pump to 2.5 mL of DMSO containing 50 mg of hyperbranched poly(BAC2-AMPD1)-PEG, 10 mg of DOX-HCl and 5 μL of triethylamine (TEA) under rapid stirring. Then the solution was dialyzed using membrane with a molecular weight cut-off of 1000 in deionized water to remove DMSO and DOX. After dialysis, aggregates of unloaded DOX were removed by filtration through a filter with a pore diameter of 0.45 μm. To measure the DOX loading capacity, DOX loaded micelle solution was lyophilized, and a certain amount of dried DOX loaded micelles was dissolved in DMSO. The solution was dialyzed using membrane with a molecular weight cut-off of 2000 in DMSO. The concentration of DOX in the dialysis solution was measured with the concentration of DOX being determined based on a calibration curve. The loading capacity and the loading efficiency were calculated:

Loading capacity = Mass of DOX loaded / Mass of DOX loaded micelles × 100%

Loading efficiency = Mass of DOX loaded / Mass of DOX added × 100 %.

5.2.6. *in vitro* DOX release of DOX loaded micelles

2 mL of the DOX loaded micelle solution in dialysis membrane with a molecular weight cut-off of 10 000 was submerged in 40 mL of PBS at 37 ^{o}C with various conditions, i.e., pH 7, pH 5, pH 7 with 10 mM of GSH respectively. At a predetermined interval, 4 mL of dialysis solution (PBS) was collected and 4 mL of fresh PBS was added. The fluorescence intensity of the

solutions at 590 nm was measured with an excitation of 440 nm, and the concentration of DOX was determined based on a calibration curve.

5.2.7. Preparation of FITC tagged micelles of hyperbranched poly(BAC2-AMPD1)-PEG

The micelle solution was reacted with excess of FITC in the presence of TEA under stirring at room temperature. After 1 day, FITC tagged micelle solution was dialyzed extensively using a membrane a molecular weight cut-off of 1000 in ample of deionized water.

5.2.8. Cellular imaging

MCF-7 and HepG2 cell lines were seeded in 8 chamber borosilicate coverglass with a cell density of 5,000 cells/chamber and were cultured in DMEM supplemented with 10% FBS and 1% penicillin-streptomycin solution in an incubator at 37^{o}C, 5% CO_2, and 95% relative humidity. The cells were allowed to adhere to the chamber bottom upon overnight incubation. Then, the medium was replaced with fresh medium which contained either with or without 0.2 mM of BSO. The cells were incubated for another 3 days before the medium was again replaced with DOX loaded micelles solution or FITC tagged micelle solution in DMEM. At a designed time interval, the medium was removed and the chamber washed with 500 µL of PBS once followed by adding 250 µL of 90 % (v/v) cold ethanol to fix the cells in dark for 10 minutes. After the ethanol was aspired, the wells were washed with 500 µL of PBS, and 200 µL of 4',6-diamidino-2-phenylindole (DAPI) (10µg/mL) was added to stain the nuclei of the cells. 5 minutes later, DAPI was removed, and

the wells were washed with 500 µL of PBS twice followed by adding 150 µL of PBS to prevent the cells from drying up. The cells were imaged under a confocal laser scanning microscope (CLSM) (FV1000, Olympus, Japan).

5.2.9. Flow cytometry analysis

MCF-7 and HepG2 cell lines were seeded in 12 well-plates with a cell density of 6 x 10^4 and 3 x 10^4cells/chamber respectively and were cultured in DMEM supplemented with 10% FBS and 1% penicillin-streptomycin solution in an incubator at 37^{o}C, 5% CO_2, and 95% relative humidity. The cells were allowed to adhere to the well bottom upon overnight incubation. Then, the medium was replaced with fresh medium which contained either with or without 0.2 mM of BSO. The cells were incubated for another 3 days before the medium was again replaced with DOX loaded micelles solution or FITC tagged micelle solution in DMEM. At a designed time interval, the medium was removed and the chamber washed with 500 µL of PBS twice and the cells were unseeded. After centrifugation, the cell pellets were dispersed in 70 % (v/v) ethanol and stored in -20 ^{o}C freezer. Lastly, the fixed cell suspensions were analysed using the BD LSR Fortessa Flow Cytometry Analyser.

5.2.10. *in vitro* cytotoxicity evaluation of samples

The *in vitro* cytotoxicity of hyperbranched poly(BAC2-AMPD1)-PEG, DOX-HCl, and DOX loaded micelles of hyperbranched poly(BAC2-AMPD1)-PEG were evaluated in MCF-7 and HepG2 cell lines. Viability of the cells was assessed by the standard thiazolyl blue [3-(4,5-dimethyliazolyl-2)-2,5-diphenyl tetrazolium bromide] (MTT) assay. This colorimetric assay allows

determination of the number of viable cells through the metabolic activity of the cells.

The cancer cells were seeded in 96-well plates with a cell density of 2,500 cells/well and were cultured in DMEM supplemented with 10% FBS and 1% penicillin-streptomycin solution in an incubator at 37 ^{o}C, 5% CO_2, and 95% relative humidity. The cells were allowed to adhere to the well bottom upon overnight incubation. Then, the medium was replaced with fresh medium which contained either with or without 0.2 mM of BSO. The cells were incubated for another 3 days before the medium was exchanged with the sample solutions of different concentrations in DMEM containing with or without 0.2 mM BSO. Meanwhile, wells containing only cell culture medium were prepared as untreated controls. At the predetermined time, the medium containing samples was aspirated and the wells were washed with 1 ×PBS solution for two times to removed non-internalized sample. Then 100 μL of DMEM and 10 μL of MTT solution (5 mg/mL in 1 ×PBS solution) were added to the wells. After incubation for 4 h at 37 ^{o}C, the solution was removed and the formazan precipitate was dissolved in 100 μL of dimethyl sulfoxide (DMSO). The absorbance intensity of the solution was then quantified spectrophotometrically using a microplate reader (TECAN SpectraFluor Plus) at 570 nm. Cell viability was expressed by the following equation:

Cell viability (%) = Abssample / Abscontroll × 100%

where Abssample was the absorbance for cells treated with samples, while Abscontroll was the absorbance for untreated control cells. All the tests were performed in multiples.

5.2.11. Measurements

Gel permeation chromatography (GPC) was performed on a Waters 2690 apparatus with two columns in series (Waters Ultrahydrogel 250 and 200) and a Waters 410 refractive index detector. A mixture of 0.5 M acetic acid/0.5 M sodium acetate was used as eluent, and poly(ethylene oxide) standards were used. Nuclear magnetic resonance (NMR) spectra were obtained on a Bruker DPX 400 MHz NMR spectrometer. A Brookhaven BIS200 laser light scattering system was used for dynamic light scattering (DLS) measurements. The light source is a power adjustable vertically polarized 35 mW argon ion laser with a wavelength of 633 nm. The scattering angle was fixed at 90^{o} for measuring the hydrodynamic radius (R_h) and the average scattering intensity. R_h values were obtained using a NNLS analysis. TEM images were obtained using a high resolution Philips CM300 transmission electron microscope (FEGTEM) at 300 kV, and the samples were prepared by dropping micelles solution onto a copper grid cover with carbon followed by drying in a desiccator. Then, the dried grid was left in 1% osmium oxide in heptane for 2 h.Fluorescence excitation and emission spectra were recorded on a Perkin–Elmer LS55 Fluorescence Spectroscopy instrument fitted with a R928-sensitive sample photomultiplier. Confocal imaging was done with Olympus Fluoview FV1000 with excitation wavelength of 405 nm while the flow cytometry analysis was done with BD LSR Fortessa Flow Cytometry Analyser.

5.3. Results and Discussion

5.3.1. Synthesis of vinyl-terminated hyperbranched poly(BAC2-AMPD1)

Michael Addition polymerization of AMPD with a double molar BAC was conducted in ethanol at 65 ^{o}C. Similar to the Michael addition polymerization of AEPZ with a double molar of diacrylate [370], the reaction of AMPD with a double molar BAC forms B'B"A intermediate first via the reaction of the 2^{o} amine (original) with BAC as shown in Scheme 5.1. As shown in Figure 5.1a, the peaks attributed to B'B"A intermediate appear, e.g., the peak d_2 at ca. 52.9 ppm, after the reaction is performed in ethanol at 65 ^{o}C for 0.25 h. At this stage, Figure 5.1a also shows that unreacted AMPD monomer still exists as reflected by the corresponding peaks, e.g., the peak c_1 at ca. 30.0 ppm. After the reaction was performed for 4 h, Figure 5.1b shows that B''A_2 intermediate is formed as reflected by the appearance of the corresponding peaks, e.g., the peak a_3 at 55.0 ppm. Vinyl-terminated hyperbranched poly(BAC2-AMPD1) is formed via the polymerization of B''A_2 intermediate. Figure 5.1c indicates that the dendritic unit is formed as reflected by the appearance of the corresponding peaks, e.g., the peak a_4 at ca. 59.7 ppm, after the reaction is performed for 48 h, with the 2^{o} amine (formed) still existing. Figure 5.1d indicates that almost all the 2^{o} amine (formed) is consumed as reflected by the disappearance of the corresponding peaks, e.g., the peak $a_{3,}$ after the reaction is performed for 240 h. Originally, the polymerization was performed in methanol at 50 ^{o}C following our previous works [64], however, the reaction was slow with the dendritic unit being formed 3 days later, and the 2^{o} amine (formed) being consumed after 28 days. When the polymerization was performed in a mixture of DMSO/water (80/20) (v/v) at 80 ^{o}C to increase the

reaction rate, no dendritic unit was formed even after 11 days. Therefore, ethanol was adopted for the polymerization.

The vinyl terminal group of hyperbranched poly(BAC2-AMPD1) was converted into amine via the reaction with excess AMPD in DMSO [370]. The complete conversion of the vinyl group to amine is indicated by the disappearance of the vinyl peaks at 125.5 ppm and 130.5 ppm as shown in Figure 5.1e. Three possible reactions may occur between the vinyl group and AMPD as shown in Scheme 5.1, i.e., the reaction between the vinyl group and 2^o amine (original), 1^o amine and the crosslinking reaction with 2 vinyl terminals, respectively. Since the reactivity sequence of the three amines of AMPD is 2^o amine (original) > 1^o amine >> 2^o amine (formed) [77,82], the vinyl group reacts with the 2^o amine (original) instead of 1^o amine when excess AMPD is presented. This is supported by the appearance of the characteristic peaks of the unit such as the peak c_2 at 29.4 ppm in Figure 5.1e. Meanwhile, the peaks attributed to the unit from the reaction with 1^o amine such as the peaks a_3 and h_3 cannot be observed. Therefore, most of the vinyl groups react with the 2^o amine (original) of AMPD forming hyperbranched poly(BAC2-AMPD1) terminated with $–NH_2$, hyperbranched poly(BAC2-AMPD1)-NH_2. The molecular weight of hyperbranched poly(BAC2-AMPD1)-NH_2 is determined to be 75.4 ± 1.1 k Dalton from Zimm plot obtained in methanol shown in Figure 5.2a. Hyperbranched poly(BAC2-AMPD1)-NH_2 is soluble in methanol, ethanol and DMSO, but not in aqueous solution.

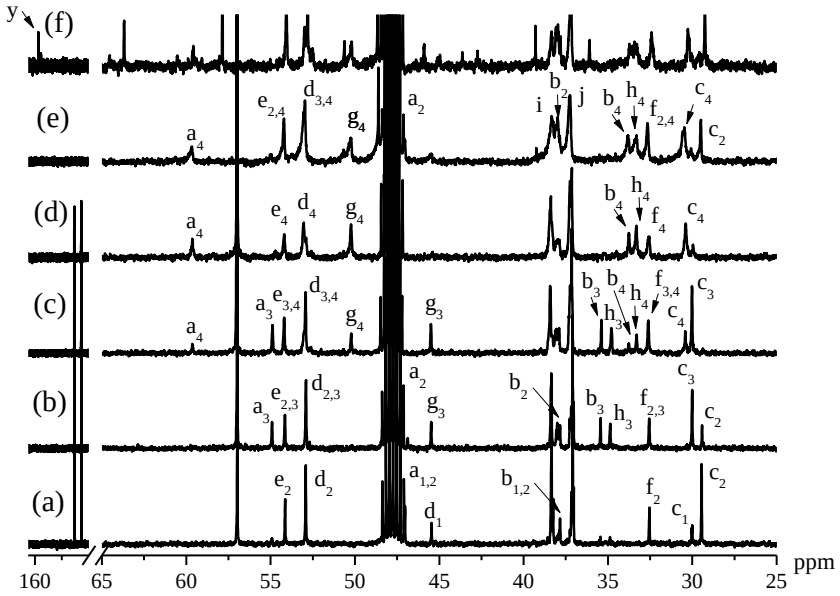

Figure 5.1. Comparison of ^{13}C NMR spectra of the product of Michael Addition polymerization of AMPD with a double molar BAC in ethanol with a monomer concentration of 25% (w/v) at 65 ^{o}C obtained a) for 0.25 h; b) for 4 h; c) for 48 h; d) for 240 h; e) after reaction with AMPD, and f) after PEGylation. The spectra were obtained in methanol-d_4.The attribution of the peaks is listed in Scheme 5.1. The peak at 57.0 ppm is attributed to residual ethanol.

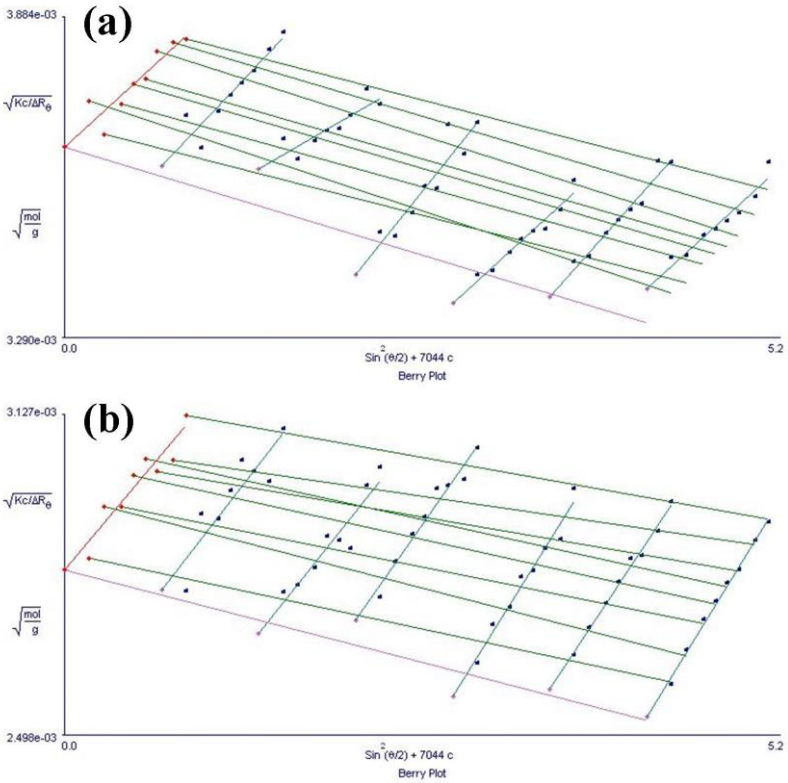

Figure 5.2. Zimm plot of a) amino-terminated hyperbranched poly(BAC2-AMPD1); b) hyperbranched poly(BAC2-AMPD1)-PEG in methanol.

5.3.2. Synthesis of hyperbranched poly(BAC2-AMPD1)-PEG

PEG has been demonstrated to have various functions including membrane penetration [273-278], prevent nonspecific protein adsorption, provide long-circulation time in blood vessel [279-284] and facilitate endocytosis [285]. So PEG was conjugated to the $–NH_2$ terminals of hyperbranched poly(BAC2-AMPD1)-NH_2 via the formation of urethane bond as shown in Scheme 5.1. To control the degree of PEG conjugation, the feeding molar ratio of PEG to the terminal $–NH_2$ was kept at 1 : 3.5. From the ^{13}C NMR spectrum shown in Figure 5.1f, the molar ratio of PEG attached is determined to be ca. 1 : 4.1 using equation E5.1.

Molar ratio of PEG / terminals = $2 \times I_{157.48} / I_{29.29}$ (E5.1)

Where $I_{157.48}$ and $I_{29.4}$ are the integral intensities of the peaks of k and c_2 at 157.5 ppm and 29.4 ppm, respectively.

Hyperbranched poly(BAC2-AMPD1)-PEG is soluble in methanol, ethanol, and DMSO. The molecular weight of hyperbranched poly(BAC2-AMPD1)-PEG is 125.6 ± 2.6 k Dalton obtained from Zimm plot in methanol shown in Figure 5.2b. So each hyperbranched poly(BAC2-AMPD1) macromolecule is conjugated with ~25 PEG chains determined using equation E5.2:

Number of PEG chains conjugated to each hyperbranched poly(BAC2-AMPD1) macromolecule = $(Mw_B – Mw_A) / 2000$ (E5.2)

Where Mw_B and Mw_A are the molecular weights of hyperbranched poly(BAC2-AMPD1)-PEG and hyperbranched poly(BAC2-AMPD1)-NH_2, respectively.

5.3.3. Self-assembly of hyperbranched poly(BAC2-AMPD1)-PEG

Polymer self-assembly occurred when deionized water was added at a rate of 0.5 ml/h into DMSO solution of hyperbranched poly(BAC2-AMPD1)-PEG. Figure 5.3a presents TEM images of the self-assembly obtained stained with OsO_4. It can be observed that the self-assembly is in the form of micelles with an average diameter of ca. 87 nm at dry state. DLS measurements show that the diameter of the swollen micelles obtained in aqueous solution is ca. 233.2 ± 13.4 nm. The CMC of the micelles was determined to be ca. 21.1 µg/mL using DLS by plotting the average scattering intensities of different polymer concentrations as shown in Figure 5.4b [77,428]. Since only the protons of polymer segments with a high mobility in solution can be observed in solution ^{1}H NMR spectrum [425-427], ^{1}H NMR spectra were used to get more information of the micelles formed. Figures 5.5a and 5.5b show ^{1}H NMR spectra of hyperbranched poly(BAC2-AMPD1)-PEG in methanol-d_4 and in D_2O obtained by dissolving directly, respectively. Although the peaks become broadened, most of the peaks in Figure 5.5a can still be observed in Figure 5.5b. Figure 5.5c shows ^{1}H NMR spectrum of micelles obtained by adding D_2O slowly into DMSO solution of hyperbranched poly(BAC2-AMPD1)-PEG followed by dialysis. In comparison with Figure 5.5b, it is obvious that only the peaks attributed to PEG can be observed which indicates that the micelles are formed with PEG shells and poly(BAC2-AMPD1) cores inaccessible to water [77,425-427]. So the micelles can only be obtained via slow addition of water into DMSO solution of hyperbranched poly(BAC2-AMPD1)-PEG rather than dissolving in water directly. So the self-assembly of hyperbranched poly(BAC2-AMPD1)-PEG is facilitated by a gradient change from a good

solvent for both the hydrophilic and hydrophobic components to a selective solvent only for the hydrophilic component.

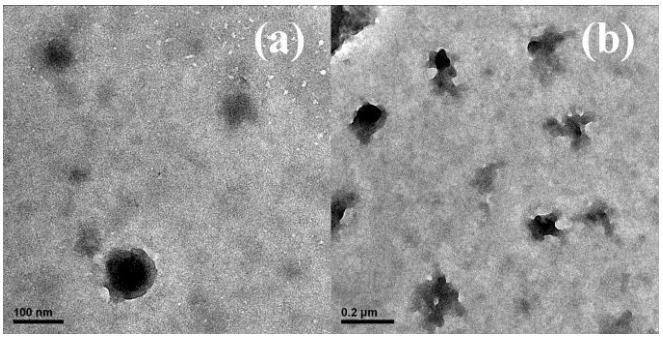

Figure 5.3. TEM images of a) micelles of hyperbranched poly(BAC2-AMPD1)-PEG stained with osmium oxide; b) DOX loaded micelles of hyperbranched poly(BAC2-AMPD1)-PEG stained with osmium oxide.

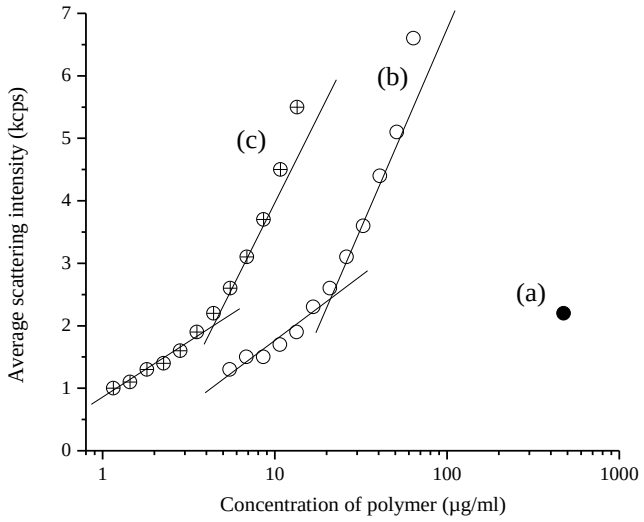

Figure 5.4. Relationship between the average scattering intensity from DLS measurements and the concentration of hyperbranched poly(BAC2-AMPD1)-PEG (µg/mL) in deionized water, a) hyperbranched poly(BAC2-AMPD1)-PEG dissolved in deionized directly; b) micelles of hyperbranched poly(BAC2-AMPD1)-PEG; c) DOX loaded micelles of hyperbranched poly(BAC2-AMPD1)-PEG.

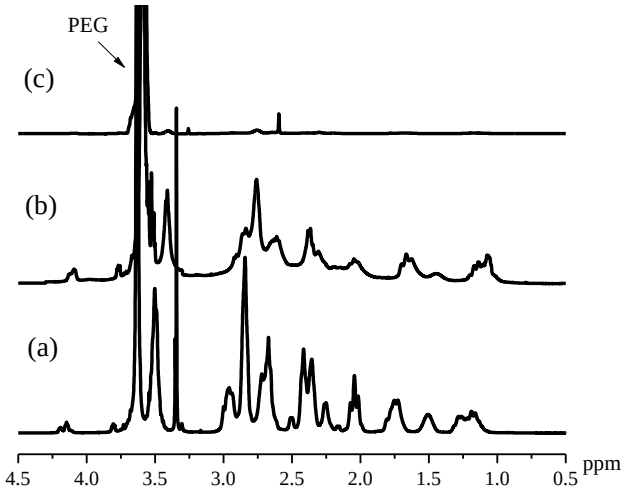

Figure 5.5. ^{1}H NMR spectra of a) hyperbranched poly(BAC2-AMPD1)-PEG in methanol-d_4; b) hyperbranched poly(BAC2-AMPD1)-PEG dissolved in D_2O directly; c) micelles of hyperbranched poly(BAC2-AMPD1)-PEG in D_2O formed by adding D_2O into DMSO followed by dialysis.

pH dependent hydrodynamic diameter of the micelles of hyperbranched poly(BAC2-AMPD1)-PEG was investigated using DLS, the results shown in Figure 5.6. As pH was decreased, the diameter of the micelles increased due to swelling induced by the protonation of the amines. Also it was shown that the average scattering intensity of the micelles declined by more than 95% in 15 minutes after incubation with 10 mM of GSH, present in Figure 5.7, which indicates that the micelles can be degraded via the reaction with GSH.

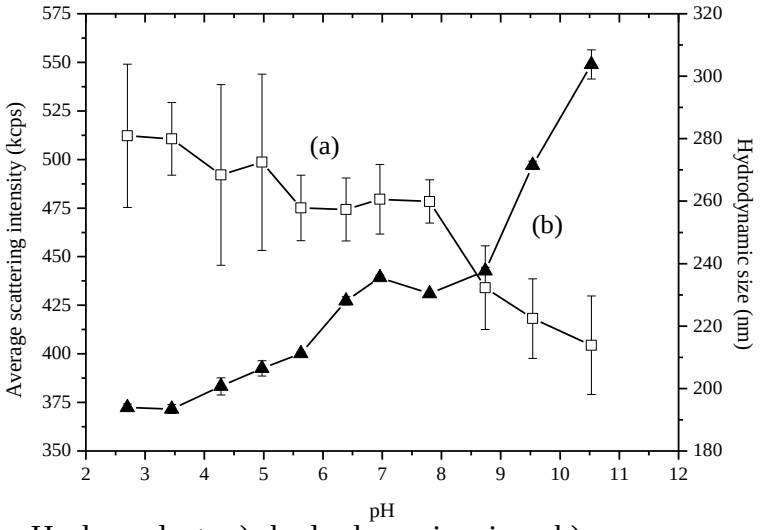

Figure 5.6. pH dependent a) hydrodynamic size; b) average scattering intensity from DLS measurement, of micelles of hyperbranched poly(BAC2-AMPD1)-PEG. All data represent mean ± SD (n = 3).

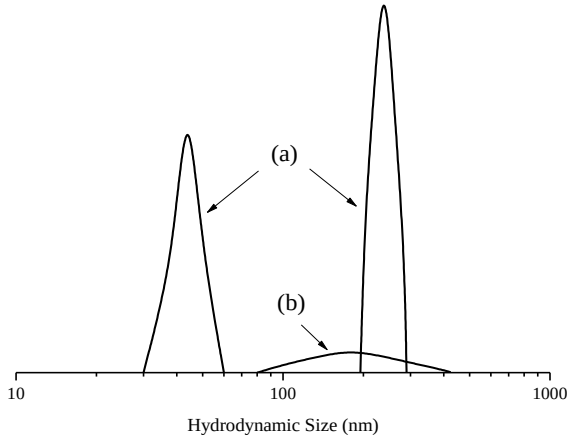

Figure 5.7. Hydrodynamic size distribution of micelles of hyperbranched poly(BAC2-AMPD1)-PEG in the presence of 10 mM GSH, a) before incubation; b) 15 min post incubation at 37 ^{o}C. (Normalized intensity)

5.3.4. DOX loaded micelles of hyperbranched poly(BAC2-AMPD1)-PEG

Anti-cancer drug, doxorubicin (DOX) which intercalate with DNA to induce cell death [432,467], was loaded into the micelles of hyperbranched poly(BAC2-AMPD1)-PEG during the self-assembly process. DOX content and loading efficiency of the micelles of hyperbranched poly(BAC2-

AMPD1)-PEG are ca. 10.5 % and ca. 52.3 %, respectively. DOX loaded micelles have a hydrodynamic diameter of ca. 193.1 ± 17.65 nm determined using DLS, and a diameter of ca. 108 nm in dry state obtained from TEM image as shown Figure 5.3b. CMC of DOX loaded micelles is 4.5 µg/ml, which is lower than the micelles without DOX as illustrated in Figure 5.4c.

The release profiles of DOX from micelles of hyperbranched poly(BAC2-AMPD1)-PEG were investigated in PBS under pH 7, pH 5, and pH 7 with 10 mM GSH, respectively, and the results are shown in Figure 5.8. The release rate of DOX is considerably faster at pH 5 than at pH 7. After 10 h, 17 % of DOX is released at pH 7 as compared to 35% at pH 5. A lower pH leads to a higher protonation degree of the amines of poly(BAC2-AMPD1) associated with a greater swelling of the micelles and therefore a faster release of DOX. When the DOX loaded micelle solution is incubated with 10 mM of GSH, a much faster release is observed with 50 % and 100% of DOX being released in 10 h and 72 h, respectively. This is caused by thiol-induced degradation leading to dissociation of the micelles.

Comparing these results to the systems described in chapter 4, we can infer that micelles self-assembled from less hydrophobic polymers which is poly(BAC2-AMPD1)-PEG tend to release the drugs more quickly. Weaker hydrophobic interactions between drugs and polymers, and less stable micelles can contribute to this rapid release significantly. Nevertheless, it is also important to note that the structures of the polymers in both cases are highly different and this may play a role in the release.

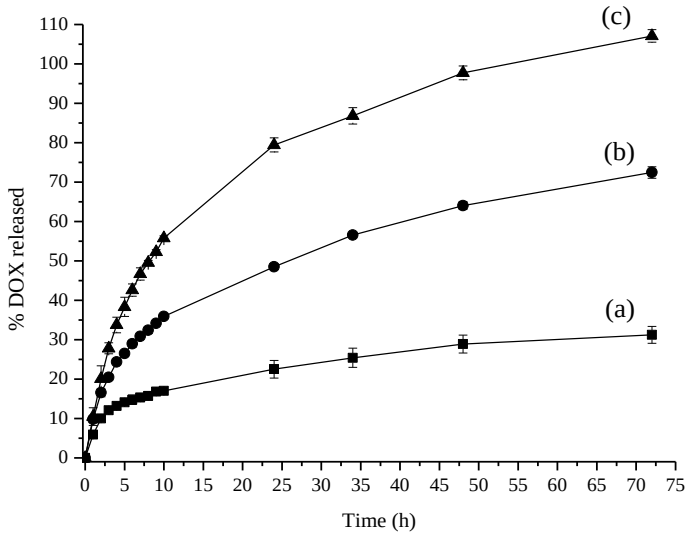

Figure 5.8. DOX release profiles of DOX loaded micelles of hyperbranched poly(BAC2-AMPD1)-PEG at (a) pH 7; (b) pH 5; (c) pH 7 with 10 mM GSH. All data represent mean ± SD (n = 3).

5.3.5. Cellular uptake of FITC tagged micelles and DOX loaded micelles

The cellular uptake of the micelles of hyperbranched poly(BAC2-AMPD1)-PEG was investigated using confocal microscopy. Although fluorescence can be observed from poly(amido amine)s similar to those amine-containing polymers [377], the micelles were tagged with FITC for accurate analysis. FITC tagged micelles were incubated with HepG2 and MCF-7 cells for 72 h. Both HepG2 and MCF-7 cells, with a high intracellular GSH level, were also incubated with 0.2 mM of BSO for 72 h to reduce the intracellular GSH concentration by ca. 4 times in order to investigate the effects of reductive potential [373]. Figure 5.9 shows the confocal microscopy images of HepG2 cells after incubation with FITC tagged micelles of hyperbranched poly(BAC2-AMPD1)-PEG for different time intervals. In HepG2 without or with BSO treatment, FITC fluorescence is detected in the cytoplasm after incubation for 5 h. This indicates that FITC tagged micelles can enter the cells

readily probably via endocytosis. The effect of BSO treatment on the HepG2 is indicated by the results of flow cytometry shown in Figure 5.10. BSO treatment results in a higher fluorescence intensity from HepG2, and the fluorescence intensity increases with the incubation time from 5 h to 72 h. In contrast, the fluorescence intensity from the cells without BSO treatment increases by ca. 40% as the incubation time increases from 5 h to 24 h, and then drops ca. 12% after 72h incubation. This might be due to that a lower reduction potential in the intracellular apartments induced by BSO treatment retards the degradation of the micelles, and therefore leads to accumulation of more FITC tagged micelles in the cytoplasm.

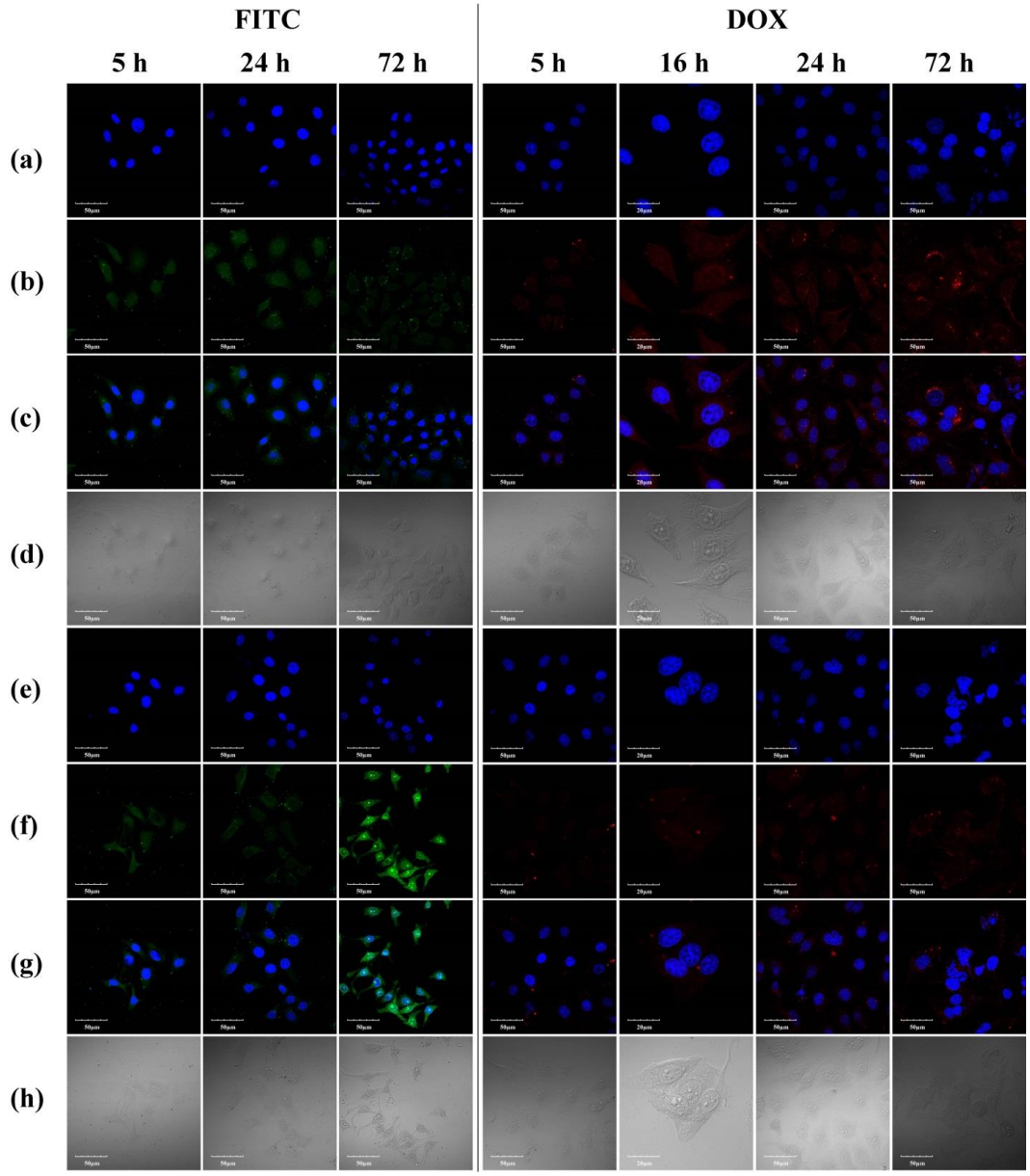

Figure 5.9. CLSM images of HepG2 incubated with FITC tagged micelles of hyperbranched poly(BAC2-AMPD1)-PEG and DOX loaded micelles of hyperbranched poly(BAC2-AMPD1)-PEG. a,e) cells with nucleus staining with DAPI; b,f) cells with FITC or DOX fluorescence; c,g) overlays of cells with nucleus staining with DAPI and FITC or DOX fluorescence; d,h) under bright field. Row (a-d) and (e-h) are results without and with BSO treatment, respectively.

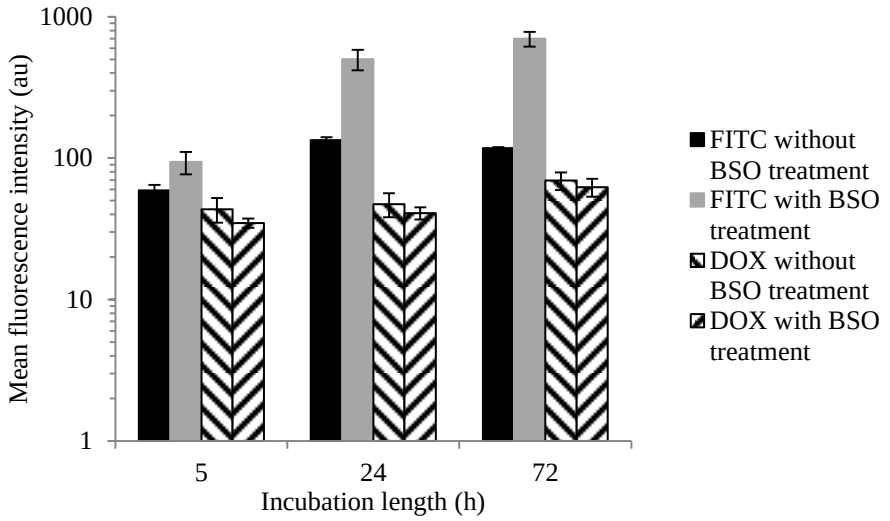

Figure 5.10. Mean FITC and DOX fluorescence intensity detected by flow cytometry when HepG2 cells were incubated with FITC tagged micelles of hyperbranched poly(BAC2-AMPD1) and DOX loaded micelles of hyperbranched poly(BAC2-AMPD1) respectively. All data represent mean ± SD. (n = 3).

Figure 5.11 shows the confocal microscopy images of MCF-7 cells after incubation with FITC tagged micelles of hyperbranched poly(BAC2-AMPD1)-PEG. Similarly the micelles can enter the cells readily without or with BSO treatment. The flow cytometry results shown in Figure 5.12 indicates that the fluorescence intensity reaches the maximum at 24 h and then decreases with time, and the effect of BSO treatment on MCF-7 cells is a negligible, which is similar to the phenomenon reported [373].

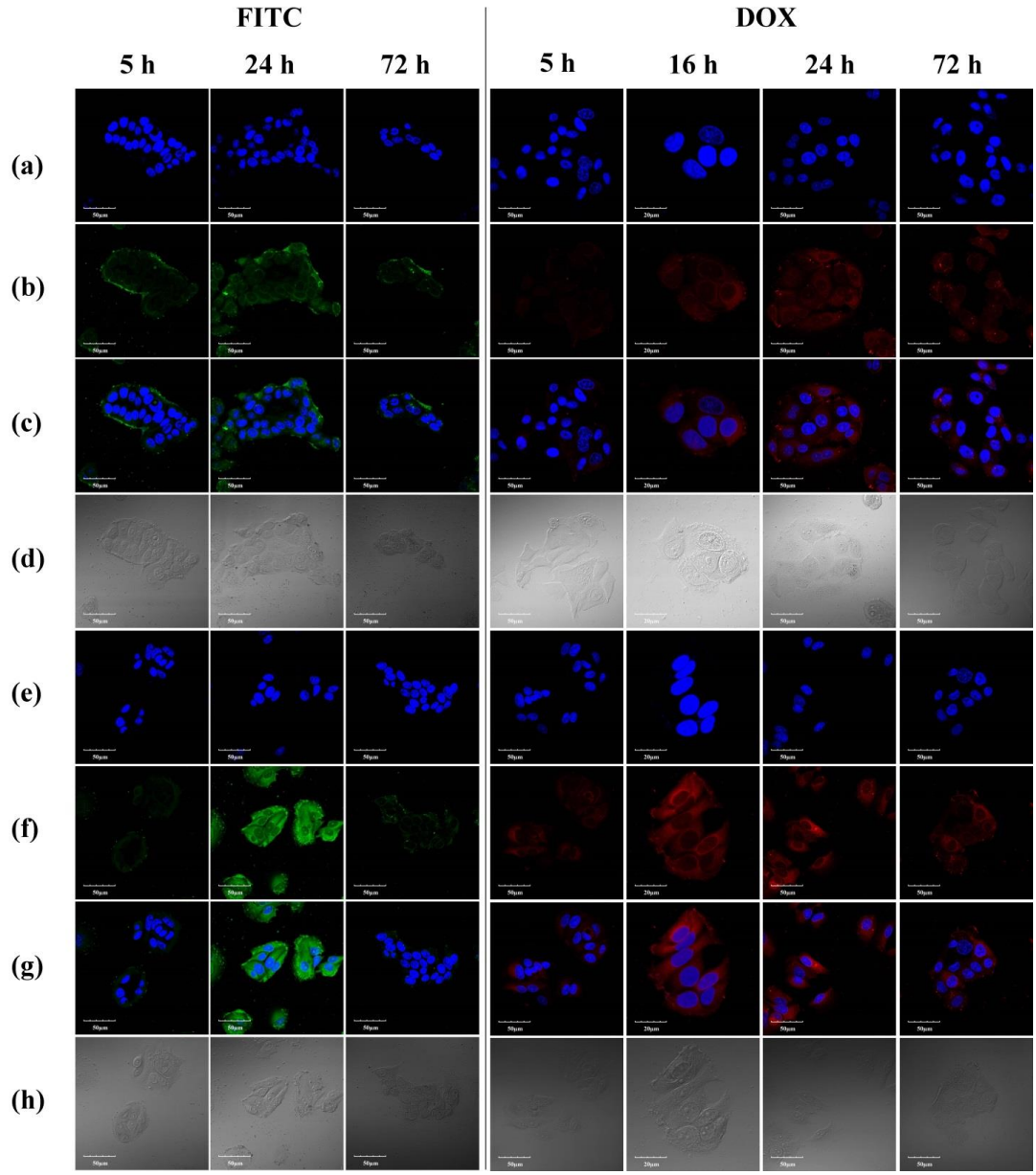

Figure 5.11. CLSM images of MCF-7 incubated with FITC tagged micelles of hyperbranched poly(BAC2-AMPD1)-PEG and DOX loaded micelles of hyperbranched poly(BAC2-AMPD1)-PEG. a,e) cells with nucleus staining with DAPI; b,f) cells with FITC or DOX fluorescence; c,g) overlays of cells with nucleus staining with DAPI and FITC or DOX fluorescence; d,h) under bright field. Row (a-d) and (e-h) are results without and with BSO treatment, respectively.

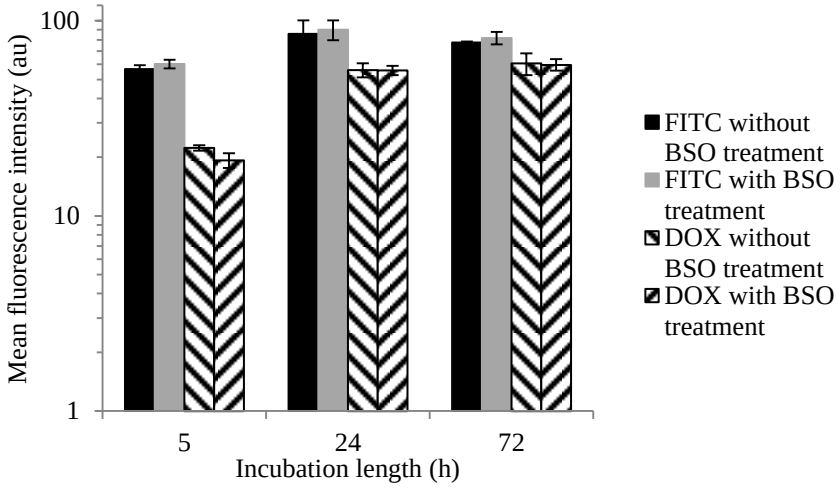

Figure 5.12. Mean FITC and DOX fluorescence intensity detected by flow cytometry when MCF-7 cells were incubated with FITC tagged micelles of hyperbranched poly(BAC2-AMPD1) and DOX loaded micelles of hyperbranched poly(BAC2-AMPD1) respectively. All data represent mean ± SD. (n = 3).

DOX loaded micelles of hyperbranched poly(BAC2-AMPD1)-PEG were incubated with HepG2 and MCF-7 cells without or with BSO treatment, respectively. As shown in Figure 5.9 and 5.11, DOX can be observed in the cytoplasm and nucleus of HepG2 and MCF-7 cells after incubation of 5 h. The results from flow cytometry shown in Figure 5.10 and 5.12 shows that DOX fluorescence intensity increase insignificantly with incubation time from 5 h to 72 h in HepG2 cells; and increase from 5 h to 24 h but level off till 72 h in MCF-7 cells. The effect of BSO treatment is negligible on the DOX fluorescence intensity in both HepG2 and MCF-7 cells.

5.3.6. *in vitro* cytotoxicity of DOX loaded micelles

in vitro cytotoxicity of hyperbranched poly(BAC2-AMPD1)-PEG and DOX loaded micelles were evaluated in HepG2 and MCF-7 without or with BSO

treatment, respectively. More than 70 % of the HepG2 cells and MCF-7 cells are viable after incubation with 200 μg/ml of hyperbranched poly(BAC2-AMPD1)-PEG for 72 h regardless of without or with BSO treatment, which shows a low cytotoxicity of the polymer as shown in Figure 5.13. Figure 5.14 and 5.15 illustrate the cytotoxicity of DOX loaded micelles of hyperbranched poly(BAC2-AMPD1)-PEG in HepG2 cells and MCF-7 cells, respectively. Figure 5.14 indicates that free DOX-HCl displays a higher cytotoxicity than DOX loaded micelles in HepG2 cells without or with BSO treatment. Furthermore, it is also reflected that BSO treatment shows insignificant effects on the cytotoxicity of free DOX-HCl and DOX loaded micelles of hyperbranched poly(BAC2-AMPD1)-PEG. Figure 5.15 shows that DOX loaded micelles of hyperbranched poly(BAC2-AMPD1)-PEG shows cytotoxicity comparable to free DOX-HCl in MCF-7 cells without or with BSO treatment, and the effects of BSO treatment is also insignificant. Since the DOX loaded micelles can release all the DOX loaded in 72 h at pH 7 with 10 mM GSH as shown in Figure 5.8, the difference in cytotoxicity of DOX loaded micelles and free DOX-HCl in HepG2 and MCF-7 cells should not be due to the incomplete release of DOX, and should be attributed to the different cell endocytosis process instead. So far, the cell endocytosis is still not well understood. Many features of nanoparticles including shape, size, and surface properties affect the cellular uptake [468,469], and endocytosis process is also cell type dependent and has many internalization routes such as clathrin-coated pit-mediated endocytosis and raft mediated endocytosis [468-470].

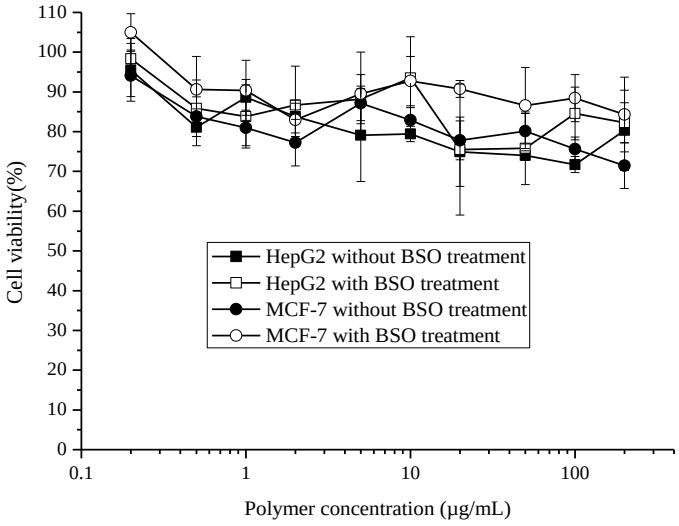

Figure 5.13. *in vitro* cytotoxicity of hyperbranched poly(BAC2-AMPD1)-PEG in HepG2 and MCF-7 with or without BSO treatment. All data represent mean ± SD. (n = 3).

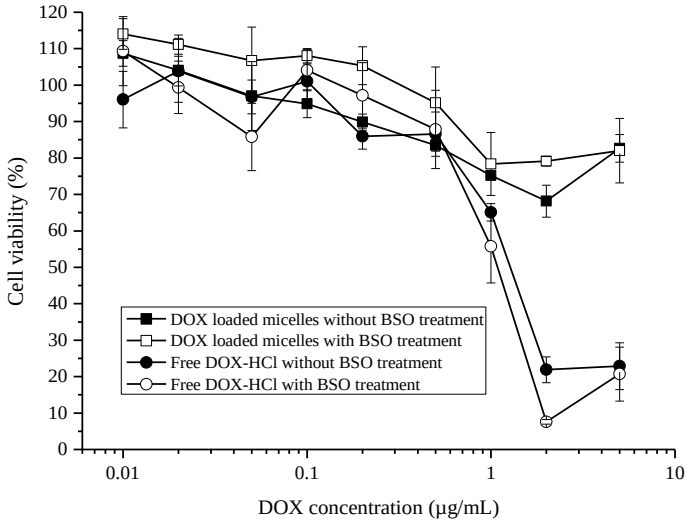

Figure 5.14. *in vitro* cytotoxicity of DOX loaded micelles of hyperbranched poly(BAC2-AMPD1)-PEG and free DOX-HCl in HepG2 with or without BSO treatment. All data represent mean ± SD. (n = 3).

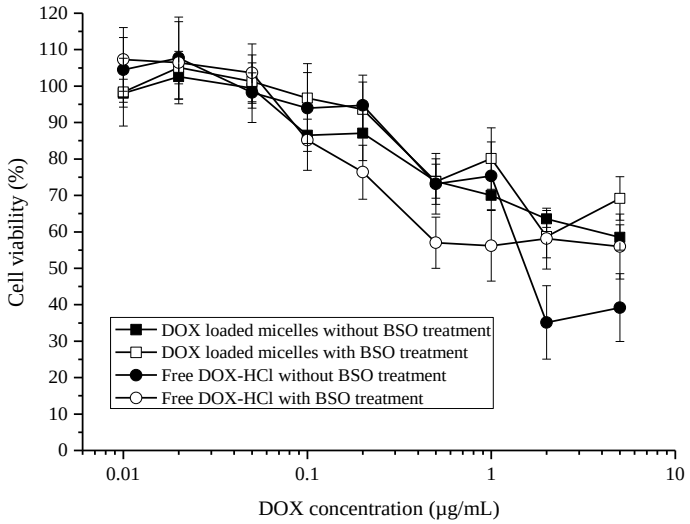

Figure 5.15. *in vitro* cytotoxicity of DOX loaded micelles of hyperbranched poly(BAC2-AMPD1)-PEG and free DOX-HCl in MCF-7 with or without BSO treatment. All data represent mean ± SD. (n = 3).

5.4. Conclusions

Vinyl terminated hyperbranched poly(amido amine)s is synthesized via Michael Addition polymerization of AMDP with a double molar BAC in ethanol. After the terminal vinyl groups is converted to primary amines via reaction with excess AMPD, PEG is conjugated to form hyperbranched poly(BAC2-AMPD1)-PEG. pH- and redox-responsive micelles with PEG shells and hydrophobic cores of poly(BAC2-AMPD1) can be formed via self-assembly of hyperbranched poly(BAC2-AMPD1)-PEG in aqueous solution, and DOX can be loaded within the micelles with loading capacity and efficiency of ca. 10.5 % and ca. 52.3 % respectively. DOX can be released faster at pH 5 and in the presence of 10 mM of GSH. The micelles of hyperbranched poly(BAC2-AMPD1)-PEG without or with DOX can enter HepG2 and MCF-7 cells readily, and DOX can be observed in the nucleus of the cells. DOX loaded micelles of hyperbranched poly(BAC2-AMPD1)-PEG can kill HepG2 and MCF-7 cells with the cytotoxicity lower or close to free

DOX. A lower reductive potential induced by BSO treatment shows insignificant effects on these performances, excluding leading to more accumulation of the micelles in HepG2 cells.

Chapter 6

A facile approach to biodegradable polydisulfide MRI contrast agent

6.1. Introduction

MRI is a powerful, non-invasive and non-radioactive diagnostic imaging technique which can provide imaging with a high spatial resolution and a multiple physical contrast, and MRI contrast agents are always needed to improve the quality of imaging to allow more accurate diagnosis of diseases [31,177]. Currently, MRI contrast agents used in clinic are small molecular gadolinium (III) (Gd(III)) chelates such as Magnevist®, Eovist® and Dotarem®. However, these MRI contrast agents have their limitations including short retention time and fast vascular extravasation due to their low molecular weight [471]. One of the approaches to overcome these limitations is to integrate small molecular Gd(III) chelates with polymers to form macromolecular MRI contrast agents which have shown to reduce vascular extravasation [177,179,472-475], are able to target tumor and have higher T_1 relaxivity [177,472-477]. However, the slow and incomplete excretion of Gd(III) ions integrated in these macromolecules can result in side effects such as nephrogenic systemic fibrosis (NSF) especially in renal dysfunctional patients [32-34], Therefore macromolecular MRI contrast agents with suitable degradation rate are needed for feasible excretion of Gd(III) chelates after imaging [478].

Besides the conventional biodegradable synthetic polymers like poly(ester)s which hydrolyse in the presence of water, several types of biodegradable polydisulfide Gd(III) based MRI contrast agents were reported with Gd(III) chelates either being linked together or being conjugated to polymer via disulfide bonds respectively. Linear macromolecular Gd(III) based MRI contrast agents with disulfide in the backbone could be prepared by copolymerization of DTPA dianhydride and disulfide containing diamine followed by forming Gd-DTPA diamide which has low chelating stability [478]. These linear macromolecular Gd(III) based MRI contrast agents showed prolonged retention time and improved *in vivo* contrast enhancement, and are degradable and readily excreted via renal filtration [479-481]. Recently a new type of polydisulfide Gd(III) based contrast agent with improved chelating stability was reported. The agent was obtained by preparing chelate containing diamine monomer with chelate units, performing condensation polymerization with disulfide containing activated dianhydride to form Gd(III) chelates [482].

Here we report a facile approach to synthesize linear biodegradable Gd(III) based macromolecular MRI contrast agent with disulfide bonds in the backbones. As shown in Scheme 6.1, the disulfide-containing poly(amido amine)s, poly(BAC-AMPD), was synthesized via Michael Addition polymerization of trifunctional amine, AMPD, and an equimolar diacrylamide, BAC. Then PEG and DTPA were conjugated via the reactions with the secondary amine remained, respectively, to form poly(BAC-AMPD)-*g*-PEG-*g*-DTPA. Poly(BAC-AMPD)-*g*-PEG-*g*-DTPA was complexed with Gd(III) ions to produce macromolecular MRI contrast agent, poly(BAC-AMPD)-*g*-PEG-*g*-Gd-DTPA. The self-assembly behaviour, thiol-induced degradation, *in*

vitro cytotoxicity and the relaxivity of poly(BAC-AMPD)-*g*-PEG-*g*-Gd-DTPA were investigated.

Scheme 6.1. Synthesis of poly(BAC-AMPD)-*g*-PEG-*g*-Gd-DTPA.

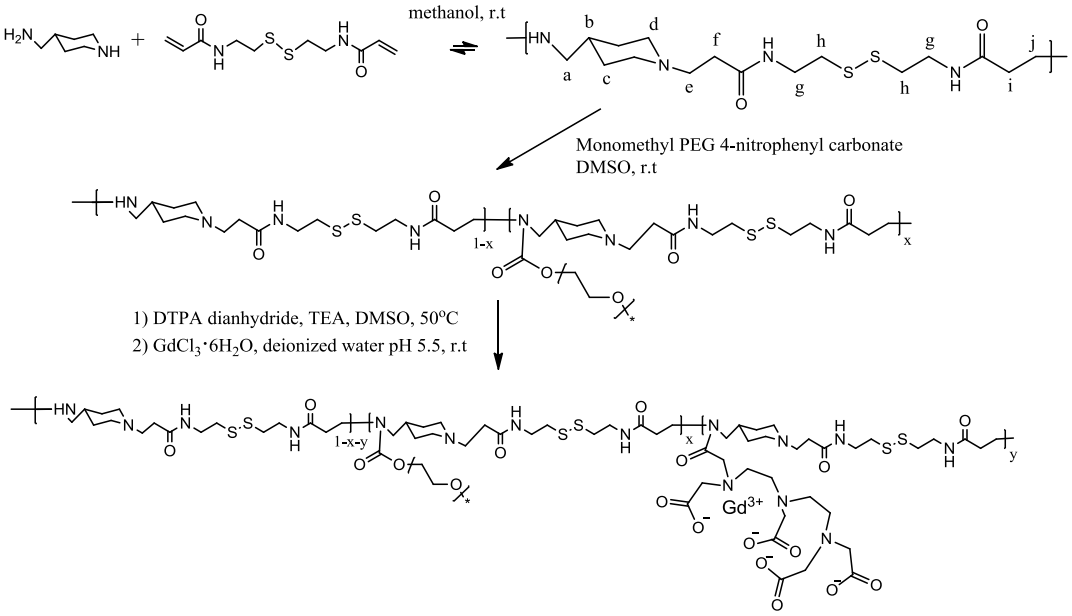

6.2. Experimental section

6.2.1. Materials

N,*N*-cystaminebis(acrylamide) (BAC) was purchased from Polysciences, Inc, 4-(aminomethyl)piperidine(AMPD) (99%) was purchased from Alfa Aesar, and DTPA dianhydride (98%), gadolinium (III) chloride hexahydrate, L-dithiothreitol (DTT), L-glutathione reduced (GSH) and xylenol orange sodium salt indicator for metal titration were purchased from Sigma Aldrich. Monomethyl PEG (~2000 g/mol) 4-nitrophenyl carbonate was prepared as in our previous report [419]. The other chemicals were of reagent grade and were used as purchased.

MCF-7 (human breast adenocarcinoma) cells and HepG2 (human hepatoma) cells were obtained from American Type Culture Collection

(ATCC, Rockville, MD). They were maintained in Dulbecco's modified eagle medium (DMEM, invitrogen) with 10% fetal bovine serum (FBS), 2 mM glutamine, 100 units/ml penicillin and 100 µg/ml streptomycin at 37 °C in an incubator with 5% CO_2 atmosphere.

6.2.2. Synthesis of poly(BAC-AMPD)

3.08 g (26.7 mmol) of AMPD were added into 40 mL of anhydrous methanol containing 6.96 g (26.7 mmol) of BAC under stirring at room temperature and argon purging. After 1 month, 0.03 g (0.27 mmol) of AMPD was added, and the reaction was continued for 1 more day. Then the solution was dialysed in methanol using membrane with a molecular weight cutting of 2000.

6.2.3. Preparation of poly(BAC-AMPD)-*g*-PEG-*g*-DTPA

10.17 g (4.5 mmol) of monomethyl PEG 4-nitrophenyl carbonate was added into 6.78 g (18 mmol) of dried poly(BAC-AMPD) dissolved in 85 mL of anhydrous dimethyl sulfoxide (DMSO) under stirring and argon purging at room temperature. 5 days later, the solution was dialyzed in methanol using membrane with a molecular weight cutting of 3500.

0.50 g (0.63 mmol) of dried poly(BAC-AMPD)-*g*-PEG in 6 mL of anhydrous DMSO was added dropwise into 9 mL of anhydrous DMSO containing 0.89 g (2.5 mmol) of DTPA dianhydride and 0.385 mL (2.7 mmol) of TEA at 50 ^{o}C under stirring and argon purging. 24 h later, the solution was dialyzed in deionized (DI) water using membrane with a molecular weight cutting of 1000 MWCO followed by lyophilized drying.

6.2.4. Complexation of poly(BAC-AMPD)-*g*-PEG-*g*-DTPA with Gd(III)

0.04 g (0.11 mmol) of gadolinium (III) chloride hexahydrate was added into 5 mL of deionized water containing 0.12 g of poly(BAC-AMPD)-*g*-PEG-*g*-DTPA at pH 5.5 under stirring at room temperature for overnight. Then excess gadolinium (III) chloride hexahydrate was removed by dialysis in deionized water using membrane with a molecular weight cutting of 1000. Xylenol orange sodium salt indicator was used to ensure a complete removal of Gd(III) ions. After all the Gd(III) ions were removed, the solution was lyophilized. Poly(BAC-AMPD)-*g*-PEG-*g*-Gd-DTPA was dissolved in deionized water for characterization.

6.2.5. *in vitro* cytotoxicity of poly(BAC-AMPD)-*g*-PEG-*g*-Gd-DTPA

Cytotoxicity of poly(BAC-AMPD)-*g*-PEG-*g*-Gd-DTPA was evaluated in MCF-7 and HepG2 cell lines. Viability of the cells was assessed by the standard thiazolyl blue [3-(4,5-dimethyliazolyl-2)-2,5-diphenyl tetrazolium bromide] (MTT) assay. This colorimetric assay allows determination of the number of viable cells through the metabolic activity of the cells.

The cancer cells were seeded in 96-well plates with a seeding density of 10,000 cells/well and were cultured in DMEM supplemented with 10% FBS and 1% penicillin-streptomycin solution in an incubator at 37^{o}C, 5% CO_2, and 95% relative humidity. The cells were allowed to adhere to the well bottom upon overnight incubation. Then the medium was replaced with the sample solutions of different concentrations. Meanwhile, wells containing only cell culture medium were prepared as untreated controls. At the predetermined time, the medium containing samples was aspirated and the

wells were washed with 1 ×PBS solution for two times to removed non-internalized sample. Then 100 μL of DMEM and 10 μL of MTT solution (5 mg/mL in 1 ×PBS solution) were added to the wells. After incubation for 4 h at 37 ^{o}C, the solution was removed and the formazan precipitate was dissolved in 100 μL of dimethyl sulfoxide (DMSO). The absorbance intensity of the solution was then quantified spectrophotometrically using a microplate reader (TECAN SpectraFluor Plus) at 570 nm. Cell viability was expressed by the following equation:

Cell viability (%) = Abssample / Abscontrol× 100%

Where Abssample was the absorbance for cells treated with samples, while Abscontrol was the absorbance for untreated control cells. All the tests were performed in multiples.

6.2.6. Degradation studies of poly(BAC-AMPD) and micelles of poly(BAC-AMPD)-*g*-PEG-*g*-Gd-DTPA

5.0 mg/mL of poly(BAC-AMPD) in pH 4.5 acetate buffer solution was treated with 10 mM of DTT at 37 ^{o}C under stirring for 2 h. GPC was applied to monitor the change in the molecular weight profile. 0.5 mg/mL of poly(BAC-AMPD)-*g*-PEG-*g*-Gd-DTPA in DI water was treated with 20 μM of GSH at 37 ^{o}C under stirring for certain time. Small amount of the samples were taken for dynamic light scattering measurement.

6.2.7. MRI T_1 relaxivity measurement

A multi-slice localization scan was used to acquire images in the transverse section (i.e. the transverse section of the barrel of the syringe) along the length

of the syringes containing the sample. The multi-slice images acquired were assessed to select slices with minimal heterogeneity and absence of bubbles. T_1 mapping was carried out with a spin-echo sequence with multiple TIs: 31 ms, 50 ms, 100 ms, 200 ms, 400 ms, 600 ms, 800 ms, 1000 ms, 1500 ms, 2000 ms, 3500 ms and 9980 ms with FOV = 56 × 75 mm, TE = 6.9 ms, TR = 10000 ms, slice thickness of 2 mm and number of slices = 1. The data was analysed using Matlab and the T_1 relaxivity calculated from homogenous regions within each sample using AMIDE as shown in Figure 6.7. Relaxivity, the gradient of the slope of relaxation rates as a function of the concentrations of the contrast agent, was then calculated.

6.2.8. Measurements

The molecular weight and distribution of poly(BAC-AMPD) was measured by gel permeation chromatography (GPC) with column and refractive index detector from Waters. The eluent was pH 4.5 acetate buffer solution with flow rate of 0.6 mL/min and the polymer concentration was 5 mg/mL. The ^{13}C and ^{1}H nuclear magnetic resonance (NMR) characterization of the polymers were done by Bruker 400 MHz NMR spectrometer with methanol-d_4 and deuterium oxide (D_2O) as solvent. The number of Gd(III) complexed was measured using the Dual-view Optima 5300 DV inductively coupled plasma optical emission spectrometry (ICP-OES). The hydrodynamic size and CMC of micelles prepared were determined by Brookhaven dynamic lightering scattering (DLS) instrument at 90^o (632.8 nm) using NNLS analysis. The micelles were also viewed under the high resolution Philips CM300 transmission electron microscope (FEGTEM), and the samples were prepared

by dropping micelles solution onto a copper grid cover with carbon followed by drying in a desiccator. Then, the dried grid was left in 1% osmium oxide in heptane for 2 h. The MRI experiments were carried out on a 7T MRI (ClinScan, BrukerBiospin GmbH, Germany) with a 20 cm bore size and a high performance gradient and shim coil (gradient strength of 63 G/cm, slew rate of 6300 T/m/s) interfaced to a Siemens console. A volume coil (diameter: 72 mm) was used for RF transmit and receive. The samples were placed at the isocentre of the magnet/coil.

6.3. Results and discussion

6.3.1. Synthesis of poly(BAC-AMPD)-*g*-PEG-*g*-Gd-DTPA

As shown in Scheme 6.1, poly(BAC-AMPD) was synthesized via Michael Addition polymerization of AMDP and an equimolar BAC in methanol. Although the reactivity sequence of the 3 amines in AMPD were 2^o amine (original) > 1^o amine >> 2^o amine (formed) [82,366], the 2^o amine (formed) participated in the polymerization process, which resulted in formation of poly(BAC-AMPD) with ~20% branching units determined via the ^{13}C NMR spectrum seen in Figure 6.1 [77]. The poly(BAC-AMPD) obtained is soluble in methanol and DMSO, but insoluble in water. Figure 6.2a and 6.3a show the GPC profile of poly(BAC-AMPD) in pH 4.5 acetate buffer solution and ^1H NMR spectrum of poly(BAC-AMPD) obtained in methanol-d_4 respectively. The molecular weight distribution of poly(BAC-AMPD) is wide with PDI of 2.6 which is reasonable for polymers obtained from multistage polymerization [82]. The two peaks in the GPC curve correspond to M_p of ca. 14034 and 1000 g/mol, respectively.

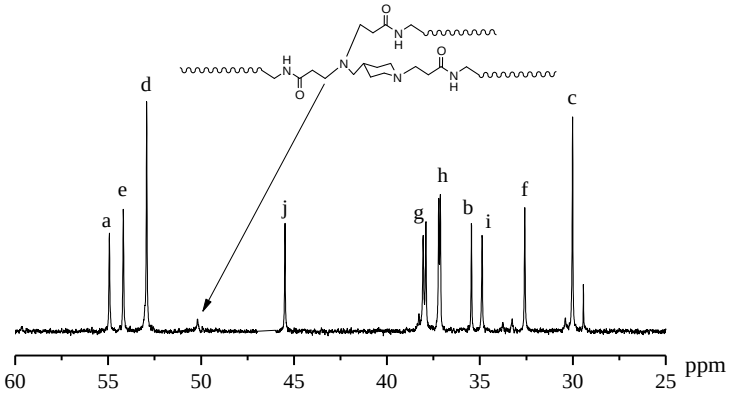

Figure 6.1. ^{13}C NMR of poly(BAC-AMPD) in methanol-d_4. (See corresponding peak attributions in scheme 6.1)

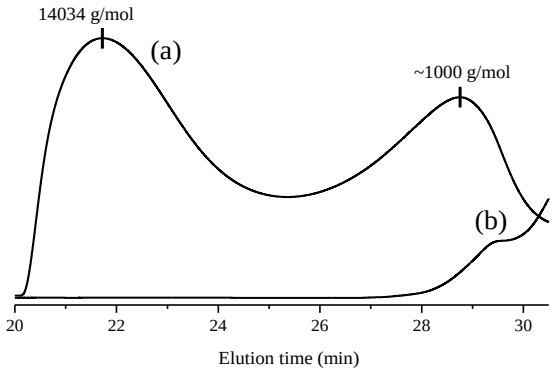

Figure 6.2. GPC spectra of poly(BAC-AMPD) incubated with 10 mM of DTT at 37 ^{o}C under stirring; a) before DTT incubation; b) 2 h after DTT incubation.

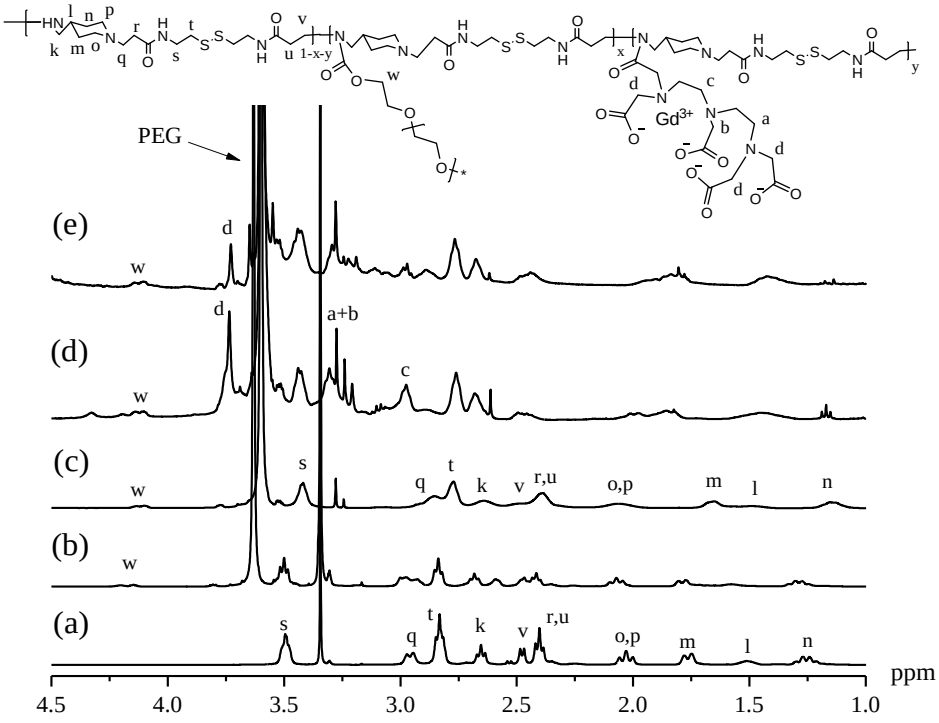

Figure 6.3. ^{1}H NMR spectrum of a) poly(BAC-AMPD) in methanol-d_4; b)poly(BAC-AMPD)-*g*-PEG in methanol-d_4; c) poly(BAC-AMPD)-*g*-PEG in D_2O; d) poly(BAC-AMPD)-*g*-PEG-*g*-DTPA in D_2O with pH 5.5; e) poly(BAC-AMPD)-*g*-PEG-*g*-DTPA in D_2O with pH 7.

PEG was grafted to poly(BAC-AMPD) via forming urethane groups through the reaction between the secondary amines in the backbone of poly(BAC-AMPD). The feed molar ratio of PEG to the 2^{o} amine in poly(BAC-AMPD) was kept at 1.25 : 5 to control the amount of PEG grafted for keeping some of the secondary amines for further functionalization. The molar ratio of the grafted PEG and BAC-AMPD unit in poly(BAC-AMPD) was determined to be 1: 5 using equation E6.1:

Molar ratio of PEG/BAC-AMPD = $I_{4.20}$ / $I_{1.29}$ (E6.1)

Where $I_{4.20}$ and $I_{1.29}$are the integral intensities of the peaks at 4.20 ppm and 1.29 ppm in Figure 6.2a, respectively.

Figures 6.3b and 6.3c shows the ^{1}H NMR spectrum of poly(BAC-AMPD)-*g*-PEG in methanol-d_4 and D_2O, respectively. Compared to Figure 6.3b, the peaks attributed to poly(BAC-AMPD) can still be observed but are noticeably broader. The relative peak intensity of the peaks in ^{1}H NMR spectrum is related to the mobility of the protons, and a broad and less intensive peak of a proton is caused by lower mobility in the solution [77,425-427]. Therefore the solubility of poly(BAC-AMPD) in aqueous solution is still not as good as in methanol, however, no species with a diameter higher than 10 nm could be observed in aqueous solution of poly(BAC-AMPD)-*g*-PEG using DLS.

DTPA was conjugated to poly(BAC-AMPD)-*g*-PEG via the reaction with the remaining secondary amines in poly(BAC-AMPD) to form amide bonds as illustrated in Scheme 6.1. Figure 6.3d shows the ^{1}H NMR spectrum of poly(BAC-AMPD)-*g*-PEG-*g*-DTPA in D_2O at pH 5.5. The grafting of DTPA is confirmed by the appearance of the characteristic peaks such as the peaks at 3.7 ppm attributed to DTPA [415,477]. However, the content of conjugated DTPA cannot be determined using ^{1}H NMR due to the self-assembly existed as discussed below.

Poly(BAC-AMPD)-*g*-PEG-*g*-Gd-DTPA was obtained through chelating with Gd(III) ions. The content of Gd(III) ions was determined using ICP-OES, and the result indicates that 1.9 out of 5 units of BAC-AMPD were complexed with Gd(III) ions. The composition of poly(BAC-AMPD)-*g*-PEG-*g*-Gd-DTPA is summarized in Table 6.1.

Table 6.1. Feed and actual molar ratio of poly(BAC-AMPD)-*g*-PEG-*g*-Gd-DTPA

	Poly(BAC-AMPD) / PEG	**Poly(BAC-AMPD) / PEG / DTPA**	**Poly(BAC-AMPD) / PEG / Gd(III)**
Feed ratio	5 / 1.25	5 / 1 / 20	5 / 1 / 4.2
Actual ratio	5 / 1	-	5 / 1 / 1.9

6.3.2. Self-assembly of poly(BAC-AMPD)-*g*-PEG-*g*-Gd-DTPA in aqueous solution

Self-assembly of poly(BAC-AMPD)-*g*-PEG-*g*-Gd-DTPA occurred in aqueous solution. Figure 6.4 shows TEM images of the micelles formed from the self-assembly of poly(BAC-AMPD)-*g*-PEG-*g*-Gd-DTPA with or without osmium oxide staining. Dark irregular regions can be observed in micelles without osmium oxide staining as shown in Figure 6.4a. These dark regions were confirmed to be rich in Gd(III) ions through energy dispersive X-ray spectroscopy. After stained with osmium oxide as shown in Figure 6.4b, the diameter of micelles was ca. 113 nm in dry state. The hydrodynamic size of the micelles in aqueous solution was determined to be ca. 188.1 ± 17.2 nm using DLS. The CMC of poly(BAC-AMPD)-*g*-PEG-*g*-Gd-DTPA in aqueous solution was determined to be ca. 60.2 µg/mL by plotting the average scattering intensity against the polymer concentrationas as illustrated in Figure 6.5 [77,428].

The structure of the self-assembly of poly(BAC-AMPD)-*g*-PEG-*g*-Gd-DTPA could not be investigated using ^{1}H NMR due to the existence of Gd(III). However, the self-assembly profile of the precursor of poly(BAC-AMPD)-*g*-PEG-*g*-DTPA could be investigated using ^{1}H NMR. As shown in

Figure 6.3d, the integral intensities of the peaks attributed to protons of AMPD unit are reduced significantly in comparison with the peaks attributed to BAC unit, e.g., ratio of the integrals of peak t and n is 3.8 times greater in Figure 2d than 2c. Meanwhile, the peaks of PEG are still obvious. This reflects that the self-assembly leads to a restricted mobility of these segments containing AMPD. Therefore, the self-assembly should be due to the formation of the ionic complex between the cationic amines of AMPD and DTPA and the anionic carbonate groups of DTPA. The ionization degree of the amine and carboxylic acid depends on pH; and a perfect polyelectrolyte complex is formed between cationic polymer and anionic polymer with an equimolar ratio between cationic group and anionic group together with the same polymer length [484]. Here there are different types of amines and carboxylic acid which have different pKa values [485,486], therefore different ionization profiles of the amine and carboxylic acid exist and result in a complicated pH dependence of the ionic complex. In comparison to Figure 6.3d, ^{1}H NMR spectrum of the assembly at pH 7, shown in Figure 6.3e, reflects that the integral intensities of the attributed to DTPA are reduced in comparison with those BAC. After Gd(III) was introduced, the formation of ionic complex still can be formed with Gd(III) being involved, and the self-assembly of poly(BAC-AMPD)-*g*-PEG-*g*-Gd-DTPA should be composed of the ionic complex with PEG shells.

The cytotoxicity of poly(BAC-AMPD)-*g*-PEG-*g*-Gd-DTPA was evaluated in MCF-7 and HepG2 cell lines. Low cytotoxicity was observed. Ca. 80% and 90% of MCF-7 and HepG2 cells are still viable after incubation with 200 μM of Gd(III) for 24 h, respectively, as shown in Figure 6.6.

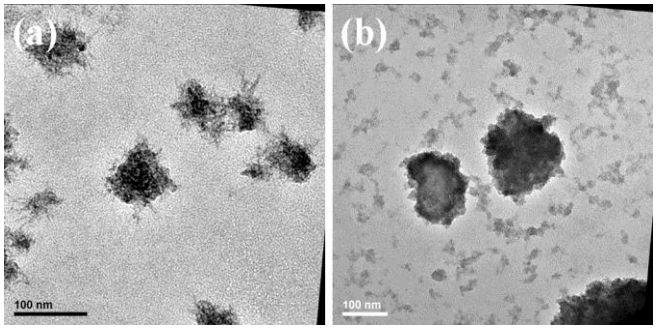

Figure 6.4. TEM images of a) unstained; b) osmium oxide stained, micelles of poly(BAC-AMPD)-*g*-PEG-*g*-Gd-DTPA.

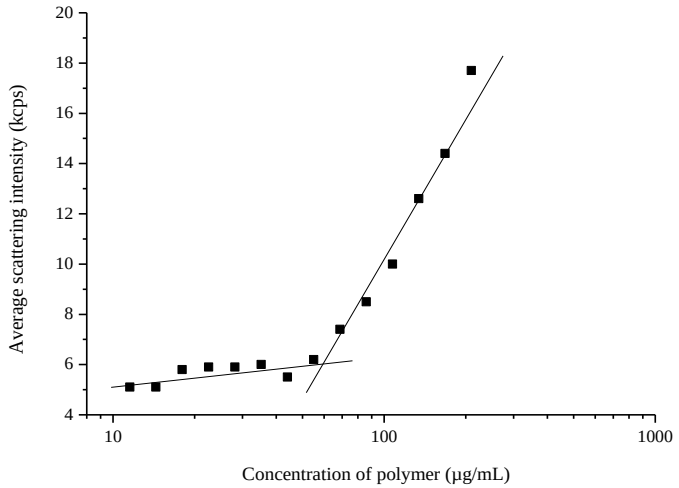

Figure 6.5. Relationship between the average scattering intensity from DLS measurements and the concentration of poly(BAC-AMPD)-*g*-PEG-*g*-Gd-DTPA (µg/mL) in deionized water.

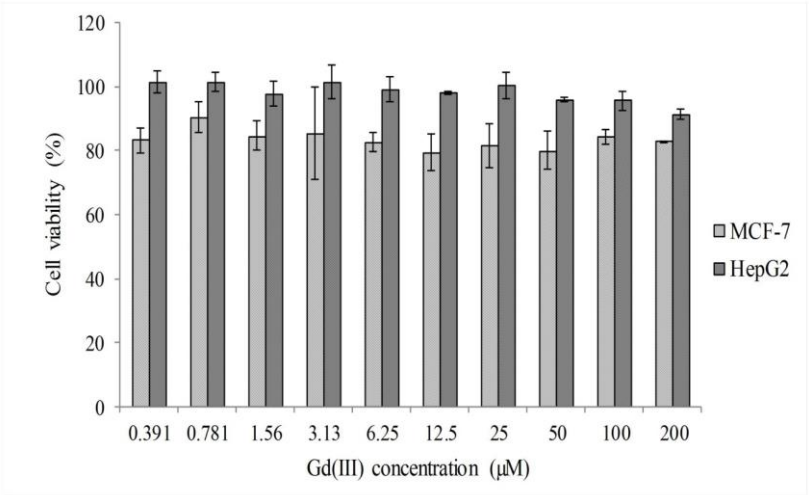

Figure 6.6. *in vitro* cytotoxicity of micelles of poly(BAC-AMPD)-*g*-PEG-*g*-Gd-DTPA in MCF-7 and HepG2. All data represent mean ± SD. (n = 3).

6.3.3. Degradation of poly(BAC-AMPD)-*g*-PEG-*g*-Gd-DTPA

The thiol-induced degradation of the backbone of poly(BAC-AMPD)-*g*-PEG-*g*-Gd-DTPA occurs readily. As shown in Figure 6.2b, almost complete degradation of poly(BAC-AMPD) can be observed in pH 4.5 acetate buffer solution in the presence of 10 mM of DTT after 2 h at 37 ^{o}C. Due to the formation of micelles via self-assembly, thiol-induced degradation of poly(BAC-AMPD)-*g*-PEG-*g*-Gd-DTPA could not be monitored using GPC. Instead the degradation of the micelles of poly(BAC-AMPD)-*g*-PEG-*g*-Gd-DTPA was monitored using DLS.

Figure 6.7 shows the change in the DLS profile of the micelles from 0.5 mg/mL of poly(BAC-AMPD)-*g*-PEG-*g*-Gd-DTPA in DI water at 37 ^{o}C in the presence of 20 μM of GSH which is close to the concentration of GSH in biological extracellular matrix. The scattering intensity decreases by 15% in 15 minutes of incubation, and another 10% and 40% in 60 minutes and 24 h respectively. From 0 h to 2h, no obvious change in the diameter of the micelles is observed. However, the increase in the diameter of the micelles becomes obvious, from ca. 206 nm at 2 h to ca. 512 nm at 24 h.

The micelles are composed of the ionic complex and PEG shells, and GSH can diffuse into the PEG shells more easily than into the ionic complex; hence the PEG segments are removed easily. When a part of the PEG shells is removed without leading to formation of aggregate, the light scattering intensity, which is dependent on the mass of the assembly formed, decreases. When more PEG shells is removed leading to the formation of aggregate of the ionic complex, the size of the assembly increases. The formation of ionic complex of AMPD, Gd-DTPA and DTPA can reduce the degradation rate, but

the inherent degradability of poly(BAC-AMPD) as shown in Figure 6.2 will ensure the degradability of the assembly of poly(BAC-AMPD)-*g*-PEG-*g*-Gd-DTPA.

Due to low concentration of GSH used, no significant change in scattering intensity and size can be observed after 24 h of incubation. Similar behaviour was observed in the degradation profile of the nanosize complex of disulfide-containing poly(amido amine)s and DNA in the presence of 10 μM of DTT [373]. Here the molar ratio of GSH / disulfide bond is only 1 / 25 and a plasma GSH concentration of 20 μM were adopted, an obvious degradation of the assembly of poly(BAC-AMPD)-*g*-PEG-*g*-Gd-DTPA could be observed. A fast degradation can be expected when ample thiol compound is presented *in vivo*.

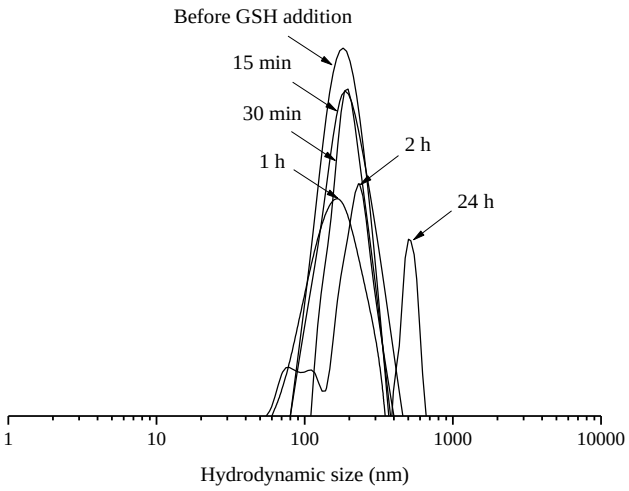

Figure 6.7. Hydrodynamic size distribution of micelles of poly(BAC-AMPD)-*g*-PEG-*g*-Gd-DTPA (0.2 mM of Gd(III)) with 20 μM of GSH. (Normalized intensity)

6.3.4. Relaxivity of poly(BAC-AMPD)-*g*-PEG-*g*-Gd-DTPA

To determine the r_1 of the micelles of poly(BAC-AMPD)-*g*-PEG-*g*-Gd-DTPA, the T_1 of different Gd(III) concentrations were measured and plotted

against Gd(III) concentration. The micelles exhibited a r_1 value of 5.90 ± 0.09 $mM^{-1}s^{-1}$ which is 50% higher than Gd-DTPA (~ 4 $mM^{-1}s^{-1}$) as seen in Figure 6.8. The micelles have greater r_1 than most small molecular Gd(III) based contrast agents, due to the reduced molecular tumbling [31,487].

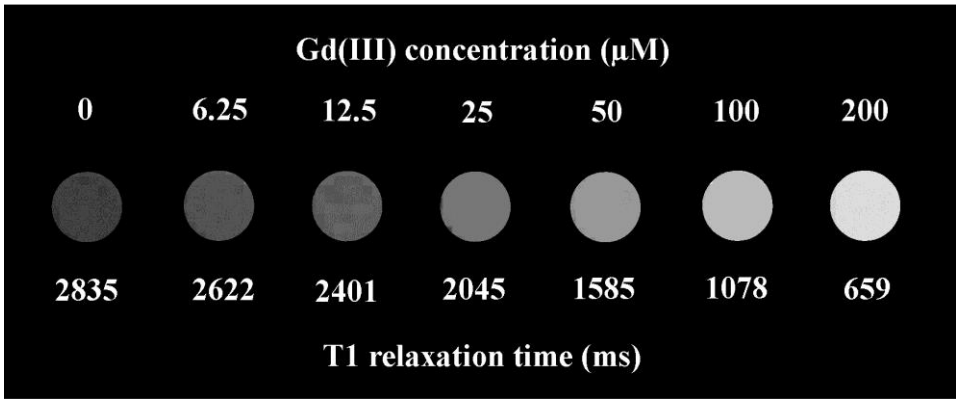

Figure 6.8. T_1 relaxation time measured at each Gd(III) concentration of the micelles of poly(BAC-AMPD)-*g*-PEG-*g*-Gd-DTPA.

6.3.5. Redox-responsive relaxivity of poly(BAC-AMPD)-*g*-PEG-*g*-Gd-DTPA

Although macromolecular Gd(III) based MRI contrast agents like the one describe above with high relaxivity can improve the sensitivity of disease diagnosis, they are unable to reflect the metabolic statues of the diseased tissues. Therefore, an interesting class of contrast agent known as activatable MRI contrast agent which exhibits a change in relaxivity value usually higher upon stimulation, is highly desired. For some of these contrast agents, they are sensitive to metal ions like Ca^{2+} [488], Zn^{2+} [489] and Fe^{2+} [490,491] which reveal the conditions of many cellular processes and metabolic mechanisms. Hypoxia conditions in many diseases like cancer and ischemic diseases can lead to variation in the pH of cellular environment [491]. There are MRI contrast agents which rely on the change in number of water molecules

coordinated (*q*) [493-495], rate of proton exchange [496,497] or rotational correlation time (τ_r) [498], to achieve activatable relaxivity in tissues with abormal pH level. Activatable MRI contrast agent can also be tuned to react to enzymatic response [499,500]. Last but not least is the redox-responsive contrast agents, these agents are exceptionally useful in the diagnosis of diseases. Louie A.Y. and coworkers developed a series of Gd(III) based activatable agents which rely on the change in *q*. In their early effort, spirobenzopyran- and (dinitro)spirobenzopyran-Gd-DO3A displayed decrease in relaxivities upon stimulation by UV or UV/NADH respectively [501,502]. Instead of raising *q* in the stable closed ring (SP) isomeric form, the indoline part interrupted water coordination and sterically hindered the access of water molecules. However, further modification on the molecule facilitated the increase in *q*, resulting in the contrast agent to exhibit a reversible positive change in relaxivity upon activation [503]. On the other hand, work on Gd-DO3A with thiol moiety demonstrated that through the reversible binding of thiol on cysteine-34 of human serum albumin, the contrast agent can exhibit an increase in relaxivity which was attributed to the reduced in τ_r [504,505].

As presented in the earlier paragraph, the micelles of poly(BAC-AMPD)-*g*-PEG-*g*-Gd-DTPA has an r_1 value of 5.90 ± 0.09 $mM^{-1}s^{-1}$. Therefore to demonstrate the redox responsive relaxivity of the contrast agents, 5 mM of DTT was added to induce the change in r_1 value. As expected, after DTT treatment shown in Figure 6.9, the micelles exhibit r_1 value of 6.48 ± 0.06 $mM^{-1}s^{-1}$ which is a ca. 10% increase in the relaxivity. Since micelles incubated at 37 ^{o}C without DTT treatment, show r_1 statistically similar to the value before incubation seen Table 6.2, the rise in relaxivity is mainly induced by

DTT reduction. As the redox interaction had no direct effect on the amines or carbonyls that coordinate the Gd(III) ions, the number of coordinated water molecules, value *q*, should stay the same before and after degradation, thus is not responsible for the change in relaxivity [494,495,499,506]. Therefore, it is likely that due to the degradation of the micelles of poly(BAC-AMPD)-*g*-PEG-*g*-Gd-DTPA in the presence of DTT, the change in micellar structure and integrity facilitates proton exchange and increase the relaxivity. This preliminary result is highly promising and exciting, showing that the micelles of poly(BAC-AMPD)-*g*-PEG-*g*-Gd-DTPA is redox activatable. The increase in relaxivity upon redox stimulation allows the pinpoint and highlight of redox related diseased tissues for example, malignant tumor, in a signal suppressed background.

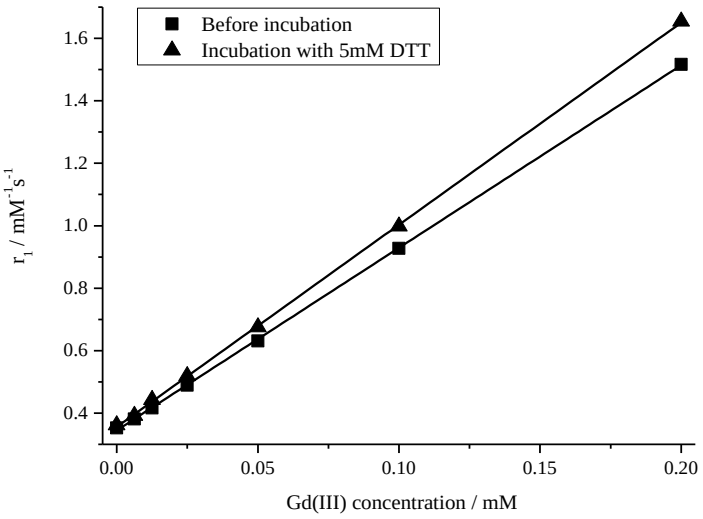

Figure 6.9. The change in relaxivity of micelles of poly(BAC-AMPD)-*g*-PEG-*g*-Gd-DTPA after incubation with 5 mM DTT.

Table 6.2: Relaxivities of micelles of poly(BAC-AMPD)-*g*-PEG-*g*-Gd-DTPA

	r_1 / $mM^{-1}s^{-1}$
Before incubation	5.90 ± 0.09
After incubation without DTT	5.82 ± 0.05
After incubation with 5mM DTT	6.48 ± 0.06

6.4. Conclusions

DTPA were conjugated to poly(BAC-AMPD)-*g*-PEG via the reaction with 2^o amines of poly(BAC-AMPD) remained. A high payload of Gd(III) chelates was achieved by conjugation to 40% of BAC-AMPD unit of poly(BAC-AMPD). Poly(BAC-AMPD)-*g*-PEG-*g*-Gd-DTPA could self-assemble to form micelles in aqueous solution due to electrostatic interactions between the cationic amines and anionic carbonate groups. The micelles consist of the cores of ionic complex of DTPA/Gd-DTPA and poly(BAC-AMPD) and the PEG shell. With a low cytotoxicity, a readily realized thiol-induced degradability and a higher r_1 poly(BAC-AMPD)-*g*-PEG-*g*-Gd-DTPA is a promising T_1 contrast agent for producing better MRI imaging with lower side effects.

Chapter 7

Redox-Responsive "Turn-on" Fluorescent Imaging with Aggregation-Induced Emission (AIE) Characteristic

7.1. Introduction

Intracellular compartments of cells are much more reductive than the extracellular matrix, and the combined redox state of cellular redox couples, like GSH/GSSG which is often regarded as the major redox buffer, forms the redox environment [43,507]. Redox homeostasis is vital in many physiological functions like oxygen homeostasis, cell adhesion, immune response, apoptosis and the defence against free radical-induced oxidative stress [44-46]. Furthermore, in particularly, oxidative stress is closely linked to many diseases such as cancer, cardiovascular diseases, diabetes, neurological disorder, ageing [508-510] e.g., a high level of GSH in tumor is related to the resistance to therapies [50].

The cellular redox environment has been explored to develop better therapeutic and diagnostic approaches. Many types of redox-responsive systems have been fabricated for safe and efficient drug and gene delivery [43,64,77,373,507,511-513]. On the other hand, suitable methods to determine the cellular redox state are also being pursued. There are very few non-invasive techniques to detect *in vivo* redox environment, such as diagnosing GSH level using $^{99}Tc^{m}$-glutathione tracer in SPECT and isotope labelled GSH as contrast agent in MRS but with low spatial resolution [514,515] and

sensitivity [516,517]. Several procedures, such as spectromic assays and gas chromatography-mass spectroscopy (GC-MS), developed to quantify *ex vivo* GSH level [44], however, these methods are invasive and sensitive to artifactual oxidation and sample manipulation [518].

Fluorescence imaging technique, usually using fluorophores, can provide cost-effective and real time diagnosis of physiological processes at a molecular level [519-522]. Through using "turn-on" fluorescent imaging probes activated by pH [523,524], enzyme [525-527], Zn^{2+} [528,529] and redox [530-534], the image contrast can be improved for the diagnosis of certain biological status due to an augmented signal to background ratio [11,535-538]. Fluorophores applied can be divided into two categories, i.e., with concentration quenching or aggregate caused quenching (ACQ) characteristic [519-535,536-539] or aggregate-induced emission (AIE) characteristic [540-542]. Fluorophores with ACQ characteristic can only be applied at a low concentration which will limit its applications. However, this disadvantage can be overcome by using fluorophores with AIE characteristic [540-542].

Redox-responsive fluorophores with ACQ characteristic have been investigated for imaging [532,543]. Redox "turn-on" fluorophore with AIE characteristic was also developed for the detection of thiol species [544], which is more promising in providing intense imaging, but it is not suitable for *in vivo* applications due to its poor biocompatibility including the poor water solubility and short circulation time in blood stream. One solution is to encapsulate fluorophore in suitable carriers such as polymers to form functional nanoparticles [545]. In order to obtain the redox-responsive

nanoparticles for biological fluorescence imaging, the polymer carrier adopted should be redox-responsive itself and preferably enhance the aggregation behaviours of the fluorophore with AIE characteristic. In this work, redox-responsive amphiphilic poly(ethylene glycol) (PEG)- and cholesterol (CE)-conjugated poly(amido amine)s, poly(BAC-AMPD)-*g*-PEG-*g*-CE [62], is applied for the preparation of redox 'turn-on" fluorescent nanoparticles with AIE characteristic. As shown in Scheme 7.1, the nanoparticles are produced by loading the fluorophore with redox "turn-on" AIE characteristic, TPE-MI, in the cores of the micelles of poly(BAC-AMPD)-*g*-PEG-*g*-CE. The PEG shells of the nanoparticles can promote penetration across the mucus membranes of many organs [273-278], prevent nonspecific proteins adsorption, provide long-circulation time in blood stream [279-284], and facilitate endocytosis [285]; and the cores displays redox "turn-on" AIE characteristic with emission intensity increasing with GSH concentration. The redox 'turn-on" fluorescence profile of the nanoparticles with AIE characteristic is demonstrated in MCF-7 and HepG2 cells. These features make the fluorescent nanoparticles developed here promising for more sensitive imaging and differentiation of cellular redox environment.

Scheme 7.1. Redox-responsive fluorescent nanoparticles.

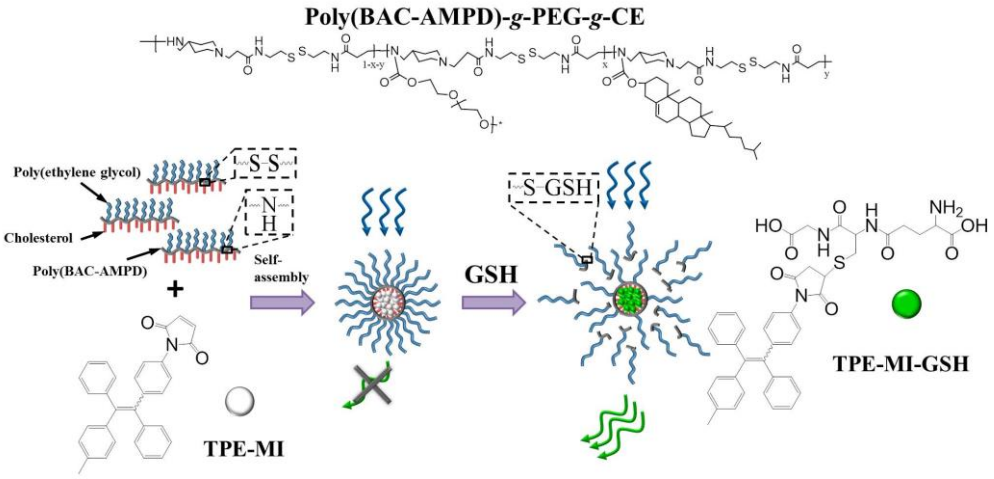

7.2. Experimental section

7.2.1. Materials

TPE-MI and poly(BAC-AMPD)-*g*-PEG-*g*-CE were prepared following the previous reports [77,544], respectively. L-glutathione (GSH) and chloroform-d from Sigma Aldrich were used as received. Dimethylsulfoxide (DMSO) and deuterium oxide (D_2O) used in this study were purchased from Tedia and Cambridge Isotope Laboratories, Inc. respectively. MCF-7 (human breast adenocarcinoma cell line) and HepG2 (human hepatoma cell line) were obtained from American Type Culture Collection (ATCC, Rockville, MD). They were maintained in Dulbecco's modified eagle medium (DMEM, invitrogen) with 10% fetal bovine serum (FBS), 2 mM of glutamine, 100 units/ml of penicillin and 100 µg/ml streptomycin at 37 °C in an incubator with 5% CO_2 atmosphere.

7.2.2. Preparation of fluorescent nanoparticles

9 mL of PBS was added at a rate of 0.25 mL/h to 1 mL of DMSO containing 10 mg of poly(BAC-AMPD)-*g*-PEG-*g*-CE and 1 mg of TPE-MI using a syringe pump. The suspension formed was dialyzed using membrane with a molecular weight cutting-off of 1000 in PBS or deionized water to remove DMSO. After dialysis, any large TPE-MI aggregates were removed by filtration through a filter with a pore diameter of 0.45 μm. Sterile solvents and apparatus were used when the nanoparticles were prepared for cell works.

To measure the content of TPE-MI, the fluorescent nanoparticles in aqueous solution was lyophilized, and a certain amount of the dried fluorescent nanoparticles was dissolved in chloroform-d for ^{1}H NMR measurement. Using equation E7.1 and E7.2, the TPE-MI loading capacity was determined.

$$\text{Molar ratio of TPE-MI/CE} = I_{7.02\text{-}7.09} / (I_{4.47} \times 14) \quad \text{(E7.1)}$$

Where $I_{7.02\text{-}7.09}$ and $I_{4.47}$ are the integral intensity of the peaks at 7.02-7.09 ppm and 4.47 ppm, respectively.

$$\text{Loading capacity (\%)} = Mw_{\text{TPE-MI loaded}} \times V_{\text{Eq(E4.1)}} \times 1.79 / (Mw_{\text{(BAC-AMPD)}} \times 4.3 + Mw_{\text{PEG}} \times 1 + Mw_{\text{CE}} \times 1.79 + Mw_{\text{TPE-MI loaded}} \times V_{\text{Eq(E4.1)}} \times 1.79) \times 100\% \quad \text{(E7.2)}$$

Where Veq(E7.1) is the molar ratio of TPE-MI / CE calculated in equation E7.1.

7.2.3. Fluorescence measurement of GSH reacted nanoparticles

A designed amount of GSH was added into 3 mL of buffer nanoparticles solution with certain concentration at 37^{o}C at a designed pH. At a

predetermined time interval, the fluorescence emission was measured under 280 nm irradiation.

7.2.4. *in vitro* cytotoxicity evaluation of samples

Cytotoxicity of micelles of poly(BAC-AMPD)-*g*-PEG-*g*-CE and the nanoparticles were evaluated in MCF-7 and HepG2 cells. Viability of the cells was assessed by the standard thiazolyl blue [3-(4,5-dimethyliazolyl-2)-2,5-diphenyl tetrazolium bromide] (MTT) assay. The cells were seeded in 96-well plates with a seeding density of 10,000 cells/well and were cultured in DMEM supplemented with 10% FBS and 1% penicillin-streptomycin solution in an incubator at 37 ^{o}C, 5% CO_2, and 95% relative humidity. The cells were allowed to adhere to the well bottom upon overnight incubation. Then the medium was replaced with the sample solutions of different concentrations. Meanwhile, wells containing only cell culture medium were prepared as untreated controls. After 24 h, the medium containing samples was aspirated and the wells were washed with 1 ×PBS solution for two times to removed non-internalized sample. Then 100 μL of DMEM and 10 μL of MTT solution (5 mg/mL in 1 ×PBS solution) were added to the wells. After incubation for 4 h at 37 ^{o}C, the solution was removed and the formazan precipitate was dissolved in 100 μL of DMSO. The absorbance intensity of the solution was then quantified spectrophotometrically using a microplate reader (TECAN SpectraFluor Plus) at 570 nm. Cell viability was expressed by the following equation:

Cell viability (%) = Abssample / Abscontroll × 100%

where Abssample was the absorbance for cells treated with samples, while Abscontroll was the absorbance for untreated control cells. All the tests were performed in multiples.

7.2.5. Cellular imaging

MCF-7 and HepG2 cells were seeded in 8 chamber borosilicate coverglass with a cell density of 5,000 cells/chamber and were cultured in DMEM supplemented with 10% FBS and 1% penicillin-streptomycin solution in an incubator at 37^{o}C, 5% CO_2, and 95% relative humidity. The cells were allowed to adhere to the chamber bottom upon overnight incubation. Then, the medium was replaced with the mixture (50% (v/v)) of DMEM and the buffer nanoparticles solution in 1 X PBS with final concentration of 0.2 mg/mL. At a predetermined time, the cells were imaged without removing the medium containing nanoparticles and fixation. As a control experiment, after 16 h of incubation with the nanoparticles, 5 mM of GSH was added to chambers followed by additional 6 h incubation.

7.2.6. Measurements

Nuclear magnetic resonance (NMR) spectra were obtained on a Bruker DPX 400 MHz NMR spectrometer. A Brookhaven BIS200 laser light scattering system was used for dynamic light scattering measurements. The light source is a power adjustable vertically polarized 35 mW argon ion laser with a wavelength of 633 nm. The scattering angle was fixed at 90 ^{o} for measuring the hydrodynamic radius (*R*h) and the average scattering intensity. *R*h values were obtained using a CONTIN analysis. TEM images were obtained using a

high resolution Philips CM300 transmission electron microscope (FEGTEM) at 300 kV, and the samples were prepared by dropping micelles suspension onto a copper grid cover with carbon followed by drying in a desiccator. Then, the dried grid was left in 1% osmium oxide in heptane for 2 h. Fluorescence emission spectra were recorded on a Perkin–Elmer LS55 Fluorescence Spectroscopy instrument fitted with a R928-sensitive sample photomultiplier. Confocal imaging was done with Olympus Fluoview FV1000 with excitation wavelength of 405 nm.

7.3. Results and Discussion

7.3.1. Characterization of fluorescent nanoparticles

Suitable formulations such as encapsulation within PEG-conjugated lipid [15-17] and bovine serum albumin (BSA) [18,19]or conjugation to chitosan [10] can improve the biocompatibility and functionality of AIE fluorophores. Here pH- and redox-responsive poly(BAC-AMPD)-*g*-PEG-*g*-CE [77] was applied for the encapsulation of the compound, TPE-MI [544],to prepare the redox 'turn-on" nanoparticles with AIE characteristic. The encapsulation was realized through self-assembly of amphiphilic poly(BAC-AMPD)-*g*-PEG-*g*-CE in phosphate buffered solution in the presence of TPE-MI, with the hydrophobic TPE-MI being loaded in the cores of the formed micelles. Figure 7.1A shows TEM images of the fluorescent nanoparticles obtained. The diameter of the nanoparticles was determined to be ca. 89 nm in dry state using TEM, and ca. 186.4 ± 14.7 nm in PBS buffer solution when measured using DLS. The content of TPE-MI in the nanoparticles is ca. 8% which was determined from ^{1}H NMR spectrum of the fluorescent nanoparticles in

chloroform-d as shown in Figure 7.1B(a). Figure 7.1B(b) shows the ^{1}H NMR spectrum of the fluorescent nanoparticles in D_2O. In comparison with Figure 7.1B(a), the peaks attributed to TPE-MI is absent in Figure 7.1B(b). Meanwhile, only the peaks attributed to PEG at ca. 3.5 ppm can be observed, and the peaks attributed to CE and poly(BAC-AMPD) disappear. This indicates that the nanoparticles consist of hydrophilic PEG shells, and hydrophobic cores of poly(BAC-AMPD), CE and TPE-MI which are inaccessible to D_2O [77,425-427]. The successful encapsulation of TPE-MI in the micelles of poly(BAC-AMPD)-*g*-PEG-*g*-CE is also confirmed by the changes in the fluorescence profile of TPE-MI after being encapsulated as described below. The cytotoxicity of the nanoparticles developed was evaluated in MCF-7 and HepG2 cells using MTT assay. As shown in Figure 7.2, the nanoparticles show low cytotoxicity, with 80% of the cells still viable when 100 µg/mL of nanoparticles are incubated with the cells for 24 h.

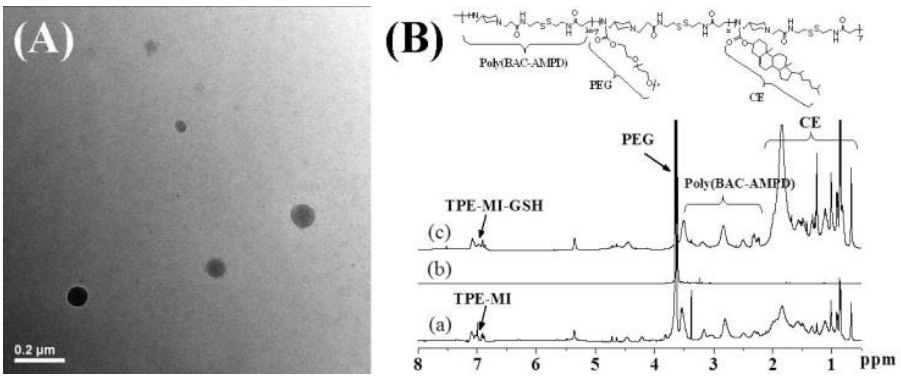

Figure 7.1. A) TEM image of the fluorescent nanoparticles stained with osmium oxide; B) ^{1}H NMR spectra of a) the fluorescent nanoparticles in chloroform-d; b)the fluorescent nanoparticles in D_2O; c) precipitate from PBS buffer solution of 0.3 mg/mL of the fluorescent nanoparticles after reaction with 2 mM of GSH for 24 h in chloroform-d.

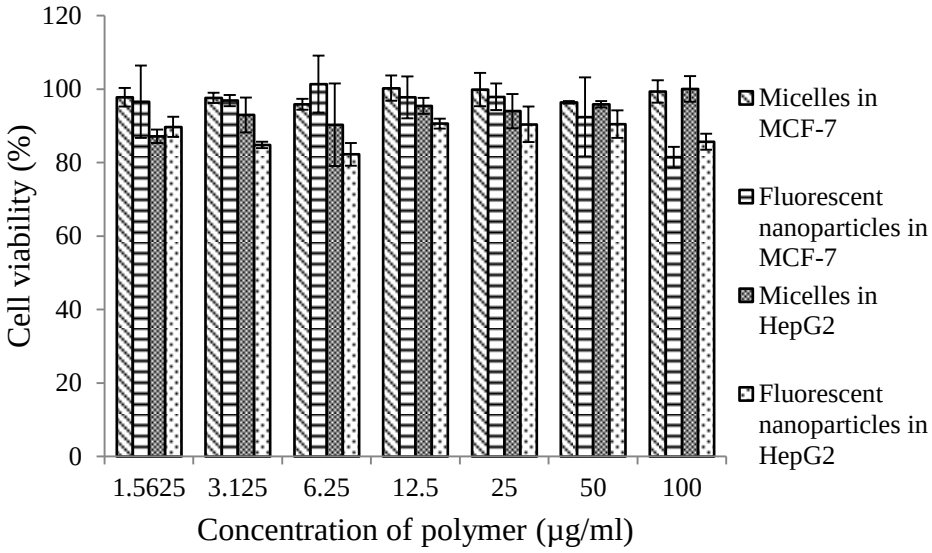

Figure 7.2. *in vitro* cytotoxicity of micelles of poly(BAC-AMPD)-*g*-PEG-*g*-CE and the fluorescent nanoparticles in MCF-7 and HepG2 cells.

7.3.2. Redox "turn on" fluorescent behaviours of nanoparticles

The nanoparticles can form a stable dispersion in PBS buffer solution as shown in Figure 7.3a because of the PEG shells and nanosize. The redox "turn-on" fluorescence profile of the nanoparticles in buffer solution was investigated in the presence of GSH. The interaction process of the nanoparticles with GSH should consist of the diffusion of GSH into the cores of the micelles, the degradation of poly(BAC-AMPD)-*g*-CE before reaching TPE-MI, and the reaction with TPE-MI to form TPE-MI-GSH. The redox-induced degradation of the micelles of poly(BAC-AMPD)-*g*-PEG-*g*-CE resulted in formation of aggregates which precipitated in the PBS buffer solution [77]. Similarly redox-induced degradation of the fluorescent nanoparticles led to obvious precipitation as shown in Figure 7.3c after reaction with 2 mM of GSH. In comparison, a stable suspension of free TPE-MI-GSH, from the reaction between free TPE-MI and GSH, in PBS buffer solution was formed as shown in Figure 7.3b. ^{1}H NMR result reflects that the

precipitate formed consists of segments with a higher content of hydrophobic CE as shown in Figure 7.1B(c), and the peaks at ca. 7 ppm which correspond to the protons of the benzenes also indicates the presence of the AIE dye in the precipitate.

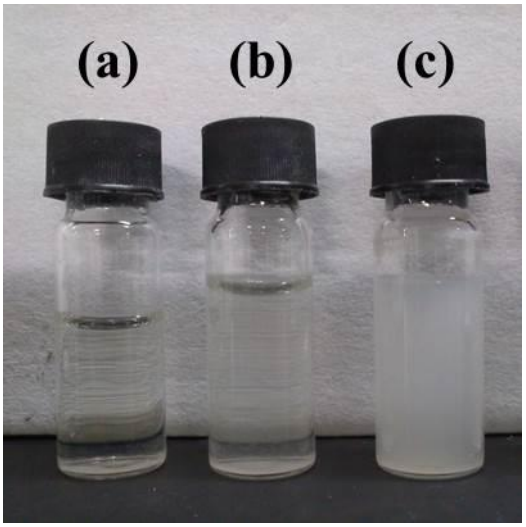

Figure 7.3. Photograph of PBS buffer solution of a) 0.3 mg/mL of fluorescent nanoparticles; b) free TPE-MI-GSH from 0.1 mg/mL of TPE-MI after reaction with 2 mM of GSH, and c) fluorescent nanoparticles (as shown in Figure 7.3a) after reaction with2 mM of GSH for 2 h.

Figure 7.4 shows the time dependent photoluminescence spectra of the PBS buffer solution of nanoparticles in the presence of 10 mM of GSH. The emission peaks are located at ca. 475 nm; and the emission intensity initially increases rapidly with time, but levels off after 60 minutes. This reflects that it takes time for GSH to diffuse into the cores of the micelles and degrade poly(BAC-AMPD)-*g*-CE before reacting with TPE-MI. TPE-MI is non-fluorescent regardless of its aggregation state, however, the product of the reaction between TPE-MI and thiol group is fluorescent due to the restricted intramolecular rotation and blockage of the non-radiative decay channels in precipitated state or being conjugated to polymer [540,544]. Here the product

of the reaction between GSH and TPE-MI, TPE-MI-GSH, might be in aggregates or dispersed in the precipitates composed of segments containing hydrophobic CE with its intramolecular rotation being restricted, which led to fluorescence.

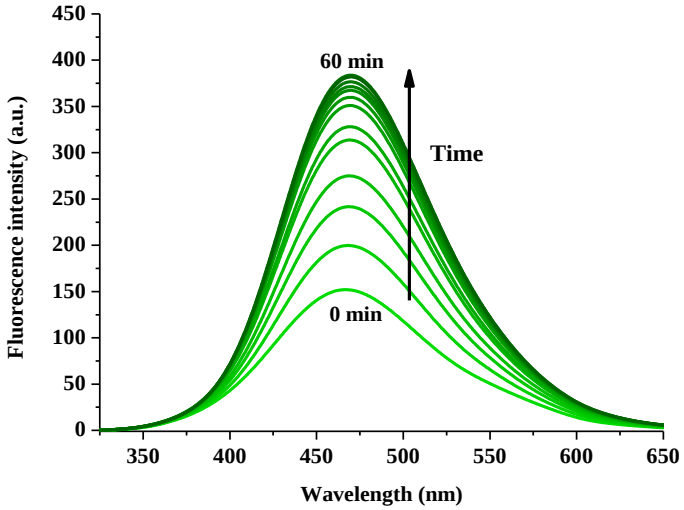

Figure 7.4. Time dependent emission spectra of PBS buffer solution of 0.1 mg/mL of fluorescent nanoparticles after reaction with 10 mM of GSH at pH 7. The time interval is 5 minutes.

Considering the physiological condition where the amount of reduced thiols in the intracellular compartments is in excess, the nanoparticles should be the limiting agents in the reaction. As a result, the tissues redox environment cannot be differentiated if the concentrations of nanoparticles endocytosized by the cells are similar. However, before all the nanoparticles can react with reduced thiols, the amount of TPE-MI-thiol formed should be related to the diffusion rate of reduced thiols. A higher concentration of reduced thiols should lead to faster diffusion, which in turn results in formation of a higher amount of the fluorescent TPE-MI-thiol with a higher fluorescent intensity. Therefore, it is meaningful to investigate the

fluorescence profile of the nanoparticles before complete reaction with reduced thiols. According to Figure 7.4, 15 minutes after treatment with 10 mM of GSH is a suitable time point when a significant fluorescence intensity augment can already be observed.

7.3.3. pH effect on fluorescent behaviours of nanoparticles

The micelles of poly(BAC-AMPD)-*g*-PEG-*g*-CE is pH responsive due to the amino groups along the polymer backbone [77], so it can be expected that pH of the buffer solution of the nanoparticles will affect the fluorescence profile. Figure 7.5 shows the pH dependent emission spectra of aqueous solution of 0.15 mg/mL of fluorescent nanoparticles after reaction with 10 mM of GSH for 15 minutes. When pH is changed from pH 3 to pH 8, the peaks remain at ca. 475 nm, but the fluorescence intensity varies. The highest emission intensity is observed at pH 7. The weaker intensity at pH 8 should be due to the slower diffusion of GSH into the less protonated and more hydrophobic cores of the nanoparticles. The emission intensity also decreases as the pH is lowered from 7 to 3. The increase in protonation degree of the amino groups is likely to cause a decline in aggregation density of the precipitate from the degradation of poly(BAC-AMPD)-*g*-CE, which should lower the restriction on the intramolecular rotation of TPE-MI-GSH formed.

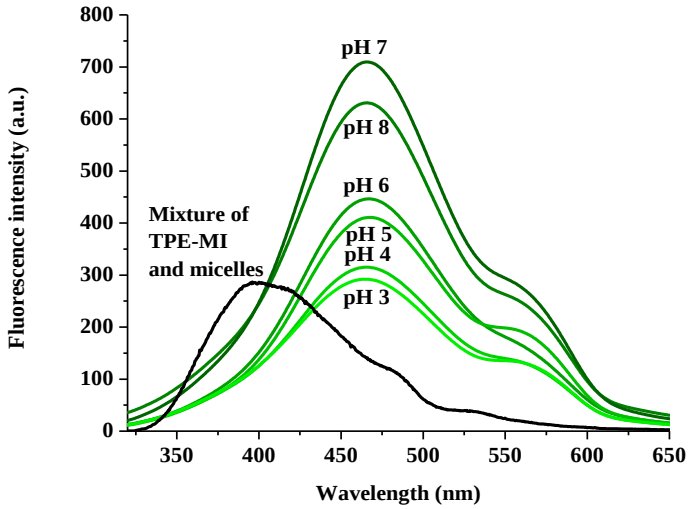

Figure 7.5. pH dependent emission spectra of aqueous solution of 0.15 mg/mL of fluorescent nanoparticles after reaction with 10 mM of GSH for 15 minutes; and emission spectrum of aqueous solution mixture of 0.067 mg/mL of free TPE-MI and 0.23 mg/mL of the micelles of poly(BAC-AMPD)-*g*-PEG-*g*-CE after reaction with 10 mM of GSH at pH 7 for 2 h.

7.3.4. Evaluation of redox environment

In a control experiment, an buffer solution of a mixture of 0.067 mg/mL of free TPE-MI and 0.23 mg/mL of the micelles of poly(BAC-AMPD)-*g*-PEG-*g*-CE at pH 7 was treated with 10 mM of GSH for 2 h, and the fluorescence emission spectrum is also shown in Figure 7.5. The peak position of the emission is ca. 400 nm, which can be taken as a summation of the emissions of free TPE-MI-GSH and poly(BAC-AMPD)-*g*-PEG-*g*-CE (amino-containing polymers were reported to be fluorescent [377,546,547].) with the peaks at 420 nm and 370 nm, respectivly as seen in Figure 7.6.In comparison, the emission peak of the fluorescent nanoparticles with TPE-MI encapsulated within the cores of the micelles shifts from 420 nm to 475 nm, and the fluorescence intensity of the nanoparticles containing 0.012 mg/mL of TPE-MI is ca. 750 a. u. much higher than ca. 300 a. u. from 0.067 mg/mL of free TPE-MI. So the nanoparticles show more than 10 times higher emission efficiency than free TPE-MI. The improved emission efficiency and red shift

might be due to a higher restriction on the intramolecular rotation of TPE-MI-GSH trapped in the precipitate composed of segments containing extremely hydrophobic CE. This observation also confirms the encapsulation of TPE-MI in the cores of the micelles as other hydrophobic species [77].

While the redox- "turn-on" fluorescence property of the nanoparticles is advantageous in improving imaging contrast, it is equally attractive to be applicable for differentiation of cellular redox environment. Thus, the relationship between the fluorescence intensity of the nanoparticles with various GSH concentrations was investigated. Figure 7.7 shows the change in the emission intensity of the PBS buffer solution of nanoparticles at pH 7 after reaction with 10 μM to 10 mM of GSH, which is the *in vivo* GSH concentration range [43,507], for 15 minutes. It can be observed that the fluorescence intensity increases with GSH concentration, and the intensity obtained after reaction with 10 mM of GSH is ca. 3 times higher than that with 10 μM of GSH. Under this condition, the amount of TPE-MI-GSH formed is dependent on the rate of GSH diffusion into the cores. A steeper concentration gradient should cause GSH to diffuse into the nanoparticles faster, resulting in the formation of a higher amount of TPE-MI-GSH. In this way, it is possible to apply the fluorescent nanoparticles to achieve differential imaging of redox environment.

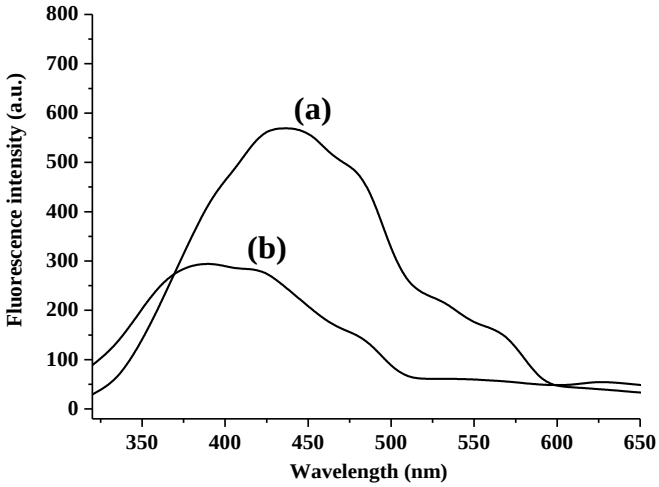

Figure 7.6. Emission spectra of a) 10 mM GSH treated free TPE-MI dispersed in pH 7 PBS; b) PBS buffer micelle solution of poly(BAC-AMPD)-*g*-PEG-*g*-CE at pH 7.

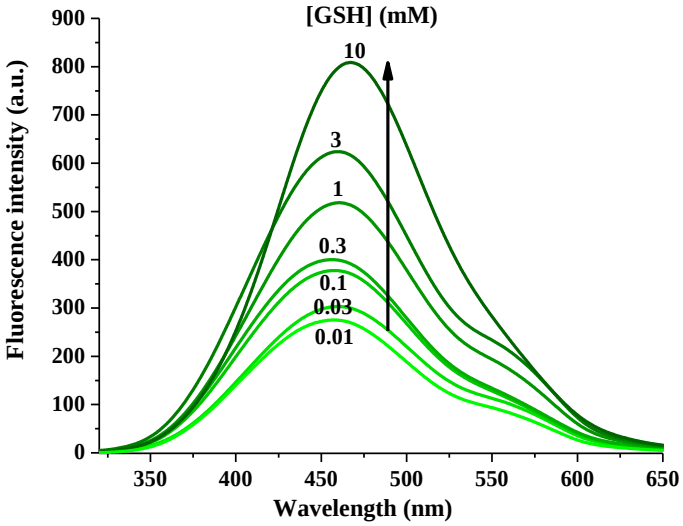

Figure 7.7. [GSH] dependent emission spectra of PBS buffer solution of 0.2 mg/mL of fluorescent nanoparticles at pH 7 after reaction with GSH for 15 minutes.

7.3.5. Enhanced cellular imaging

Redox 'turn-on" fluorescent behaviour of the fluorescent nanoparticles was evaluated in MCF-7 and HepG2 cells, which have a high intracellular GSH level [373]. Typical results are presented in Figures7.8 and 7.9. Figures 7.8a, 7.8e, 7.8c and 7.8g illustrate the confocal microscopy images of MCF-7 and

HepG2 cells incubated with the fluorescent nanoparticles for 22 h respectively. Note that the cells were imaged without removing the medium containing the nanoparticles and fixation. Figure 7.8a and 7.8c shows that only the fluorescence signal within the cytoplasm of live MCF-7 and HepG2 cells can be seen, and an obvious contrast between the intracellular compartments and the culture medium can observed. After the nanoparticles were endocytosized by the cells, the free reduced thiol-containing species diffused into the nanoparticles, degraded the cores and reacted with the encapsulated TPE-MI to form fluorescent species. In contrast, the concentration of free reduced thiol-containing species in the medium was so low that no redox-"turn-on" fluorescence could be observed from those nanoparticles that remained outside of the cells. However, when 5 mM of GSH was added into the medium after 16 h of incubation as positive control, the nanoparticles in the medium, either well dispersed or aggregated, became fluorescent as shown in Figures 7.8b and 7.8d. Since the MCF-7 and HepG2 cells incubated with 5mM of GSH are still healthy and have the integrity of their cell membrane retained, the brightening of the background is should not be due to to the leakage of the fluorescent nanoparticles back into the medium.

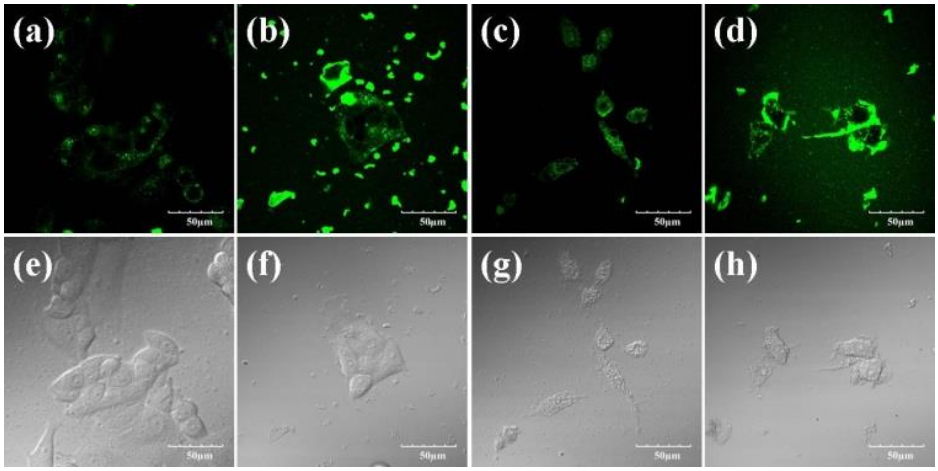

Figure 7.8. Confocal microscopy imaging of live MCF-7(a,b,e,f) and HepG2 (c,d,g,h) cells after incubation with the fluorescent nanoparticles for a,c,e,g) 22 h; b,d,f,h) 16 h followed by additional 6 h incubation with 5 mM of GSH without removing the medium containing the nanoparticles and fixation.

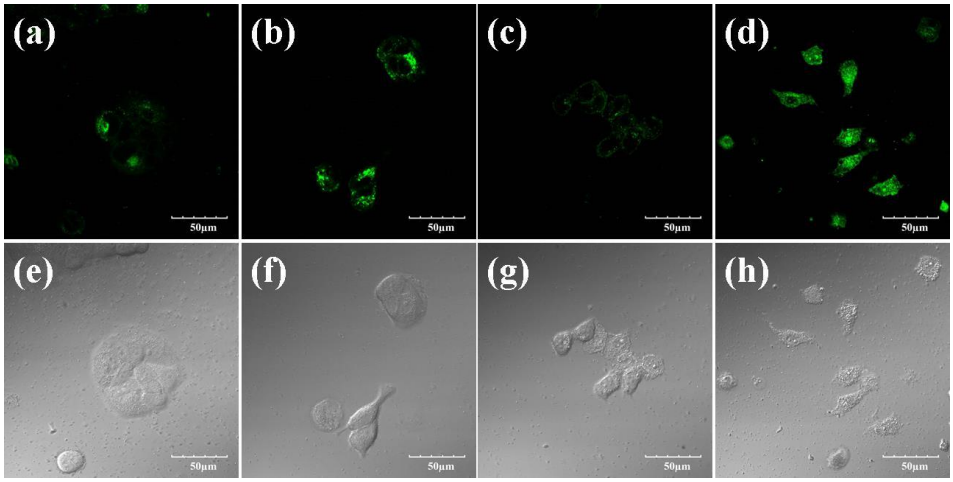

Figure 7.9. Confocal microscopy imaging of live MCF-7 (a,b,e,f) and HepG2 (c,d,g,h) cells after incubation with the fluorescent nanoparticles for a,c,e,g) 6 h; b,d,f,h) 30 h without removing the medium containing the nanoparticles and fixation.

7.4. Conclusions

Redox-responsive nanoparicles with AIE characteristic are developed for achieving redox-responsive fluorescence imaging. The fluorescent nanoparticles are obtained by encapsulating redox-responsive fluorophores with AIE characteristic in redox responsive polymers via self-assembly. The

nanoparticles obtained are nanosize with PEG shells and have low cytotoxicity, and show redox "turn-on" fluorescence with AIE characteristic. The encapsulated TPE-MI displayed a higher efficiency and red shift in emission in comparison to free TPI-MI upon reaction with GSH. It took ca. 60 min for the fluorescent nanoparticles to reach the maximum intensity after reaction with 10 mM of GSH. Before reaching the maximum intensity, the fluorescence intensity is pH dependent with the highest intensity obtained at pH 7 within a range of pH 3 – 8; and it is important that the fluorescence intensity increases with GSH concentration, which make it possible to image the level of thiol species. The redox- "turn-on" fluorescence behaviour of the fluorescent nanoparticles with AIE characteristic was verified in MCF-7 and HepG2 cells. The fluorescent nanoparticles provided obvious imaging contrast between the intracellular compartments and extracellular matrix. These features make the fluorescent probes promising for bioimaging with a high contrast and differentiation of cellular redox environment. The *in vivo* applications will be investigated.

Chapter 8

Conclusions and Future Recommendations

8.1. Conclusions

In general, linear, branched, and hyperbranched redox-responsive poly(amido amine)s are obtained, and thereon delivery systems developed have been demonstrated to be promising for safe and efficient delivery of anti-cancer drug, DOX, preparation of safe macromolecular MRI contrast agents, and fluorescence imaging agents to provide imaging with improved contrast and indication of redox level. Further, the following key points can be concluded:

- Linear poly(BAC-AMPD) was produced by applying a mixture of 40% methanol and 60% DMSO (v/v) as a solvent for Michael Addition polymerization of trifunctional amine, AMPD, with an equimolar diacrylamide, BAC. Amphiphilic poly(BAC-AMPD)-*g*-PEG-*g*-CE was obtained by conjugating PEG and cholesterol onto the linear poly(BAC-AMPD) through reactions with the 2^{o} amine groups. Self-assembly of poly(BAC-AMPD)-*g*-PEG-*g*-CE in aqueous solution formed micelles with PEG shells and cores composed of poly(BAC-AMPD) and CE. DOX could be successfully loaded into the micelles, and DOX loaded micelles showed pH- and redox-responsive drug release and could also form redox-induced aggregates. These factors contribute to the higher efficacy of the DOX loaded micelles of poly(BAC-AMPD)-*g*-PEG-*g*-CE in killing cancer cells than free drug. The biodegradability and high efficacy of DOX loaded micelles in killing cancer cells render poly(BAC-AMPD)-*g*-PEG-*g*-

CE promising for preparation of drug delivery system for safe and efficient cancer chemotherapy.

- Vinyl terminated hyperbranched poly(amido amimes) was synthesized via Michael addition polymerization of AMDP with double molar of BAC in ethanol. After converting the terminal vinyl groups to primary amines via reaction with excess AMPD, PEG was conjugated to form hyperbranched poly(BAC2-AMPD1)-PEG. pH- and redox-responsive micelles with PEG shells and hydrophobic cores of poly(BAC2-AMPD1) can be formed via self-assembly of hyperbranched poly(BAC2-AMPD1)-PEG in aqueous solution. In comparison with linear and 20% branched poly(BAC-AMPD)-*g*-PEG, hyperbranched poly(BAC2-AMPD1)-PEG formed the largest micelles with the highest DOX loading capacity and loading efficiency. In terms of DOX release profile, more DOX were released at pH 5 and with 10 mM GSH. Endocytosis of micelles and DOX loaded micelles of hyperbranched poly(BAC2-AMPD1)-PEG was readily realized by HepG2 and MCF-7 regardless of GSH level, but a lower GSH level in HepG2 might result in a slower degradation of the micelles. However, differing GSH level shows unnoticeable effects on the degradation profiles of the micelles in MCF-7 cells. Imaging and quantifying the DOX levels and distribution in HepG2 and MCF-7 cells indicate that significant amount of DOX can be located within the nucleus. In comparison with free DOX-HCl, DOX-loaded micelles of hyperbranched poly(BAC2-AMPD1)-PEG displays a lower and comparable cytotoxicity in HepG2 and MCF-7 cells, respectively.

- DTPA were conjugated to poly(BAC-AMPD)-*g*-PEG via the reaction with 2^{o} amines of poly(BAC-AMPD) remained. A high payload of Gd(III) chelates was achieved by conjugation to 40% of BAC-AMPD unit of poly(BAC-AMPD). Poly(BAC-AMPD)-*g*-PEG-*g*-Gd-DTPA could self-assemble to form micelles in aqueous solution due to electrostatic interactions between the cationic amines and anionic carbonate groups. The micelles consist of the cores of ionic complex of DTPA/Gd-DTPA and poly(BAC-AMPD) and the PEG shell. With a low cytotoxicity, a readily realized thiol-induced degradability and a higher r_1 poly(BAC-AMPD)-*g*-PEG-*g*-Gd-DTPA is a promising T_1 contrast agent for producing better MRI imaging with lower side effects.

- Redox-responsive nanoparicles with AIE characteristic are developed for achieving redox-responsive fluorescence imaging. The fluorescent nanoparticles are obtained by encapsulating redox-responsive fluorophores with AIE characteristic in redox responsive polymers via self-assembly. The nanoparticles obtained are nanosize with PEG shells and have low cytotoxicity, and show redox "turn-on" fluorescence with AIE characteristic. The encapsulated TPE-MI displayed a higher efficiency and red shift in emission in comparison to free TPI-MI upon reaction with GSH. It took ca. 60 min for the fluorescent nanoparticles to reach the maximum intensity after reaction with 10 mM of GSH. Before reaching the maximum intensity, the fluorescence intensity is pH dependent with the highest intensity obtained at pH 7 within a range of pH 3 – 8; and it is important that the fluorescence intensity increases with GSH concentration, which make it possible to image the level of thiol species. The redox "turn-

on" fluorescence behaviour of the fluorescent nanoparticles with AIE characteristic was verified in MCF-7 and HepG2 cells. The fluorescent nanoparticles provided obvious imaging contrast between the intracellular compartments and extracellular matrix. These features make the fluorescent probes promising for bioimaging with a high contrast and differentiation of cellular redox environment. The *in vivo* applications will be investigated.

8.2. Future recommendations

Although the PEG- and cholesterol- grafted linear poly(BAC-AMPD) based DOX delivery system discussed in chapter 4 is highly stable and more effective in killing cancer cells than free DOX-HCl, it has relatively low drug loading capacity and has a very slow DOX release rate after the initial burst release which may not be suitable for some treatment. Therefore, these are some suggestions which may be able to overcome these issues.

- As mentioned in chapter 5, the loading capacity of a delivery system is affected by a few factors and one of them is the compatibility of the hydrophobic polymer/molecules and the drugs used. Therefore, to improve the loading capacity of this system, a variety of hydrophobic polymers/molecules, ranging from long linear ones like C_{12} alky chains, or small compact hydrophobic molecules like phenylalanine and aromatic molecules, can be tested to solubilize the drugs within the micelles core. This work can be very tedious but with the right hydrophobic polymer/molecule, the loading capacity of the system can definitely be enhanced.

- As for hastening the DOX release rate, similarly the hydrophobic content of the amphiphilic polymer can be altered. Either grafting lesser number of cholesterol or substitute cholesterol with slight lesser hydrophobic molecules like C_8 alky chain. This reduced in hydrophobicity might decrease the attraction of DOX and allow faster release.

Although the above suggestions might overcome the issue of low drug loading capacity and slow DOX release, the change in the hydrophobic component might also alter the degradation characteristic of the system which is the formation of aggregate upon degradation, a property that can be useful in killing cancer cells.

The hyperbranched poly(BAC2-AMPD1)-PEG based delivery system in chapter 5 has a higher DOX loading capacity and can release all of its loaded DOX in a considerable rate but the cytotoxicity of the system is not ideal.

- Since the cytotoxicity of a system depends heavily both on the drug release profile and cellular uptake of the system, improvement can be made in this area. Clearly shown in the result in chapter 5, the DOX loaded micelles upon stimulated is able to fully release its loaded DOX in 72 h. Thus, the likely possible reason for its low cytotoxicity is its poor cellular uptake and this can be improved by conjugating the system with targeting ligands and cell penetrating peptides. For example, arginine-glycine-aspartic acid (RGD) peptide is well known for its high and specific affinity for $\alpha_v\beta_3$-integrin which are over-expressed in endothelial cells during angiogenesis of tumors and deoxyglucosamine which is an analog of glucose is reported

to be rapidly taken by tumor due to its over-expressed glucose transporters while cell penetrating peptides facilitate the endocytosis of the nanoparticles by the cells. With numerous primary amines available, conjugation processes like using NHS esters and imidoesters reaction or even condensation with carboxylic acids to form amide bonds can be done easily.

- Furthermore, it also interesting to investigate how the amphiphilic polymers, which are very unlike conventional linear diblock polymers in term of structure, conform to form micelles with core/shell structure.
- For the hyperbranched poly(amido amine)s, besides self-assembling into micelles, it is possible to form unimolecular micelles. Unlike conventional micelles where many polymer chains self-assemble to form one micelle, unimolecular micelles do not face stability/dissociation issue which is commonly associated to polymeric or surfactant micelles under certain conditions like high salt and low polymer concentration. As the hyperbranched poly(amido amine)s is insoluble in water, the hydrophilicity of the polymer must be improved via reaction with water soluble monomer like *N*,*N*-methylenebis(acrylamide). With well-proportioned ratio, the resulting hyperbranched poly(amido amine)s is water soluble and still degradable. Making use of the plentiful surface amines, moieties with different functions like targeting ligands (as mentioned above), cell penetrating peptides, fluorescence dyes and Gd(III) chelates can be conjugated. Furthermore, with structural voids present, drugs still can be loaded, thus achieving multiple functional capabilities. However, an challenge for this approach is the polydispersity of the

hyperbranched poly(amido amine)s synthesized. More optimum polymerization conditions must be explored to narrow the polydispersity of the polymer.

The redox-induced biodegradable macromolecular MRI contrast agent in chapter 6 has shown to be able to degrade in the biological extracellular conditions. However, to improve the system, more works can be done.

- The r_1 value of this system is not high enough when compared with many macromolecular MRI contrast agent. A possible reason is the complexation of the cationic AMPD and the anionic DTPA might have repel water molecules from the Gd(III) ions. Therefore, different methods can be employed to ensure the Gd-DTPA is located on the surface of the micelles instead of within the micelles. One such method is via nanoprecipitation. With hydrophobic interaction as the driving force for the self-assembly, the Gd-DTPA which is water soluble will be forced to the outer region of the micelles.
- In chapter 6.3.5, the redox-induced biodegradable macromolecular MRI contrasat agent has shown to have redox-responsive relaxivity. However, the increase in relaxivity is not sufficient. Therefore to improve this, a practical approach is to lower the initial r_1 of the contrast agent and a possible way is to increase the hydrophobicity of the polymer to expel more water molecules out of the micellar core where most of the Gd(III) ions are located. Thus, reducing the number of water molecules coordinated to the Gd(III) ions and lower the r_1 value.

Although the redox-responsive bioimaging agent mentioned in chapter 7 can enhance imaging contrast and has to potential to differentiate redox environment, the wavelengths that it can be excited and it emits is not suitable to *in vivo* imaging.

- For maximum tissue penetration, radiation in the near infra-red (NIR) region is often mentioned and used in *in vivo* fluorescence imaging. Therefore, to make this system for practical for clinical use, like imaging of sub-surface tissue, the encapsulation of suitable dye to form NIR bioimaging agent is needed.
- Furthermore, like mentioned earlier the redox-responsive bioimaging agent can also be conjugated with targeting ligand or cell-penetrating peptides to improve cellular uptake. This allows high concentration of fluorescent nanoparticles to accumulate in targeted tissue and thus can further improve imaging contrast.

More applications of poly(amido amine)s can also be explored in the area of gene delivery. A popular and common approach to delivery gene is to complex negatively charged gene to positively charged polymers, an prime example is poly(ethylenimine) (PEI). Since poly(amido amine)s have numerous amount of amine groups, the polymers might be a suitable polymer candidate for gene delivery. Furthermore, the presence of disulfide bonds in the polymers can aid in the release of gene in nucleus where the level of GSH is significant high.

Besides gene delivery, the anti-bacterial properties of poly(amido amine)s can also be investigated. The cationic nature of poly(amido amine)s

helps the polymers to get adsorbed and diffuse through the bacterial cell wall which are usually negatively charged. Then, the polymers can reach the cell membrane and disrupt its integrity.

Here, the poly(amido amine)s developed have been demonstrated in both drug delivery and imaging applications. On the basis of these understanding, theranostic systems which combine diagnosis and treatment in one platform can also be developed. A theranostic system from linear, branched and hyperbranched poly(BAC-AMPD) can be fabricated by physically or chemically integrate drugs and imaging moiety in one system.

References

[1] C. A. Lipinski, F. Lombardo, B. W. Dominy, and P. J. Feeney, *Advanced Drug Delivery Reviews*, **2001**, *46*, 3-26.

[2] A. M. Fernandez, K. Van derpoorten, L. Dasnois, K. Lebtahi, V. Dubois, T. J. Lobl, S. Gangwar, C. Oliyai, E. R. Lewis, D. Shochat, and A. Trouett, *Journal of Medicinal Chemistry*, **2001**, *44*, 3750-3753.

[3] V. P. Torchilin, *Pharmaceutical Research*, **2007**, *24*, 1-16.

[4] L. Brannon-Peppas and J. O. Blanchette, *Advanced Drug Delivery Reviews*, **2004**, *56*, 1649-1659.

[5] I. Brigger, C. Dubernet, and P. Couvreur, *Advanced Drug Delivery Reviews*, **2002**, *54*, 631-651.

[6] Z. Liao, H. Wang, X. Wang, P. Zhao, S. Wang, W. Su, and J. Chang, *Advanced Functional Materials*, **2011**,*21*, 1179-1186.

[7] Y. Liu, Z. Chen, C. Liu, D. Yu, Z. Lu, and N. Zhang, *Biomaterials*, **2011**, *32*, 5167-5176.

[8] W. L. Zhang, D. W. Yong, J. Huang, J. H. Yu, S. Y. Liu, and M. X. Fan, *Journal of Applied Polymer Science*, **2011**, *120*, 2596-2605.

[9] S. Y. Jeong, H. J. Kim, B. K. Kwak, H. Y. Lee, H. Seong, B. C. Shin, S. H. Yuk, S. J. Hwang, and S. H. Cho, *Nanoscale Research Letters*, **2010**, *5*, 1970-1976.

[10] K. Shiraishi, K. Kawano, Y. Maitani, and M. Yokoyama, *Journal of Controlled Release*, **2010**, *148*, 160-167.

[11] S. Luo, E. Zhang, Y. Su, T. Cheng, and C. Shi, *Biomaterials*, **2011**, *32*, 7127-7138.

[12] J. V. Frangioni, *Current Opinion in Chemical Biology*, **2003**, *7*, 626-634.

[13] M. Rawat, D. Singh, S. Saraf, and S. Saraf, *Biological and Pharmaceutical Bulletin*, **2006**, *29*, 1790-1798.

[14] N. Nishiyama and K. Kataoka, *Pharmacology and Therapeutics*, **2006**, *112*, 630-648.

[15] J. L. Geng, K. Li, W. Qin, L. Ma, G. G. Gurzadyan, B. Z. Tang, and B. Liu, *Small*, **2013**, *9*, 2012-2019.

[16] J. L. Geng, K. Li, D. Ding, X. H. Zhang, W. Qin, J. Z. Liu, B. Z. Tang, and B. Liu, *Small*, **2012**, *8*, 3655-3663.

[17] K. Li, W. Qin, D. Ding, N. Tomczak, J. L. Geng, R. R. Liu, J. Z. Liu, X. H. Zhang, H. W. Liu, B. Liu, and B. Z. Tang, *Scientific Reports*, **2013**, *3*.

[18] D. Ding, K. Li, W. Qin, R. Y. Zhan, Y. Hu, J. Z. Liu, B. Z. Tang, and B. Liu, *Advanced Healthcare Materials*, **2013**, *2*, 500-507.

[19] W. Qin, D. Ding, J. Z. Liu, W. Z. Yuan, Y. Hu, B. Liu, and B. Z. Tang, *Advanced Functional Materials*, **2012**, *22*, 771-779.

[20] Z. K. Wang, S. J. Chen, J. W. Y. Lam, W. Qin, R. T. K. Kwok, N. Xie, Q. L. Hu, and B. Z. Tang, *Journal of the American Chemical Society*, **2013**, *135*, 8238-8245.

[21] S. Stolnik, L. Illum, and S. S. Davis, *Advanced Drug Delivery Reviews*, **1995**, *16*, 195-214.

[22] H. Maeda, *Bioconjugate Chemistry*, **2010**, *21*, 797-802.

[23] H. Maeda, T. Sawa, and T. Konno, *Journal of Controlled Release*, **2001**, *74*, 47-61.

[24] K. Greish, *Methods in molecular biology*, **2010**, *624*, 25-37.

[25] S. Iwaki, K. Hanaoka, W. Piao, T. Komatsu, T. Ueno, T. Terai, and T. Nagano, *Bioorganic and Medicinal Chemistry Letters*, **2012**, *22*, 2798-2802.

[26] Technical information on Cremophor® EL Castor Oil, *BASF*, **2008**.

[27] N. P. Desai, V. Trieu, L. Y. Hwang, R. Wu, P. Soon-Shiong and W. J. Gradishar, *Anti-Cancer Drugs*, **2008**, *19*, 899-909.
[28] A. Hioki, A. Wakasugi, K. Kawano, Y. Hattori and Y. Maitani, *Biological and Pharmaceutical Bulletin*, **2010**, *33*, 1466-1470.;
[29] P. Panwar, B. Pandey, P. C. Lakhera and K. P. Singh, *International Journal of Nanomedicine*, **2010**, *5*, 101-108.
[30] a) N. Desai, V. Trieu, Z. Yao, L. Louie, S. Ci, A. Yang, C. Tao, T. De, B. Beals, D. Dykes, P. Noker, R. Yao, E. Labo, M. Hawkins and P. Soon-Shiong, *Clinical Cancer Research*, **2006**, *12*, 1317-1324. b) E. A. Murphy, B. K. Majeti, r. Mukthavaram, L. M. Acevedo, L. A. Barnes and D. A, Cheresh, *Molecular Cancer Therapeutics*, **2011**, *10*, 972-982.
[31] W. Cheng, Y. Ping, Y. Zhang, K. H. Chuang, and Y. Liu, *Journal of Healthcare Engineering*, **2013**, *4*, 23-46.
[32] P. H. Kuo, E. Kanal, A. K. Abu-Alfa, and S. E. Cowper, *Radiology*, **2007**, *242*, 647-649.
[33] H. S. Thomsen, P. Marckmann, and V. B. Logager, *Cancer Imaging*, **2007**, *7*, 130-137.
[34] A. Deo, M. Fogel, and S. E. Cowper, *Clinical Journal of the American Society Nephrology*, **2007**, *2*, 264-267.
[35] M. Goyen, *Radiography*, **2007**, *13*, 85-89.
[36] M. G. Wikstrom, M. E. Moseley, D. L. White, J. W. Dupon, J. L. Winkelhake, J. Kopplin, and R. C. Brasch, *Investigative Radiology*, **1989**, *24*, 609-615.
[37] H. Daldrup, D. M. Shames, M. Wendland, Y. Okuhata, T. M. Link, W. Rosenau, Y. Lu, and R. C. Brasch, *American Journal of Roentgenology*, **1998**, *171*, 941-949.
[38] A. Gossmann, Y. Okuhata, D. M. Shames, T. H. Helbich, T. P. L. Roberts, M. F. Wendland, S. Huber, and R. C. Brasch, *Radiology*, **1999**, *213*, 265-272.
[39] C. F. Van Dijke, R. C. Brasch, T. P. L. Roberts, N. Weidner, A. Mathur, D. M. Shames, J. S. Mann, F. Demsar, P. Lang, and H. C. Schwickert, *Radiology*, **1996**, *198*, 813-818.
[40] K. Turetschek, S. Huber, E. Floyd, T. Helbich, T. P. L. Roberts, D. M. Shames, K. S. Tarlo, M. F. Wendland, and R. C. Brasch, *Radiology*, **2001**, *218*, 562-569.
[41] L. Brannon-Peppas and J. O. Blanchette, *Advanced Drug Delivery Reviews*, **2004**, *56*, 1649-1659.
[42] J. M. Estrela, A. Ortega, and E. Obrador, *Critical Reviews in Clinical Laboratory Sciences*, **2006**, *43*, 143-181.
[43] F. Q. Schafer and G. R. Buettner, *Free Radical Biology and Medicine*, **2001**, *30*, 1191-1212.
[44] G. Kroemer, B. Dallaporta, and M. Resche-Rigon, *Annual Review of Physiology*, **1998**, *60*, 619-642
[45] E. Cadenas and K. J. A. Davies, *Free Radical Biology and Medicine*, **2000**, *29*, 222-230.
[46] M. Valko, D. Leibfritz, J. Moncol, M. T. D. Cronin, M. Mazur, and J. Telser, *The International Journal of Biochemistry and Cell Biology*, **2007**, *39*, 44-84.
[47] Z. Djuric, V. K. Malviya, G. Deppe, J. Malone, D. L. McGunagle, L. K. Heilbrun, B. A. Reading, and W. D. Lawrence, *Journal of Cancer Research and Clinical Oncology*, **1990**, *116*, 379-383.
[48] G. K. Balendiran, R. Dabur, and D. Fraser, *Cell Biochemistry and Function*, **2004**, *22*, 343-352.
[49] R. Franco, O. J. Schoneveld, A. Pappa, and M. I. Panayiotidis, *Archives of Physiology and Biochemistry*, **2007**, *113*, 234-258.
[50] A. A. Stavrovskaya, *Biochemistry*, **2000**, *65*, 95-106.

[51] Y. C. Wang, Y. Li, T. M. Sun, M. H. Xiong, J. Wu, Y. Y. Yang, and J. Wang, *Macromolecular Rapid Communications*, **2010**, *31*, 1201-1206.
[52] L. P. Lv, J. P. Xu, X. S. Liu, G. Y. Liu, X. Yang, and J. Ji, *Macromolecular Chemistry and Physics*, **2010**, *211*, 2292-2300.
[53] A. N. Koo, H. J. Lee, S. E. Kim, J. H. Chang, C. Park, C. Kim, J. H. Park, and S. C. Lee, *Chemical Communications*, **2008**, *48*, 6570-6572.
[54] A. Zhang, Z. Zhang, F. Shi, J. Ding, C. Xiao, X. Zhuang, C. He, L. Chen, and X. Chen, *Soft Matter*, **2013**, *9*, 2224-2233.
[55] A. N. Koo, K. H. Min, H. J. Lee, S. U. Lee, K. Kim, I. Chan Kwon, S. H. Cho, S. Y. Jeong, and S. C. Lee, *Biomaterials*, **2013**, *33*, 1489-1499.
[56] K. O. Jung, D. J. Siegwart, H. I. Lee, G. Sherwood, L. Peteanu, J. O. Hollinger, K. Kataoka, and K. Matyjaszewski, *Journal of the American Chemical Society*, **2007**, *129*, 5939-5945.
[57] S. Cajot, D. Schol, F. Danhier, V. Préat, M. C. Gillet De Pauw, and C. Jérôme, *Macromolecular Bioscience*, **2013**, *13*, 1661-1670.
[58] Y. Cheng, C. He, C. Xiao, J. Ding, K. Ren, S. Yu, X. Zhuang, and X. Chen, *Polymer Chemistry*, **2013**, *4*, 3851-3858.
[59] J. O. Kim, G. Sahay, A. V. Kabanov, and T. K. Bronich, *Biomacromolecules*, **2010**, *11*, 919-926.
[60] B. Gyarmati, B. Vajna, Á. Némethy, K. László, and A. Szilágyi, *Macromolecular Bioscience*, **2013**, *13*, 633-640.
[61] Y. Li, K. Xiao, J. Luo, W. Xiao, J. S. Lee, A. M. Gonik, J. Kato, T. A. Dong, and K. S. Lam, *Biomaterials*, **2011**, *32*, 6633-6645.
[62] J. H. Ryu, R. T. Chacko, S. Jiwpanich, S. Bickerton, R. P. Babu, and S. Thayumanavan, *Journal of the American Chemical Society*, **2010**, *132*, 17227-17235.
[63] Y. Xu, F. Meng, R. Cheng, and Z. Zhong, *Macromolecular Bioscience*, **2009**, *9*, 1254-1261.
[64] D. C. Wu, X. J. Loh, Y. L. Wu, C. L. Lay, and Y. Liu, *Journal of the American Chemical Society*, **2010**, *132*, 15140-15143.
[65] K. Kataoka, A. Harada, and Y. Nagasaki, *Advanced Drug Delivery Reviews*, **2001**, *47*, 113-131.
[66] H. Sun, B. Guo, R. Cheng, F. Meng, H. Liu, and Z. Zhong, *Biomaterials*, **2009**, *30*, 6358-6366.
[67] H. Sun, B. Guo, X. Li, R. Cheng, F. Meng, H. Liu, and Z. Zhong, *Biomacromolecules*, **2010**, *11*, 848-854.
[68] T. Thambi, H. Y. Yoon, K. Kim, I. C. Kwon, C. K. Yoo, and J. H. Park, *Bioconjugate Chemistry*, **2011**, *22*, 1924-1931.
[69] L. Y. Tang, Y. C. Wang, Y. Li, J. Z. Du, and J. Wang, *Bioconjugate Chemistry*, **2009**, *20*, 1095-1099.
[70] T. Thambi, G. Saravanakumar, J. U. Chu, R. Heo, H. Ko, V. G. Deepagan, J. H. Kim, and J. H. Park, *Macromolecular. Research*, **2013**, *21*, 100-107.
[71] Wang, J., Yang, G., Guo, X., Tang, Z., Zhong, Z., and Zhou, S. *Biomaterials*, **2014**, *35*, 3080-3090.
[72] X. Zhang, F. Du, J. Huang, W. Lu, S. Liu, and J. Yu, *Colloids and Surfaces B: Biointerfaces*, **2012**, *100*, 155-162.
[73] C. Yu, C. Gao, S. Lü, C. Chen, Y. Huang, and M. Liu, *Chemical Engineering Journal*, **2013**, *228*, 290-299.
[74] J. H. Ryu, R. Roy, J. Ventura, and S. Thayumanavan, *Langmuir*, **2010**, *26*, 7086-7092.
[75] M. Cao, H. Jin, W. Ye, P. Liu, L. Wang, and H. Jiang, *Journal of Applied Polymer Science*, **2012**, *123*, 3137-3144.
[76] J. Li, M. Huo, J. Wang, J. Zhou, J. M. Mohammad, Y. Zhang, Q. Zhu, A. Y. Waddad, and Q. Zhang, *Biomaterials*, **2012**, *33*, 2310-2320.

[77] W. Cheng, J. N. Kumar, Y. Zhang, and Y. Liu, *Macromolecular Bioscience*, **2014**,*14*, 347-358.
[78] Y. Sun, X. Yan, T. Yuan, J. Liang, Y. Fan, Z. Gu, and X. Zhang, *Biomaterials*, **2010**, *31*, 7124-7131.
[79] P. Luo, Y. Luo, J. Huang, W. Lu, D. Luo, J. Yu, and S. Liu, *Colloids and Surfaces B: Biointerfaces*, **2013**, *109*, 167-175.
[80] J. Liu, Y. Pang, W. Huang, Z. Zhu, X. Zhu, Y. Zhou, and D. Yan, *Biomacromolecules*, **2011**, *12*, 2407-2415.
[81] R. S. Navath, B. Wang, S. Kannan, R. Romero, and R. M. Kannan, *Journal of Controlled Release*, **2010**, *142*, 447-456.
[82] D. Wu, Y. Liu, C. He, T. Chung, and S. Goh, *Macromolecules*, **2004**, *37*, 6763-6770.
[83] Y. Liu, D. Wu, Y. Ma, G. Tang, S. Wang, C. He, T. Chung, and S. Goh, *Chemical Communications*, **2003**, *9*, 2630-2631.
[84] J. Khandare and T. Minko, *Progress in Polymer Science*, **2006**, *31*, 359-397.
[85] P. Liu, B. Shi, C. Yue, G. Gao, P. Li, H. Yi, M. Li, B. Wang, Y. Ma, and L. Cai, *Polymer Chemistry*, **2013**, *4*, 5793-5799.
[86] X. Zhang, K. Achazi, D. Steinhilber, F. Kratz, J. Dernedde, and R. Haag, *Journal of Controlled Release*, **2014**, *174*, 209-216.
[87] X. Q. Li, H. Y. Wen, H. Q. Dong, W. M. Xue, G. M. Pauletti, X. J. Cai, W. J. Xia, D. Shi, and Y. Y. Li, *Chemical Communications*, **2011**, *47*, 8647-8649.
[88] R. S. Navath, Y. E. Kurtoglu, B. Wang, S. Kannan, R. Romero, and R. M. Kannan, *Bioconjugate Chemistry*, **2008**, *19*, 2446-2455.
[89] S. McRae Page, M. Martorella, S. Parelkar, I. Kosif, and T. Emrick, *Molecular Pharmaceutics*, **2013**, *10*, 2684-2692.
[90] Z. Xu, D. Wang, S. Xu, X. Liu, X. Zhang, and H. Zhang, *Chemistry - An Asian Journal*, **2014**, *9*, 199-205.
[91] M. Xu, J. Qian, A. Suo, H. Wang, X. Yong, X. Liu, and R. Liu, *Carbohydrate Polymers*, **2013**, *98*, 181-188.
[92] H. Cho, J. Bae, V. K. Garripelli, J. M. Anderson, H. W. Jun, and S. Jo, *Chemical. Communication*, **2012**, *48*, 6043-6045.
[93] M. Volpato, N. Abou-Zeid, R. W. Tanner, L. T. Glassbrook, J. Taylor, I. Stratford, P. M. Loadman, M. Jaffar, and R. M. Phillips, *Molecular Cancer Therapeutics*, **2007**, *6*, 3122-3130.
[94] S. T. Huang, Y. X. Peng, and K. L. Wang, *Biosensors and Bioelectronics*, **2008**, *23*, 1793-1798.
[95] R. A. Cairns, I. S. Harris, and T. W. Mak, *Nature Reviews Cancer*, **2011**, *11*, 85-95.
[96] K. Ulbrich and V. Subr, *Advanced Drug Delivery Reviews*, **2004**, *56*, 1023-1050.
[97] J. Yao, Y. Ruan, T. Zhai, J. Guan, G. Tang, H. Li, and S. Dai, *Polymer*, **2011**, *52*, 3396-3404.
[98] Y. Y. Li, S. H. Hua, W. Xiao, H. Y. Wang, X. H. Luo, C. Li, S. X. Cheng, X. Z. Zhang, and R. X. Zhuo, *Journal of Materials Chemistry*, **2011**, *21*, 3100-3106.
[99] C. Liu, X. Gan, and Y. Chen, *Starch*, **2011**, *63*, 503-511.
[100] M. A. Malana, J.-U. D. Bukhari, and R. Zohra, *Designed Monomers and Polymers*, **2014**, *17*, 266-274.
[101] K. S. Soppimath, A. R. Kulkarni, and T. M. Aminabhavi, *Journal of Controlled Release*, **2001**, *75*, 331-345.
[102] C. L. Lay, J. N. Kumar, C. K. Liu, X. Lu, and Y. Liu, *Macromolecular Rapid Communications*, **2013**, *34*, 1563-1568.
[103] C. L. Lay, H. R. Tan, X. Lu, and Y. Liu, *Chemistry - A European Journal*, **2011**, *17*, 2504-2509.

[104] Y. Shang, F. Ding, L. Xiao, H. Deng, Y. Du, and X. Shi, *Carbohydrate Polymers*, **2014**, *102*, 413-418.
[105] J. Varshosaz, F. Hassanzadeh, H. Sadeghi-aliabadi, Z. Larian, and M. Rostami, *Chemistry - A European Journal*, **2014**, *240*, 133-146.
[106] D. Liu, H. Hu, J. Zhang, X. Zhao, X. Tang, and D. Chen, *Chemical and Pharmaceutical Bulletin*, **2011**, *59*, 63-71.
[107] J. Liang, W. L. Wu, X. D. Xu, R. X. Zhuo, and X. Z. Zhang, *Colloids and Surfaces B: Biointerfaces*, **2014**, *114*, 398-403.
[108] R. P. Johnson, Y. I. Jeong, E. Choi, C. W. Chung, D. H. Kang, S. O. Oh, H. Suh, and I. Kim, *Advanced Functional Materials*, **2012**, *22*, 1058-1068.
[109] G. Chang, C. Li, W. Lu, and J. Ding, *Macromolecular Bioscience*, **2010**, *10*, 1248-1256.
[110] E. S. Lee, K. T. Oh, D. Kim, Y. S. Youn, and Y. H. Bae, *Journal of Controlled Release*, **2007**, *123*, 19-26.
[111] E. S. Lee, Z. Gao, D. Kim, K. Park, I. C. Kwon, and Y. H. Bae, *Journal of Controlled Release*, **2008**, *129*, 228-236.
[112] V. A. Sethuraman and Y. H. Bae, *Journal of Controlled Release*, **2007**, *118*, 216-224.
[113] Y. Bae, S. Fukushima, A. Harada, and K. Kataoka, *Angewandte Chemie International Edition*, **2003**, *42*, 4640-4643.
[114] Y. Bae, N. Nishiyama, S. Fukushima, H. Koyama, M. Yasuhiro, and K. Kataoka, *Bioconjugate Chemistry*, **2005**, *16*, 122-130.
[115] Y. Bae, W. D. Jang, N. Nishiyama, S. Fukushima, and K. Kataoka, *Molecular Biosystems*, **2005**, *1*, 242-250.
[116] A. Ponta and Y. Bae, *Pharmaceutical Research*, **2010**, *27*, 2330-2342.
[117] Y. Bae, A. W. G. Alani, N. C. Rockich, T. S. Z. C. Lai, and G. S. Kwon, *Pharmaceutical Research*, **2010**, *27*, 2421-2432.
[118] H. J. Lee and Y. Bae, *Pharmaceutical Research*, **2013**, *30*, 478-488.
[119] M. D. Howard, A. Ponta, A. Eckman, M. Jay, and Y. Bae, *Pharmaceutical Research*, **2011**, *28*, 2435-2446.
[120] H. J. Lee and Y. Bae, *Pharmaceutical Research*, **2013**, *30*, 2077-2086.
[121] S. Akter, B. F. Clem, H. J. Lee, J. Chesney, and Y. Bae, *Pharmaceutical Research*, **2012**, *29*, 847-855.
[122] E. R. Gillies, A. P. Goodwin, and J. M. J. Fréchet, *Bioconjugate Chemistry*, **2004**, *15*, 1254-1263.
[123] H. Wang, J. He, M. Zhang, Y. Tao, F. Li, K. C. Tam, and P. Ni, *Journal of Materials Chemistry B*, **2013**, *1*, 6596-6607.
[124] H. He, S. Chen, J. Zhou, Y. Dou, L. Song, L. Che, X. Zhou, X. Chen, Y. Jia, J. Zhang, S. Li, and X. Li, *Biomaterials*, **2013**, *34*, 5344-5358.
[125] I. Lee, M. Park, Y. Kim, O. Hwang, G. Khang, and D. Lee, *International Journal of Pharmaceutics*, **2013**, *448*, 259-266.
[126] M. Krämer, J. F. Stumbé, H. Türk, S. Krause, A. Komp, L. Delineau, S. Prokhorova, H. Kautz, and R. Haag, *Angewandte Chemie International Edition*, **2002**, *41*, 4252-4256.
[127] T. Suzawa, S. Nagamura, H. Saito, S. Ohta, N. Hanai, J. Kanazawa, M. Okabe, and M. Yamasaki, *Journal of Controlled Release*, **2002**, *79*, 229-242.
[128] B. Law, R. Weissleder, and C. H. Tung, *Biomacromolecules*, **2006**, *7*, 1261-1265.
[129] M. T. Basel, T. B. Shrestha, D. L. Troyer, and S. H. Bossmann, *ACS Nano*, **2011**, *5*, 2162-2175.
[130] D. E. Chung and F. Kratz, *Bioorganic and Medicinal Chemistry Letter*, **2006**, *16*, 5157-5163.
[131] J. R. Tauro and R. A. Gemeinhart, *Molecular Pharmaceutics*, **2005**, *2*, 435-438.

[132] J. R. Tauro and R. A. Gemeinhart, *Bioconjugate Chemistry*, **2005**, *16*, 1133-1139.
[133] K. Y. Choi, M. Swierczewska, S. Lee, and X. Chen, *Theranostics*, **2012**, *2*, 156-179.
[134] M. J. Vicent, F. Greco, R. I. Nicholson, A. Paul, P. C. Griffiths, and R. Duncan, *Angewandte Chemie International Edition*, **2005**, *44*, 4061-4066.
[135] R. Satchi, T. A. Connors, and R. Duncan, *British Journal of Cancer*, **2001**, *85*, 1070-1076.
[136] T. A. Denison and Y. H. Bae, *Journal of Controlled Release*, **2012**, *164*, 187-191.
[137] D. E. Meyer, B. C. Shin, G. A. Kong, M. W. Dewhirst, and A. Chilkoti, *Journal of Controlled Release*, **2001**, *74*, 213-224.
[138] M. Curcio, U. Gianfranco Spizzirri, F. Iemma, F. Puoci, G. Cirillo, O. I. Parisi, and N. Picci, *European Journal of Pharmaceutics and Biopharmaceutics*, **2010**, *76*, 48-55.
[139] H. Zhang, Q. Yan, Y. Kang, L. Zhou, H. Zhou, J. Yuan, and S. Wu, *Polymer*, **2012**, *53*, 3719-3725.
[140] T. C. Stover, Y. S. Kim, T. L. Lowe, and M. Kester, *Biomaterials*, **2008**, *29*, 359-369.
[141] S. Fujishige, K. Kubota, and I. Ando, *The Journal of Physical Chemistry*, **1989**, *93*, 3311-3313.
[142] K. Na, V. T. Sethuraman, and Y. H. Bae, *Anti-Cancer Agents in Medicinal Chemistry*, **2006**, *6*, 525-535.
[143] N. Sanoj Rejinold, P. R. Sreerekha, K. P. Chennazhi, S. V. Nair, and R. Jayakumar, *International Journal of Biological Macromolecules*, **2011**, *49*, 161-172.
[144] M. Nakayama, T. Okano, T. Miyazaki, F. Kohori, K. Sakai, and M. Yokoyama, Journal of Controlled Release, 2006, 115, 46-56.
[145] D. C. Wu, Y. Liu, and C. B. He, *Macromolecules*, **2008**, *41*, 18-20.
[146] D. Needham and M. W. Dewhirst, *Advanced Drug Delivery Reviews*, **2001**, *53*, 285-305.
[147] L. Paasonen, T. Laaksonen, C. Johans, M. Yliperttula, K. Kontturi, and A. Urtti, *Journal of Controlled Release*, **2007**, *122*, 86-93.
[148] A. Agarwal, M. A. MacKey, M. A. El-Sayed, and R. V. Bellamkonda, *ACS Nano*, **2011**, *5*, 4919-4926.
[149] M. B. Yatvin, H. Muhlensiepen, W. Porschen, J. N. Weinstein, and L. E. Feinendegen, *Cancer Research*, **1981**, *41*, 1602-1607.
[150] K. Kakinuma, R. Tanaka, H. Takahashi, Y. Sekihara, M. Watanabe, and M. Kuroki, *International Journal of Hyperthermia*, **1996**, *12*, 157-165.
[151] J. N. Weinstein, R. L. Magin, R. L. Cysyk, and D. S. Zaharko, *Cancer Research*, **1980**, *40*, 1388-1395.
[152] J. B. Bassett, J. R. Tacker, R. U. Anderson, and D. Bostwick, *The Journal of Urology*, **1988**, *139*, 634-636.
[153] L. Paasonen, T. Sipilä, A. Subrizi, P. Laurinmäki, S. J. Butcher, M. Rappolt, A. Yaghmur, A. Urtti, and M. Yliperttula, *Journal of Controlled Release*, **2010**, *147*, 136-143.
[154] R. Regmi, S. R. Bhattarai, C. Sudakar, A. S. Wani, R. Cunningham, P. P. Vaishnava, R. Naik, D. Oupicky, and G. Lawes, *Journal of Materials Chemistry*, **2010**, *20*, 6158-6163.
[155] P. Pradhan, J. Giri, F. Rieken, C. Koch, O. Mykhaylyk, M. Döblinger, R. Banerjee, D. Bahadur, and C. Plank, *Journal of Controlled Release*, **2010**, *142*, 108-121.
[156] H. Y. Huang, S. H. Hu, C. S. Chian, S. Y. Chen, H. Y. Lai, and Y. Y. Chen, *Journal of Materials Chemistry*, **2012**, *22*, 8566-8573.

[157] A. E. Mengesha, R. J. Wydra, J. Z. Hilt, and P. M. Bummer, *Pharmaceutical Research*, **2013**, *30*, 3214-3224.
[158] B. Bondurant and D. F. O'Brien, *Journal of the American Chemical Society*, **1998**, *120*, 13541-13542.
[159] A. Mueller, B. Bondurant, and D. F. O'Brien, *Macromolecules*, **2000**, *33*, 4799-4804.
[160] S. Punnamaraju, H. You, and A. J. Steckl, *Langmuir*, **2012**, *28*, 7657-7664.
[161] A. Yavlovich, A. Singh, S. Tarasov, J. Capala, R. Blumenthal, and A. Puri, *Journal of Thermal Analysis and Calorimetry*, **2009**, *98*, 97-104.
[162] P. Shum, J. M. Kim, and D. H. Thompson, *Advanced Drug Delivery Reviews*, **2001**, *53*, 273-284.
[163] E. G. Randles and P. R. Bergethon, *Langmuir*, **2013**, *29*, 1490-1497.
[164] J. Wu, J. Pepe, and M. Rincón, *Ultrasonics*, **2006**, *44*, 21-25.
[165] S. Mitragotri, *Nature Reviews Drug Discovery*, **2005**, *4*, 255-260.
[166] J. M. Escoffre, J. Piron, A. Novell, and A. Bouakaz, *Molecular Pharmaceutics*, **2011**, *8*, 799-806.
[167] R. R. Patil, S. A. Guhagarkar, and P. V. Devarajan, *Critical Reviews in Therapeutics Drug Carrier System*, **2008**, *25*, 1-61.
[168] B. Geers, I. Lentacker, N. N. Sanders, J. Demeester, S. Meairs, and S. C. De Smedt, *Journal of Controlled Release*, **2011**, *152*, 249-256.
[169] I. Lentacker, B. Geers, J. Demeester, S. C. De Smedt, and N. N. Sanders, *Molecular Therapy*, **2010**, *18*, 101-108.
[170] N. Y. Rapoport, A. M. Kennedy, J. E. Shea, C. L. Scaife, and K. H. Nam, *Journal of Controlled Release*, **2009**, *138*, 268-276.
[171] C. H. Wang, S. T. Kang, Y. H. Lee, Y. L. Luo, Y. F. Huang, and C. K. Yeh, *Biomaterials*, **2012**, *33*, 1939-1947.
[172] T. J. Evjen, E. A. Nilssen, S. Rögnvaldsson, M. Brandl, and S. L. Fossheim, *European Journal of Pharmaceutics and Biopharmaceutics*, **2010**, *75*, 327-333.
[173] E. Hagtvet, T. J. Evjen, D. R. Olsen, S. L. Fossheim, and E. A. Nilssen, *Journal of Drug Targeting*, **2011**, *19*, 701-708.
[174] K. Brindle, *Nature Reviews Cancer*, **2008**, *8*, 94-107.
[175] R. Weissleder and M. J. Pittet, *Nature*, **2008**, *452*, 580-589.
[176] S. Aime, D. D. Castelli, S. G. Crich, E. Gianolio, and E. Terreno, *Accounts of Chemical Research*, **2009**, *42*, 822-831.
[177] P. Caravan, J. J. Ellison, T. J. McMurry, and R. B. Lauffer, *Chemical Reviews*, **1999**, *99*, 2293-2352.
[178] W. B. Lin, T. Hyeon, G. M. Lanza, M. Q. Zhang, and T. J. Meade, *MRS Bulletin*, **2009**, *34*, 441-448.
[179] A. J. L. Villaraza, A. Bumb, and M. W. Brechbiel, *Chemical Reviews*, **2010**, *110*, 2921-2959.
[180] H. Pettersson, J. Eliasson, N. Egund, B. Rooser, H. Willen, A. Rydholm, N. O. Berg, and S. Holtas, *Skeletal Radiology*, **1988**, *17*, 319-323.
[181] R. Crisci, E. Di Cesare, L. Lupattelli, and G. F. Coloni, *European Journal of Cardio-thoracic Surgery*, **1997**, *11*, 214-217.
[182] J. M. Hawnaur, R. J. Johnson, G. Read, and I. Isherwood, *Clinical Radiology*, **1993**, *47*, 302-310.
[183] C. J. Zech, K. A. Herrmann, M. F. Reiser, and S. O. Schoenberg, *Magnetic Resonance in Medical Science*, **2007**, *6*, 43-52.
[184] L. Vander Elst, F. Maton, S. Laurent, F. Seghi, F. Chapelle, and R. N. Muller, *Magnetic Resonance in Medicine*, **1997**, *38*, 604-614.
[185] K. Shimada, H. Isoda, Y. Hirokawa, S. Arizono, T. Shibata, and K. Togashi, *European Radiology*, **2010**, *20*, 2690-2698.

[186] O. Clement, A. Muhler, V. S. Vexler, R. Kuwatsuru, Y. Berthezene, W. Rosenau, and R. C. Brasch, *Journal of Magnetic Resonance Imaging*, **1993**, *3*, 71-77.
[187] Z. Tyeklar, S. U. Dunham, K. Midelfort, D. M. Scott, H. Sajiki, K. Ong, R. B. Lauffer, P. Caravan, and T. J. McMurry, *Inorganic Chemistry*, **2007**, *46*, 6621-6631.
[188] P. Caravan, N. J. Cloutier, M. T. Greenfield, S. A. McDermid, S. U. Dunham, J. W. M. Bulte, J. Amedio, R. J. Looby, R. M. Supkowski, J. Horrocks, T. J. McMurry, and R. B. Lauffer, *Journal of the American Chemical Society*, **2002**, *124*, 3152-3162.
[189] P. Caravan, G. Parigi, J. M. Chasse, N. J. Cloutier, J. J. Ellison, R. B. Lauffer, C. Luchinat, S. A. McDermid, M. Spiller, and T. J. McMurry, *Inorganic Chemistry*, **2007**, *46*, 6632-6639.
[190] K. Turetschek, E. Floyd, T. Helbich, T. P. L. Roberts, D. M. Shames, M. F. Wendland, W. O. Carter, and R. C. Brasch, *Journal of Magnetic Resonance Imaging*, **2001**, *14*, 237-242.
[191] C. Chen, J. S. Cohen, C. E. Myers, and M. Sohn, *FEBS Letters*, **1984**, *168*, 70-74.
[192] O. Galindev, M. Dalantai, W. S. Ahn, and Y. K. Shim, *Journal of Porphyrins and Phthalocyanines*, **2009**, *13*, 823-831.
[193] J. L. Sessler, T. D. Mody, G. W. Hemmi, V. Lynch, S. W. Young, and R. A. Miller, *Journal of the American Chemical Society*, **1993**, *115*, 10366-10367.
[194] S. I. Hashemy, J. S. Ungerstedt, F. Zahedi Avval, and A. Holmgren, *Journal of Biological Chemistry*, **2006**, *281*, 10691-10697.
[195] G. M. Richards and M. P. Mehta, *Expert Opinion on Pharmacotherapy*, **2007**, *8*, 351-359.
[196] J. A. Park, J. J. Lee, J. C. Jung, D. Y. Yu, C. Oh, S. Ha, T. J. Kim, and Y. Chang, *Chembiochem*, **2008**, *9*, 2811-2813.
[197] W. Zhang, Y. Chen, D. J. Guo, Z. W. Huang, L. Cai, and L. He, *European Journal of Radiology*, **2011**, *79*, 369-374.
[198] P. A. Sukerkar, K. W. MacRenaris, T. J. Meade, and J. E. Burdette, *Molecular Pharmaceutics*, **2011**, *8*, 1390-1400.
[199] A. Pais, C. Gunanathan, R. Margalit, I. E. Biton, A. Yosepovich, D. Milstein, and H. Degani, *Cancer Research*, **2011**, *71*, 7387-7397.
[200] E. C. Unger, T. A. Fritz, C. Tilcock, and T. E. New, *Journal of Magnetic Resonance Imaging*, **1991**, *1*, 689-693.
[201] K. Nwe, L. H. Bryant, and M. W. Brechbiel, *Bioconjugate Chemistry*, **2010**, *21*, 1014-1017.
[202] W. C. Floyd, P. J. Klemm, D. E. Smiles, A. C. Kohlgruber, V. C. Pierre, J. L. Mynar, J. M. J. Frechet, and K. N. Raymond, *Journal of the American Chemical Society*, **2011**, *133*, 2390-2393.
[203] J. J. Yang, J. H. Yang, L. X. Wei, O. Zurkiya, W. Yang, S. Y. Li, J. Zou, Y. B. Zhou, A. L. W. Maniccia, H. Mao, F. Q. Zhao, R. Malchow, S. M. Zhao, J. Johnson, X. P. Hu, E. Krogstad, and Z. R. Liu, *Journal of the American Chemical Society*, **2008**, *130*, 9260-9267.
[204] P. Caravan, *Accounts of Chemical Research*, **2009**, *42*, 851-862.
[205] L. R. Opsahl, E. E. Uzgiris, and D. R. Vera, *Academic Radiology*, **1995**, *2*, 762-767.
[206] G. P. Yan, M. L. Liu, and L. Y. Li, *Bioconjugate Chemistry*, **2005**, *16*, 967-971.
[207] F. R. Ye, T. Y. Ke, E. K. Jeong, X. L. Wang, Y. G. Sung, M. Johnson, and Z. R. Lu, *Molecular Pharmaceutics*, **2006**, *3*, 507-515.
[208] C. B. Sirlin, D. R. Vera, J. A. Corbeil, M. B. Caballero, R. B. Buxton, and R. F. Mattrey, *Academic Radiology*, **2004**, *11*, 1361-1369.

[209] T. H. Helbich, A. Gossman, P. A. Mareski, B. Raduchel, T. P. L. Roberts, D. M. Shames, M. Muhler, K. Turetschek, and R. C. Brasch, *Journal of Magnetic Resonance Imaging*, **2000**, *11*, 694-701.
[210] D. R. Vera, M. H. Buonocore, E. R. Wisner, R. W. Katzberg, and R. C. Stadalnik, *Academic Radiology*, **1995**, *2*, 497-506.
[211] J. P. Andre, C. F. G. C. Geraldes, J. A. Martins, A. E. Merbach, M. I. M. Prata, A. C. Santos, J. J. P. de Lima, and E. Toth, *Chemistry - A European Journal*, **2004**, *10*, 5804-5816.
[212] P. Baia, J. P. Andre, C. F. G. C. Geraldes, J. A. Martins, A. E. Merbach, and T. Toth, *European Journal of Inorganic Chemistry*, **2005**, *11*, 2110-2119.
[213] S. Laus, A. Sour, R. Ruloff, E. Toth, and A. E. Merbach, *Chemistry - A European Journal*, **2005**, *11*, 3064-3076.
[214] S. Laus, R. Ruloff, E. Toth, and A. E. Merbach, *Chemistry - A European Journal*, **2003**, *9*, 3555-3566.
[215] J. Rudovsky, J. Kotek, P. Hermann, I. Lukes, V. Mainero, and S. Aime, *Organic and Biomolecular Chemistry*, **2005**, *3*, 112-117.
[216] M. M. Ali, M. Woods, P. Caravan, A. C. L. Opina, M. Spiller, J. C. Fettinger, and A. D. Sherry, *Chemistry - A European Journal*, **2008**, *14*, 7250-7258.
[217] N. Sato, H. Kobayashi, A. Hiraga, T. Saga, K. Togashi, J. Konishi, and M. W. Brechbiel, *Magnetic Resonance in Medicine*, **2001**, *46*, 1169-1173.
[218] H. Kobayashi, S. Kawamoto, R. A. Star, T. A. Waldmann, Y. Tagaya, and M. W. Brechbiel, *Cancer Research*, **2003**, *63*, 271-276.
[219] H. Kobayashi, S. Kawamoto, R. A. Star, T. A. Waldmann, M. W. Brechbiel, and P. L. Choyke, *Bioconjugate Chemistry*, **2003**, *14*, 1044-1047.
[220] A. T. Yordanov, H. Kobayashi, S. J. English, K. Reijnders, D. Milenic, M. C. Krishna, J. B. Mitchell, and M. W. Brechbiel, *Journal of Materials Chemistry*, **2003**, *13*, 1523-1525.
[221] C. C. Cyran, Y. J. Fu, H. J. Raatschen, V. Rogut, B. Chaopathomkul, D. M. Shames, M. F. Wendland, B. M. Yeh, and R. C. Brasch, *Journal of Magnetic Resonance Imaging*, **2008**, *27*, 581-589.
[222] C. Kojima, B. Turkbey, M. Ogawa, M. Bernardo, C. A. S. Regino, L. H. Bryant, P. L. Choyke, K. Kono, and H. Kobayashi, *Nanomedicine: Nanotechnology, Biology, and Medicine*, **2011**, *7*, 1001-1008.
[223] K. Luo, G. Liu, W. She, Q. Wang, G. Wang, B. He, H. Ai, Q. Gong, B. Song, and Z. Gu, *Biomaterials*, **2011**, *32*, 7951-7960.
[224] K. Nwe, D. E. Milenic, G. L. Ray, Y. S. Kim, and M. W. Brechbiel, *Molecular Pharmaceutics*, **2012**, *9*, 374-381.
[225] H. Kobayashi, N. Sato, T. Saga, Y. Nakamoto, T. Ishimori, S. Toyama, K. Togashi, J. Konishi, and M. W. Brechbiel, *European Journal of Nuclear Medicine*, **2000**, *27*, 1334-1339.
[226] S. D. Konda, M. I. C. H. Aref, M. A. R. T. Brechbiel, and E. C. Wiener, *Investigative Radiology*, **2000**, *35*, 104-113.
[227] S. D. Konda, S. T. E. V. Wang, M. A. R. T. Brechbiel, and E. C. Wiener, *Investigative Radiology*, **2002**, *37*, 199-204.
[228] S. Konda, M. Aref, S. Wang, M. Brechbiel, and E. Wiener, *Magnetic Resonance Materials in Physics, Biology and Medicine*, **2001**, *12*, 104-113.
[229] E. C. Wiener, S. H. E. E. Konda, A. M. B. E. Shadron, M. A. R. T. Brechbiel, and O. T. T. O. Gansow, *Investigative Radiology*, **1997**, *32*, 748-754.
[230] C. A. Boswell, P. K. Eck, C. A. S. Regino, M. Bernardo, K. J. Wong, D. E. Milenic, P. L. Choyke, and M. W. Brechbiel, *Molecular Pharmaceutics*, **2008**, *5*, 527-539.
[231] Z. L. Cheng, D. L. J. Thorek, and A. Tsourkas, *Angewandte Chemie International Edition*, **2010**, *49*, 346-350.

[232] Miyake, Y., Kimura, Y., Ishikawa, S., Tsujita, H., Miura, H., Narazaki, M., Matsuda, T., Tabata, Y., Yano, T., Toshimitsu, A., and Kondo, *Tetrahedron Letters*, **2012**, *53*, 4580-4583.
[233] P. J. Klemm, W. C. Floyd, D. E. Smiles, J. M. J. Fréchet, and K. N. Raymond, *Contrast Media and Molecular Imaging*, **2012**, *7*, 95-99.
[234] U. Schmiedl, M. D. Ogan, M. E. Moseley, and R. C. Brasch, *American Journal of Roentgenology*, **1986**, *147*, 1263-1270.
[235] R. B. Lauffer and T. J. Brady, *Magnetic Resonance Imaging*, **1985**, *3*, 11-16.
[236] H. Paajanen, T. Reisto, I. Hemmila, M. Komu, P. Niemi, and M. Kormano, *Magnetic Resonance in Medicine*, **1990**, *13*, 38-43.
[237] K. P. Aicher, J. W. Dupon, D. L. White, S. L. Aukerman, M. E. Moseley, R. Juster, W. Rosenau, J. L. Winkelhake, and R. C. Brasch, *Cancer Research*, **1990**, *50*, 7376-7381.
[238] A. S. Krishnan, A. A. Neves, M. M. De Backer, D. E. Hu, B. Davletov, M. I. Kettunen, and K. M. Brindle, *Radiology*, **2008**, *246*, 854-862.
[239] D. Artemov, N. Mori, R. Ravi, and Z. M. Bhujwalla, *Cancer Research*, **2003**, *63*, 2723-2727.
[240] D. Shahbazi-Gahrouei, M. Williams, S. Rizvi, and B. J. Allen, *Journal of Magnetic Resonance Imaging*, **2001**, *14*, 169-174.
[241] D. Shahbazi-Gahrouei, S. M. Rizvi, M. A. Williams, and B. J. Allen, *Australasian Physical and Engineering Sciences in Medicine*, **2002**, *25*, 31-38.
[242] Y. Kuriu, E. Otsuji, S. Kin, Y. Nakase, K. I. Fukuda, K. Okamoto, A. Hagiwara, and H. Yamagishi, *Journal of Surgical Oncology*, **2006**, *94*, 144-148.
[243] E. C. Unger, W. G. Totty, and D. M. Neufeld, *Investigative Radiology*, **1985**, *20*, 693-700.
[244] W. T. Anderson-Berg, M. Strand, and T. E. Lempert, *Journal of Nuclear Medicine*, **1986**, *27*, 829-833.
[245] G. Ratzinger, P. Agrawal, W. Körner, J. Lonkai, H. M. H. F. Sanders, E. Terreno, M. Wirth, G. J. Strijkers, K. Nicolay, and F. Gabor, *Biomaterials*, **2010**, *31*, 8716-8723.
[246] K. Shiraishi, K. Kawano, T. Minowa, Y. Maitani, and M. Yokoyama, *Journal of Controlled Release*, **2009**, *136*, 14-20.
[247] E. Nakamura, K. Makino, T. Okano, T. Yamamoto, and M. Yokoyama, *Journal of Controlled Release*, **2006**, *114*, 325-333.
[248] S. Kaida, H. Cabral, M. Kumagai, A. Kishimura, Y. Terada, M. Sekino, I. Aoki, N. Nishiyama, T. Tani, and K. Kataoka, *Cancer Research*, **2010**, *70*, 7031-7041.
[249] X. Li, Y. Qian, T. Liu, X. Hu, G. Zhang, Y. You, and S. Liu, *Biomaterials*, **2011**, *32*, 6595-6605.
[250] T. Liu, Y. Qian, X. Hu, Z. Ge, and S. Liu, *Journal of Materials Chemistry*, **2012**, *22*, 5020-5030.
[251] T. Liu, X. Li, Y. Qian, X. Hu, and S. Liu, *Biomaterials*, **2012**, *33*, 2521-2531.
[252] T. Bui, J. Stevenson, J. Hoekman, S. Zhang, K. Maravilla, and R. J. Y. Ho, *PLoS ONE*, **2010**, *5*, 1-7.
[253] S. Aime, D. D. Castelli, S. G. Crich, E. Gianolio, and E. Terreno, *Accounts of Chemical Research*, **2009**, *42*, 822-831.
[254] E. C. Unger, T. Winokur, P. MacDougall, J. Rosenblum, M. Clair, R. Gatenby, and C. Tilcock, *Radiology*, **1989**, *171*, 81-85.
[255] W. Li, B. Su, S. Meng, L. Ju, L. Yan, Y. Ding, Y. Song, W. Zhou, H. Li, L. Tang, Y. Zhao, and C. Zhou, *European Journal of Radiology*, **2011**, *80*, 598-606.

[256] A. Korotcov, L. Shan, H. Meng, T. Wang, R. Sridhar, Y. Zhao, X. J. Liang, and P. C. Wang, *Journal of Nanoscience and Nanotechnology*, **2010**, *10*, 7545-7549.
[257] K. M. Ward, A. H. Aletras, and R. S. Balaban, *Journal of Magnetic Resonance*, **2000**, *143*, 79-87.
[258] W. Lin, J. L. Vivero-Escoto, K. M. L. Taylor-Pashow, R. C. Huxford, J. Della Rocca, C. Okoruwa, H. An, and W. Lin, *Small*, **2011**, *7*, 3519-3528.
[259] Y. Shao, X. Tian, W. Hu, Y. Zhang, H. Liu, H. He, Y. Shen, F. Xie, and L. Li, *Biomaterials*, **2012**, *33*, 6438-6446.
[260] Y. Wu, X. Xu, Q. Tang, and Y. Li, *Nanotechnology*, **2012**, *23*, 205103-205108.
[261] A. Datta, J. M. Hooker, M. Botta, M. B. Francis, S. Aime, and K. N. Raymond, *Journal of the American Chemical Society*, **2008**, *130*, 2546-2552.
[262] L. Moriggi, C. Cannizzo, E. Dumas, C. R. Mayer, A. Ulianov, and L. Helm, *Journal of the American Chemical Society*, **2009**, *131*, 10828-10829.
[263] Y. Song, X. Y. Xu, K. W. MacRenaris, X. Q. Zhang, C. A. Mirkin, and T. J. Meade, *Angewandte Chemie International Edition*, **2009**, *48*, 9143-9147.
[264] a) P. J. Endres, K. W. MacRenaris, S. Vogt, and T. J. Meade, *Bioconjugate Chemistry*, **2008**, *19*, 2049-2059; b) R. Cilliers, Y. Song, E.K. Kohlmeir, A. C. Larson, R.A. Omary, and T. J. Meade, *Magnetic Resonance in Medicine*, **2008**, *59*, 898-902; c) H. S. Chong, H. A. Song, S. Lim, K. MacRenaris, X. Ma, H. Lee, P. Bui, and T, J. Meade, *Bioorgainc & Medicinal Chemistry Letters*, **2008**, *18*, 2505-2508.
[265] C. Y. Shu, F. D. Corwin, J. F. Zhang, Z. J. Chen, J. E. Reid, M. H. Sun, W. Xu, J. H. Sim, C. R. Wang, P. P. Fatouros, A. R. Esker, H. W. Gibson, and H. C. Dorn, *Bioconjugate Chemistry*, **2009**, *20*, 1186-1193.
[266] J. F. Zhang, P. P. Fatouros, C. Y. Shu, J. Reid, L. S. Owens, T. Cai, H. W. Gibson, G. L. Long, F. D. Corwin, Z. J. Chen, and H. C. Dorn, *Bioconjugate Chemistry*, **2010**, *21*, 610-615.
[267] G. Oberdörster, E. Oberdörster , and J. Oberdörster, *Environmental Health Perspectives*, **2005**, *113*, 823-839.
[268] W. H. De Jong and P. J. A. Borm, *International Journal of Nanomedicine*, **2008**, *3*, 133-149.
[269] M. Vert, *Biomacromolecules*, **2005**, *6*, 538-546.
[270] Y. Luo and G. D. Prestwich, *Expert Opinion on Therapeutic Patent*, **2001**, *11*, 1395-1410.
[271] R. Mehta, V. Kumar, H. Bhunia, and S. N. Upadhyay, *Journal of Macromolecular Science Polymer Reviews*, **2005**, *45*, 325-349.
[272] J. M. Anderson and M. S. Shive, *Advanced Drug Delivery Reviews*, **1997**, *28*, 5-24.
[273] S. K. Lai, D. E. O'Hanlon, S. Harrold, S. T. Man, Y. Y. Wang, R. Cone, and J. Hanes, *Proceedings of the National Academy of Sciences of the United States of America*, **2007**, *104*, 1482-1487.
[274] S. K. Lai, Y. Y. Wang, and J. Hanes, *Advanced Drug Delivery Reviews*, **2009**, *61*, 158-171.
[275] Y. Cu and W. M. Saltzman, *Molecular Pharmaceutics*, **2009**, *6*, 173-181.
[276] J. S. Suk, S. K. Lai, Y. Y. Wang, L. M. Ensign, P. L. Zeitlin, M. P. Boyle, and J. Hanes, *Biomaterials*, **2009**, *30*, 2591-2597.
[277] B. C. Tang, M. Dawson, S. K. Lai, Y. Y. Wang, J. S. Suk, M. Yang, P. Zeitlin, M. P. Boyle, J. Fu, and J. Hanes, *Proceedings of the National Academy of Sciences of the United States of America*, **2009**, *106*, 19268-19273.
[278] Y. Y. Wang, S. K. Lai, J. S. Suk, A. Pace, R. Cone, and J. Hanes, *Angewandte Chemie International Edition*, **2008**, *47*, 9726-9729.

[279] D. D. Lasic, D. Papahadjopoulos, in *Medical Applications of Liposomes*, Elsevier Science, Amsterdam **1998**.
[280] J. C. M. Lee, H. Bermudez, B. M. Discher, M. A. Sheehan, Y. Y. Won, F. S. Bates, and D. E. Discher, *Biotechnology and Bioengineering*, **2001**, *73*, 135-145.
[281] M. Antonietti and S. Forster, *Advanced Materials*, **2003**, *15*, 1323-1333.
[282] D. E. Discher and A. Eisenberg, *Science*, **2002**, *297*, 967-973.
[283] V. P. Torchilin, *Nature Reviews Drug Discovery*, **2005**, *4*, 145-160.
[284] G. Prencipe, S. M. Tabakman, K. Welsher, Z. Liu, A. P. Goodwin, L. Zhang, J. Henry, and H. J. Dai, *Journal of the American Chemical Society*, **2009**, *131*, 4783-4787.
[285] C. L. Lay, H. Q. Liu, D. C. Wu, and Y. Liu, *Chemistry - A European Journal*, **2010**, *16*, 3001-3004.
[286] S. C. Kim, D. W. Kim, Y. H. Shim, J. S. Bang, H. S. Oh, S. W. Kim, and M. H. Seo, *Journal of Controlled Release*, **2001**, *72*, 191-202.
[287] F. Ahmed and D. E. Discher, *Journal of Controlled Release*, **2004**, *96*, 37-53.
[288] M. Tobío, R. Gref, A. Sánchez, R. Langer, and M. J. Alonso, *Pharmaceutical Research*, **1998**, *15*, 270-275.
[289] J. W. Kostanski, B. C. Thanoo, and P. P. DeLuca, *Pharmaceutical Development and Technology*, **2000**, *5*, 585-596.
[290] B. Jeong, Y. H. Bae, D. S. Lee, and S. W. Kim, *Nature*, **1997**, *388*, 860-862.
[291] E. Gautier, P. Fuertes, P. Cassagnau, J. P. Pascault, and E. Fleury, *Journal of Polymer Sciene Part A*, **2009**, *47*, 1440-1449.
[292] C. C. Chu, *Journal of Biomedical Materials Research*, **1981**, *15*, 795-804.
[293] C. C. Chu, *Journal of Biomedical Materials Research*, **1981**, *15*, 19-27.
[294] R. B. Bourne, P. R. Andreae, J. B. Finlay, and F. Marquis, *Canadian Journal of Surgery*, **1988**, *31*, 43-45.
[295] R. A. Miller, J. M. Brady, and D. E. Cutright, *Journal of Biomedical Materials Research*, **1977**, *11*, 711-719.
[296] A. M. Reed and D. K. Gilding, *Polymer*, **1981**, *22*, 494-498.
[297] Y. Koyamatsu, T. Hirano, Y. Kakizawa, F. Okano, T. Takarada, and M. Maeda, *Journal of Controlled Release*, **2014**, *173*, 89-95.
[298] S. H. Lee, H. Mok, Y. Lee, and T. G. Park, *Journal of Controlled Release*, **2011**, *152*, 152-158.
[299] H. S. Yoo and T. G. Park, *Journal of Controlled Release*, **2001**, *70*, 63-70.
[300] S. Cohen, T. Yoshioka, M. Lucarelli, L. H. Hwang, and R. Langer, *Pharmaceutical Research*, **1991**, *8*, 713-720.
[301] F. J. Van Natta, J. W. Hill, and W. H. Carothers, *Journal of the American Chemical Society*, **1934**, *56*, 455-457.
[302] J. Cayuela, V. Bounor-Legaré, P. Cassagnau, and A. Michel, *Macromolecules*, **2006**, *39*, 1338-1346.
[303] F. V. Burkersroda, L. Schedl, and A. Göpferich, *Biomaterials*, **2002**, *23*, 4221-4231.
[304] M. A. Woodruff and D. W. Hutmacher, *Progress in Polymer Science*, **2010**, *35*,1217-1256.
[305] C. Shasteen and Y. B. Choy, *Biomedical Engineering Letters*, **2011**, *1*, 163-167.
[306] H. Yin, C. Gong, S. Shi, X. Liu, Y. Wei, and Z. Qian, *Journal of Biomedical Materials Research Part B Applied Biomaterials*, **2010**, *92*, 129-137.
[307] C. Gong, Y. Wang, X. Wang, X. Wei, Q. Wu, B. Wang, P. Dong, L. Chen, F. Luo, and Z. Qian, *Journal of Nanoparticle Research*, **2011**, *13*, 721-731.
[308] M. Gou, X. Zheng, K. Men, J. Zhang, B. Wang, L. Lv, X. Wang, Y. Zhao, F. Luo, L. Chen, X. Zhao, Y. Wei, and Z. Qian, *Pharmaceutical Research*, **2009**, *26*, 2164-2173.

[309] C. Mohanty, S. Acharya, A. K. Mohanty, F. Dilnawaz, and S. K. Sahoo, *Nanomedicine*, **2010**, *5*, 433-449.
[310] Y. J. Park, J. Y. Lee, Y. S. Chang, J. M. Jeong, J. K. Chung, M. C. Lee, K. B. Park, and S. J. Lee, *Biomaterials*, **2002**, *23*, 873-879.
[311] X. Duan, P. Wang, K. Men, X. Gao, M. Huang, M. Gou, L. Chen, Z. Qian, and Y. Wei, *Nanoscale*, **2012**, *4*, 2400-2407.
[312] R. Feng, W. Zhu, Z. Song, L. Zhao, and G. Zhai, *Journal of Nanoparticle Research*, **2013**, *15*, 1748-1759.
[313] M. S. Kim, K. S. Seo, H. Hyun, G. Khang, S. H. Cho, and H. B. Lee, *Journal of Applied Polymer Science*, **2006**, *102*, 1561-1567.
[314] N. Kumar, R. S. Langer, and A. J. Domb, *Advanced Drug Delivery Reviews*, **2002**, *54*, 889-910.
[315] J. P. Jain, S. Modi, A. J. Domb, and N. Kumar, *Journal of Controlled Release*, **2005**, *103*, 541-563.
[316] D. S. Katti, S. Lakshmi, R. Langer, and C. T. Laurencin, *Advanced Drug Delivery Reviews*, **2002**, *54*, 933-961.
[317] K. W. Leong, P. D'Amore, M. Marletta, and R. Langer, *Journal of Biomedical Materials Research*, **1986**, *20*, 51-64.
[318] K. W. Leong, J. Kost, E. Mathiowitz, and R. Langer, *Biomaterials*, **1986**, *7*, 364-371.
[319] D. J. Quick, K. K. Macdonald, and K. S. Anseth, *Journal of Controlled Release*, **2004**, *97*, 333-343.
[320] A. S. Determan, B. G. Trewyn, V. S. Y. Lin, M. Nilsen-Hamilton, and B. Narasimhan, *Journal of Controlled Release*, **2004**, *100*, 97-109.
[321] M. Chiba, J. Hanes, and R. Langer, *Biomaterials*, **1997**, *18*, 893-901.
[322] E. S. Park, M. Maniar, and J. C. Shah, *Journal of Controlled Release*, **1998**, *52*, 179-189.
[323] K. W. Leong, B. C. Brott, and R. Langer, *Journal of Biomedical Materials Research*, **1985**, *19*, 941-955.
[324] V. K. Yellepeddi, A. Kumar, and S. Palakurthi, *Expert Opinion on Drug Delivery*, **2009**, *6*, 835-850.
[325] V. J. Venditto, C. A. S. Regino, and M. W. Brechbiel, *Molecular Pharmaceutics*, **2005**, *2*, 302-311.
[326] H. Yang and W. J. Kao, *Journal of Biomaterials Science, Polymer Edition*, **2006**, *17*, 3-19.
[327] B. Devarakonda, N. Li, and M. M. de Villiers, *AAPS PharmSciTech*, **2005**, *6*, 504-512.
[328] O. M. Milhem, C. Myles, N. B. McKeown, D. Attwood, and A. D'Emanuele, *International Journal of Pharmaceutics*, **2000**, *197*, 239-241.
[329] K. Jain, P. Kesharwani, U. Gupta, and N. K. Jain, *International Journal of Pharmaceutics*, **2010**, *394*, 122-142.
[330] R. Duncan and L. Izzo, *Advanced Drug Delivery Review*, **2005**, *57*, 2215-2237.
[331] J. C. Roberts, M. K. Bhalgat, and R. T. Zera, *Journal of Biomedical Materials Research*, **1996**, *30*, 53-65.
[332] N. Karoonuthaisiri, K. Titiyevskiy, and J. L. Thomas, *Colloids and Surfaces B: Biointerfaces*, **2003**, *27*, 365-375.
[333] S. Hong, A. U. Bielinska, A. Mecke, B. Keszler, J. L. Beals, X. Shi, L. Balogh, B. G. Orr, J. Baker, and M. M. Banaszak Holl, *Bioconjugate Chemistry*, **2004**, *15*, 774-782.
[334] A. Asthana, A. S. Chauhan, P. V. Diwan, and N. K. Jain, *AAPS PharmSciTech*, **2005**, *6*, 536-542.
[335] D. Bhadra, S. Bhadra, S. Jain, and N. K. Jain, *International Journal of Pharmaceutics*, **2003**, *257*, 111-124.

[336] P. C. Naha, M. Davoren, F. M. Lyng, and H. J. Byrne, *Toxicology and Applied Pharmacology*, **2010**, *246*, 91-99.
[337] N. Malik, R. Wiwattanapatapee, R. Klopsch, K. Lorenz, H. Frey, J. W. Weener, E. W. Meijer, W. Paulus, and R. Duncan, *Journal of Controlled Release*, **2000**, *65*, 133-148.
[338] R. Jevprasesphant, J. Penny, R. Jalal, D. Attwood, N. B. McKeown, and A. D'Emanuele, *International Journal of Pharmaceutics*, **2003**, *252*, 263-266.
[339] R. B. Kolhatkar, K. M. Kitchens, P. W. Swaan, and H. Ghandehari, *Bioconjugate Chemistry*, **2007**, *18*, 2054-2060.
[340] C. L. Waite, S. M. Sparks, K. E. Uhrich, and C. M. Roth, *BMC Biotechnology*, **2009**, *9*, 38-47.
[341] L. Wang, Z. Wang, G. Ma, W. Lin, and S. Chen, *Langmuir*, **2013**, *29*, 8914-8921.
[342] J. S. Choi, K. Nam, J. Y. Park, J. B. Kim, J. K. Lee, and J. S. Park, *Journal of Controlled Release*, **2004**, *99*, 445-456.
[343] R. Q. Huang, Y. H. Qu, W. L. Ke, J. H. Zhu, Y. Y. Pei, and C. Jiang, *The Journal of the Federation of American Societies for Experimental Biology*, **2007**, *21*, 1117-1125.
[344] J. Zhou, J. Wu, N. Hafdi, J. P. Behr, P. Erbacher, and L. Peng, *Chemical Communications*, **2006**, *22*, 2362-2364.
[345] A. K. Patri, J. F. Kukowska-Latallo, and J. Baker, *Advanced Drug Delivery Reviews*, **2005**, *57*, 2203-2214.
[346] Y. Wang, X. Cao, R. Guo, M. Shen, M. Zhang, M. Zhu, and X. Shi, *Polymer Chemistry*, **2011**, *2*, 1754-1760.
[347] C. Kojima, K. Kono, K. Maruyama, and T. Takagishi, *Bioconjugate Chemistry*, **2000**, *11*, 910-917.
[348] L. Jia, J. P. Xu, H. Wang, and J. Ji, *Colloids and Surfaces B: Biointerfaces*, **2011**, *84*, 49-54.
[349] J. Bryant, M. W. Brechbiel, C. Wu, J. W. M. Bulte, V. Herynek, and J. A. Frank, *Journal of Magnetic Resonance Imaging*, **1999**, *9*, 348-352.
[350] M. Polásek, P. Hermann, J. A. Peters, C. F. G. C. Geraldes, and I. Lukes, *Bioconjugate Chemistry*, **2009**, *20*, 2142-2153.
[351] Z. Jászberényi, L. Moriggi, P. Schmidt, C. Weidensteiner, R. Kneuer, A. E. Merbach, L. Helm, and E. Tóth, *Journal of Biological Inorganic Chemistry*, **2007**, *12*, 406-420.
[352] J. Franchini and P. Ferruti, *Journal of Bioactive and Compatible Polymer*, **2004**, *19*, 221-236.
[353] B. D. Mather, K. Viswanathan, K. M. Miller, and T. E. Long, *Progress in Polymer Science*, **2006**, *31*, 487-531.
[354] P. R. Krishna, A. Sreeshailam, and R. Srinivas, *Tetrahedron*, **2009**, *65*, 9657-9672.
[355] A. Manfredi, E. Ranucci, M. Suardi, and P. Ferruti, *Journal of Bioactive and Compatible Polymer*, **2007**, *22*, 219-231.
[356] P. Ferruti, E. Ranucci, F. Bignotti, L. Sartore, P. Bianciardi, and M. A. Marchisio, *Journal of Biomaterials Science, Polymer Edition*, **1995**, *6*, 833-844.
[357] P. Ferruti, M. E. Ranucci, L. Sartore, F. Bignottii, M. A. Marchisio, P. Bianciardi, and F. M. Veronese, *Biomaterials*, **1994**, *15*, 1235-1241.
[358] E. Ranucci, G. Spagnoli, P. Ferruti, D. Sgouras, and R. Duncan, *Journal of Biomaterials Science, Polymer Edition*, **1991**, *2*, 303-315.
[359] R. B. Arote, H. L. Jiang, Y. K. Kim, M. H. Cho, Y. J. Choi, and C. S. Cho, *Expert Opinion on Drug Delivery*, **2011**,*8*, 1237-1246.
[360] P. Ferruti, S. Bianchi, E. Ranucci, F. Chiellini, and V. Caruso, *Macromolecular Bioscience*, **2005**, *5*, 613-622.

[361] M. Piest, M. Ankoné, and J. F. J. Engbersen, *Journal of Controlled Release*, **2013**, *169*, 266-275.
[362] C. Lin, Z. Zhong, M. C. Lok, X. Jiang, W. E. Hennink, J. Feijen, and J. F. J. Engbersen, *Bioconjugate Chemistry*, **2007**, *18*, 138-145.
[363] M. Liu, J. Chen, Y. P. Cheng, Y. N. Xue, R. X. Zhuo, and S. W. Huang, *Macromolecular Bioscience*, **2010**, *10*, 384-392.
[364] Y. Sun, X. Yan, T. Yuan, J. Liang, Y. Fan, Z. Gu, and X. Zhang, *Biomaterials*, **2010**, *31*, 7124-7131.
[365] H. Fan, J. Huang, Y. Li, J. Yu, and J. Chen, *Polymer*, **2010**, *51*, 5107-5114.
[366] D. Wang, Y. Liu, Z. Hu, C. Hong, and C. Pan, *Polymer*, **2005**, *46*, 3507-3514.
[367] Z. Zheng, C. Pan, D. Wang, and Y. Liu, *Macromolecular Chemistry and Physics*, **2005**, *206*, 2182-2189.
[368] C. Lin, Z. Zhong, M. C. Lok, X. Jiang, W. E. Hennink, J. Feijen, and J. F. J. Engbersen, *Journal of Controlled Release*, **2006**, *116*, 130-137.
[369] D. Wang, Y. Liu, C. Y. Hong, and C. Y. Pan, *Polymer*, **2006**, *47*, 3799-3806.
[370] D. Wu, Y. Liu, L. Chen, C. He, T. S. Chung, and S. H. Goh, *Macromolecules*, **2005**, *38*, 5519-5525.
[371] D. Wang, Y. Liu, C. Y. Hong, and C. Y. Pan, *Journal of Polymer Science: Part A*, **2005**, *43*, 5127-5137.
[372] J. Chen, C. Wu, and D. Oupický, *Biomacromolecules*, **2009**, *10*, 2921-2927.
[373] Y. Ping, D. Wu, J. N. Kumar, W. Cheng, C. L. Lay, and Y. Liu, *Biomacromolecules*, **2013**, *14*, 2083-2094.
[374] F. Martello, M. Piest, J. F. J. Engbersen, and P. Ferruti, *Journal of Controlled Release*, **2012**, *164*, 372-379.
[375] Y. Z. You, C. Y. Hong, and C. Y. Pan, *Macromolecules*, **2009**, *42*, 573-575.
[376] W. Yang, C. Y. Pan, X. Q. Liu, and J. Wang, *Biomacromolecules*, **2011**, *12*, 1523-1531.
[377] X. Pan, G. Wang, C. L. Lay, B. H. Tan, C. He, and Y. Liu, *Scientific Report*, **2013**, *3*.
[378] W. Yang, C. Y. Pan, M. D. Luo, and H. B. Zhang, *Biomacromolecules*, **2010**, *11*, 1840-1846.
[379] Z. Yu, M. Cui, J. Yan, and Y. You, *Science China Chemistry*, **2013**, *53*, 1663-1668.
[380] D. Wang, Z. Q. Yu, C. Y. Hong, and Y. Z. You, *European Polymer Journal*, **2013**, *49*, 4189-4194.
[381] W. Yang and C. Y. Pan, *Macromolecular Rapid Communications*, **2009**, *30*, 2096-2101.
[382] G. Harald, *NMR Spectroscopy: Basic Principles, Concepts, and Applications in Chemistry*, John. Wiley & Sons, New York, **1995**.
[383] J. F. Rabek, *Experimental Methods in Polymer Chemistry*, John. Wiley & Sons, New York, **1980**, 419.
[384] J. Benjamin, *Laser Light Scattering*, Academic Press, Inc. San Diego, **1991**.
[385] D.B. Willaim and C. B. Carter, *Transmission Electron Microscopy A Textbook for Materials Science*, Springer, **2009**.
[386] *An Introduction to Fluorescence Spectroscopy*, PerkinElmer, **2000**.
[387] T. Mosmann, *Journal of Immunological Methods*, **1983**,*65*, 55-63.
[388] J. B. Pawley, *Handbook of Biological Confocal Microscopy Third Edition*, Springer, **2006**.
[389] A. C. Bakke, *Laboratory Medicine*, **2001**, **32**, 207.
[390] A. Gabizon, R. Isacson, E. Libson, B. Kaufman, B. Uziely, R. Catane, C. G. Ben-Dor, E. Rabello, Y. Cass, T. Peretz, A. Sulkes, R. Chisin, and Y. Barenholz, *Acta Oncologica*, **1994**, *33*, 779-786.
[391] M. R. Green, G. M. Manikhas, S. Orlov, B. Afanasyev, A. M. Makhson, P. Bhar, and M. J. Hawkins, *Annals of Oncology*, **2006**, *17*, 1263-1268.

[392] E. S. Gil and S. M. Hudson, *Progress in Polymer Science*, **2004**, *29*, 1173-1222.
[393] M. A. C. Stuart, W. T. S. Huck, J. Genzer, M. Müller, C. Ober, M. Stamm, G. B. Sukhorukov, I. Szleifer, V. V. Tsukruk, M. Urban, F. Winnik, S. Zauscher, I. Luzinov, and S. Minko, *Nature Materials*, **2010**, *9*, 101-113.
[394] C. De Las Heras Alarcon, S. Pennadam, and C. Alexander, *Chemical Society Reviews*, **2005**, *34*, 276-285.
[395] C. M. Schilli, M. Zhang, E. Rizzardo, S. H. Thang, Y. K. Chong, K. Edwards, G. Karlsson, and A. H. E. Müller, *Macromolecules*, **2004**, *37*, 7861-7866.
[396] R. A. Cairns, I. S. Harris, and T. W. Mak, *Nature Reviews Cancer*, **2011**, *11*, 85-95.
[397] R. M. Sawant, J. P. Hurley, S. Salmaso, A. Kale, E. Tolcheva, T. S. Levchenko, and V. P. Torchilin, *Bioconjugate Chemistry*, **2006**, *17*, 943-949.
[398] K. Kataoka, T. Matsumoto, M. Yokoyama, T. Okano, Y. Sakurai, S. Fukushima, K. Okamoto, and G. S. Kwon, *Journal of Controlled Release*, **2000**, *64*, 143-153.
[399] M. Hrubý, C. Konák, and K. Ulbrich, *Journal of Controlled Release*, **2005**, *103*, 137-148.
[400] J. Rodríguez-Hernández and S. Lecommandoux, *Journal of the American Chemical Society*, **2005**, *127*, 2026-2027.
[401] E. S. Lee, K. Na, and Y. M. Bae, *Nano Letters*, **2005**, *5*, 325-329.
[402] J. C. Leroux, E. Roux, D. Le Garrec, K. Hong, and D. C. Drummond, *Journal of Controlled Release*, **2001**, *72*, 71-84.
[403] F. Q. Schafer and G. R. Buettner, *Free Radical Biology and Medicine*, **2001**, *30*, 1191-1212.
[404] M. P. Gamcsik, M. S. Kasibhatla, S. D. Teeter, and O. M. Colvin, *Biomarkers*, **2012**, *17*, 671-691.
[405] J. Chen, X. Qiu, J. Ouyang, J. Kong, W. Zhong, and M. M. Q. Xing, *Biomacromolecules*, **2011**, *12*, 3601-3611.
[406] S. Cerritelli, D. Velluto, and J. A. Hubbell, *Biomacromolecules*, **2007**, *8*, 1966-1972.
[407] B. Remant, B. Thapa, and P. Xu, *Molecular Pharmaceutics*, **2012**, *9*, 2719-2729.
[408] H. Kim, S. Kim, C. Park, H. Lee, H. J. Park, and C. Kim, *Advanced Materials*, **2010**, *22*, 4280-4283.
[409] Y. Yan, A. P. R. Johnston, S. J. Dodds, M. M. J. Kamphuis, C. Ferguson, R. G. Parton, E. C. Nice, J. K. Heath, and F. Caruso, *ACS Nano*, **2010**, *4*, 2928-2936.
[410] K. Wang, G. F. Luo, Y. Liu, C. Li, S. X. Cheng, R. X. Zhuo, and X. Z. Zhang, *Polymer Chemistry*, **2012**, *3*, 1084-1090.
[411] Y. J. Pan, Y. Y. Chen, D. R. Wang, C. Wei, J. Guo, D. R. Lu, C. C. Chu, and C. C. Wang, *Biomaterials*, **2012**, *33*, 6570-6579.
[412] Y. L. Li, L. Zhu, Z. Liu, R. Cheng, F. Meng, J. H. Cui, S. J. Ji, and Z. Zhong, *Angewandte Chemie International Edition*, **2009**, *48*, 9914-9918.
[413] H. H. Bae, M. Y. Cho, J. H. Hong, H. Poo, M. H. Sung, and Y. T. Lim, *Journal of Microbiology and Biotechnology*, **2012**, *22*, 1782-1789.
[414] L. V. Christensen, C. W. Chang, J. K. Won, W. K. Sung, Z. Zhong, C. Lin, J. F. J. Engbersen, and J. Feijen, *Bioconjugate Chemistry*, **2006**, *17*, 1233-1240.
[415] X. Wang, Y. He, J. Wu, C. Gao, and Y. Xu, *Biomacromolecules*, **2010**, *11*, 245-251.
[416] R. Wang, L. Zhou, Y. Zhou, G. Li, X. Zhu, H. Gu, X. Jiang, H. Li, J. Wu, L. He, X. Guo, B. Zhu, and D. Yan, *Biomacromolecules*, **2010**, *11*, 489-495.
[417] Z. Q. Yu, J. J. Yan, Y. Z. You, and Q. H. Zhou, *International Journal of Nanomedicine*, **2012**, *7*, 5819-5832.

[418] D. Wu, Y. Liu, C. He, T. Chung, and S. Goh, *Macromolecules*, **2004**, *37*, 6763-6770.
[419] C. L. Lay, H. Q. Liu, D. Wu, and Y. Liu, *Chemistry - A European Journal*, **2010**, *16*, 3001-3004.
[420] W. Zhang, Y. Li, L. Liu, Q. Sun, X. Shuai, W. Zhu, and Y. Chen, *Biomacromolecules*, **2010**, *11*, 1331-1338.
[421] L. Cheng and D. Cao, *Langmuir*, **2009**, *25*, 2749-2756.
[422] S. Cohen, G. Coué, D. Beno, R. Korenstein, and J. F. J. Engbersen, *Biomaterials*, **2012**, *33*, 614-623.
[423] E. Emilitri, E. Ranucci, and P. Ferruti, *Journal of Polymer Science Part A*, **2005**, *43*, 1404-1416.
[424] G. Prencipe, S. M. Tabakman, K. Welsher, Z. Liu, A. P. Goodwin, L. Zhang, J. Henry, and H. Dai, , *Journal of the American Chemical Society*, **2009**, *131*, 4783-4787.
[425] J. V. M. Weaver, Y. Tang, S. Liu, P. D. Iddon, R. Grigg, N. C. Billingham, S. P. Armes, R. Hunter, and S. P. Rannard, *Angewandte Chemie International Edition*, **2004**, *43*, 1389-1392.
[426] Y. Li, B. S. Lokitz, and C. L. McCormick, *Angewandte Chemie International Edition*, **2006**, *45*, 5792-5795.
[427] C. L. Lay, H. R. Tan, X. Lu, and Y. Liu, *Chemistry - A European Journal*, **2011**, *17*, 2504-2509.
[428] H. Hussain, B. H. Tan, C. S. Gudipati, C. B. He, Y. Liu, and T. P. Davis, *Langmuir*, **2009**, *25*, 5557-5564.
[429] J. Panyam and V. Labhasetwar, *Pharmaceutical Research*, **2003**, *20*, 212-220.
[430] A. K. Larsen, A. E. Escargueil, and A. Skladanowski, *Pharmacology and Therapeutics*, **2000**, *85*, 217-229.
[431] H. Jin, D. A. Heller, R. Sharma, and M. S. Strano, *ACS Nano*, **2009**, *3*, 149-158.
[432] H. Carvalho, L. M. Garrido, R. L. A. Furlan, G. Padilla, M. Agnoletto, T. Guecheva, J. A. P. Henriques, J. Saffi, and C. F. M. Menck, *Cancer Chemotherapy and Pharmacology*, **2010**, *65*, 989-994.
[433] Y. Wang and S. M. Grayson, *Advanced Drug Delivery Reviews*, **2012**, *64*, 852-865.
[434] M. Calderón, R. Graeser, F. Kratz, and R. Haag, *Bioorganic and Medicinal Chemistry Letter*, **2009**, *19*, 3725-3728.
[435] L. Zhu, C. Tu, B. Zhu, Y. Su, Y. Pang, D. Yan, J. Wu, and X. Zhu, *Polymer Chemistry*, **2011**, *2*, 1761-1768.
[436] S. Lee, K. Saito, H. R. Lee, M. J. Lee, Y. Shibasaki, Y. Oishi, and B. S. Kim, *Biomacromolecules*, **2012**, *13*, 1190-1196.
[437] J. Liu, W. Huang, Y. Pang, X. Zhu, Y. Zhou, and D. Yan, *Biomacromolecules*, **2010**, *11*, 1564-1570.
[438] P. Kolhe, J. Khandare, O. Pillai, S. Kannan, M. Lieh-Lai, and R. Kannan, *Pharmaceutical Research*, **2004**, *21*, 2185-2195.
[439] O. Perumal, J. Khandare, P. Kolhe, S. Kannan, M. Lieh-Lai, and R. M. Kannan, *Bioconjugate Chemistry*, **2009**, *20*, 842-846.
[430] M. Hu, M. Chen, G. Li, Y. Pang, D. Wang, J. Wu, F. Qiu, X. Zhu, and J. Sun, *Biomacromolecules*, **2012**, *13*, 3552-3561.
[441] X. Huang, G. Song, S. Yu, and I. Kim, *Journal of Materials Science*, **2013**, *48*, 5163-5170.
[442] L. Qiu and Y. Bae, *Pharmaceutical Research*, **2006**, *23*, 1-30.
[443] P. Kolhe, E. Misra, R. M. Kannan, S. Kannan, and M. Lieh-Lai, *International Journal of Pharmaceutics*, **2003**, *259*, 143-160.

[444] S. Kannan, P. Kolhe, V. Raykova, M. Glibatec, R. M. Kannan, M. Lieh-Lai, and D. Bassett, *Journal of Biomaterials Science Polymer Edition*, **2004**, *15*, 311-330.
[445] H. Zhang, C. Zhao, H. Cao, G. Wang, L. Song, G. Niu, H. Yang, J. Ma, and S. Zhu, *Biomaterials*, **2010**, *31*, 5445-5454.
[446] Y. Pang, J. Liu, Y. Su, J. Wu, L. Zhu, X. Zhu, D. Yan, and B. Zhu, *Polymer Chemistry*, **2011**, *2*, 1661-1670.
[447] Y. Zhou, Z. Guo, Y. Zhang, W. Huang, Y. Zhou, and D. Yan, *Macromolecular Bioscience*, **2009**, *9*, 1090-1097.
[448] J. Zou, Y. Zhao, and W. Shi, *Journal of Physical Chemistry B*, **2006**, *110*, 2638-2642.
[449] X. Li, Y. Qian, T. Liu, X. Hu, G. Zhang, Y. You, and S. Liu, *Biomaterials*, **2011**, *32*, 6595-6605.
[450] S. Aryal, M. Prabaharan, S. Pilla, and S. Gong, *International Journal of Biological Macromolecules*, **2009**, *44*, 346-352.
[451] C. Kontoyianni, Z. Sideratou, T. Theodossiou, L. A. Tziveleka, D. Tsiourvas, and C. M. Paleos, *Macromolecular Bioscience*, **2008**, *8*, 871-881.
[452] Y. Pang, J. Liu, Y. Su, B. Zhu, W. Huang, Y. Zhou, X. Zhu, and D. Yan, *Science China Chemistry*, **2010**, *53*, 2497-2508.
[453] M. Prabaharan, J. J. Grailer, S. Pilla, D. A. Steeber, and S. Gong, *Biomaterials*, **2009**, *30*, 3009-3019.
[454] Y. Wu, F. Jiao, S. Han, T. Fan, Y. Liu, W. Li, L. Hu, Y. Zhao, and C. Chen, *Nanomedicine: Nanotechnology, Biology and Medicine*, **2011**, *7*, 945-954.
[455] X. Zeng, Y. Zhang, Z. Wu, P. Lundberg, M. Malkoch, and A. M. Nyström, *Journal of Polymer Science A Polymer Chemistry*, **2012**, *50*, 280-288.
[456] W. Su, X. h. Luo, H. f. Wang, L. Li, J. Feng, X. Z. Zhang, and R. x. Zhuo, *Macromolecular Rapid Communications*, **2011**, *32*, 390-396.
[457] J. Liu, W. Huang, Y. Pang, X. Zhu, Y. Zhou, and D. Yan, *Langmuir*, **2010**, *26*, 10585-10592.
[458] J. Liu, Y. Pang, W. Huang, X. Zhu, Y. Zhou, and D. Yan, *Biomaterials*, **2010**, *31*, 1334-1341.
[459] J. Liu, Y. Pang, W. Huang, X. Huang, L. Meng, X. Zhu, Y. Zhou, and D. Yan, *Biomacromolecules*, **2011**, *12*, 1567-1577.
[460] S. Kim, Y. Shi, J. Y. Kim, K. Park, and J. X. Cheng, *Expert Opinion on Drug Delivery*, **2009**, *7*, 49-62.
[461] S. K. Patel, A. Lavasanifar, and P. Choi, *Biomacromolecules*, **2009**, *10*, 2584-2591.
[462] R. Nagarajan, M. Barry, and E. Ruckenstein, *Langmuir*, **1986**, *2*, 210-215.
[463] C. Allen, D. Maysinger, and A. Eisenberg, *Colloids and Surfaces B: Biointerfaces*, **1999**, *16*, 3-27.
[464] C. M. Paleos, D. Tsiourvas, Z. Sideratou, and L. A. Tziveleka, *Expert Opinion on Drug Delivery*, **2010**, *7*, 1387-1398.
[467] G. P. Sartiano and W. E. Lynch, *Clinical Research*, **1978**, *26*, 60.
[468] T. G. Iversen, T. Skotland, and K. Sandvig, *Nano Today*, **2011**, *6*, 176-185.
[469] R. A. Petros and J. M. DeSimone, *Nature Reviews Drug Discovery*, **2010**, *9*, 615-627.
[470] L. Rajendran, H. J. Knolker, and K. Simons, *Nature Reviews Drug Discovery*, **2010**, *9*, 29-42.
[471] A. Bumb, M. W. Brechbiel, and P. Choyke, *Acta Radiologica*, **2010**, *51*, 751-767.
[472] S. Mornet, S. Vasseur, F. Grasset, and E. Duguet, *Journal of Materials Chemistry*, **2004**, *14*, 2161-2175.
[473] S. E. Matthews, C. W. Pouton, and M. D. Threadgill, *Advanced Drug Delivery Reviews*, **1996**, *18*, 219-267.

[474] A. Accardo, D. Tesauro, L. Aloj, C. Pedone, and G. Morelli, *Coordination Chemistry Reviews*, **2009**, *253*, 2193-2213.
[475] S. Langereis, A. Dirksen, T. M. Hackeng, M. H. P. Van Genderen, and E. W. Meijer, *New Journal of Chemistry*, **2007**, *31*, 1152-1160.
[476] Z. R. Lu, F. Ye, and A. Vaidya, *Journal of Controlled Release*, **2007**, *122*, 269-277.
[477] R. Brasch, C. Pham, D. Shames, T. Roberts, K. Van Dijke, N. Van Bruggen, J. Mann, S. Ostrowitzki, and O. Melnyk, *Journal of Magnetic Resonance Imaging*, **1997**, *7*, 68-74.
[478] Z. R. Lu, A. M. Mohs, Y. Zong, and Y. Feng, *International Journaol of Nanomedicine*, **2006**, *1*, 31-40.
[479] Y. Zong, X. Wang, K. C. Goodrich, A. M. Mohs, D. L. Parker, and Z. R. Lu, *Magnetic Resonance in Medicine*, **2005**, *53*, 835-842.
[480] Y. Zong, X. Wang, E. K. Jeong, D. L. Parker, and Z. R. Lu, *Magnetic Resonance Imaging*, **2009**, *27*, 503-511.
[481] Y. Zong, J. Guo, T. Ke, A. M. Mohs, D. L. Parker, and Z. R. Lu, *Journal of Controlled Release*, **2006**, *112*, 350-356.
[482] Z. Ye, X. Wu, M. Tan, J. Jesberger, M. Grisworld, and Z. R. Lu, *Contrast Media and Molecular Imaging*, **2013**, *8*, 220-228.
[483] E. Nakamura, K. Makino, T. Okano, T. Yamamoto, and M. Yokoyama, *Journal of Controlled Release*, **2006**, *114*, 325-333.
[484] A. Harada and K. Kataoka, *Science*, **1999**, *283*, 65-67.
[485] K. A. Deal, R. J. Motekaitis, A. E. Martell, and M. J. Welch, *Journal of Medicinal Chemistry*, **1996**, *39*, 3096-3106.
[486] G. Sun, D. Wu, Y. Liu, C. He, T. S. Chung, and S. H. Goh, *Polymer*, **2005**, *46*, 3355-3362.
[487] Y. Li, M. Beija, S. Laurent, L. v. Elst, R. N. Muller, H. T. T. Duong, A. B. Lowe, T. P. Davis, and C. Boyer, *Macromolecules*, **2012**, *45*, 4196-4204.
[488] W. H. Li, G. Parigi, M. Fragai, C. Luchinat, and T. J. Meade, *Inorganic Chemistry*, **2002**, *41*, 4018-4024.
[489] A. C. Esqueda, J. A. López, G. Andreu-de-Riquer, J. C. Alvarado- Monzón, J. Ratnakar, A. J. M. Lubag, A. D. Sherry, and L. M. De León-Rodríguez, *Journal of the American Chemical Society*, **2009**, *131*, 11387-11391.
[490] J. Paris, C. Gameiro, V. Humblet, P. K. Mohapatra, V. Jacques, and J. F. Desreux, *Inorganic Chemistry*, **2006**, *45*, 5092-5102.
[491] T. N. Parac-Vogt, L. Vander Elst, K. Kimpe, S. Laurent, C. Burtéa, F. Chen, R. Van Deun, Y. Ni, R. N. Muller, and K. Binnemans, *Contrast Media and Molecular Imaging*, **2006**, *1*, 267-278.
[492] E. Pérez -Mayoral, V. Negri, J. Soler- Padrós, S. Cerdán, and P. Ballesteros, *European Journal of Radiology*, **2008**, *67*, 453-458.
[493] C. Tu, E. A. Osborne, and A. Y. Louie, *Annals of Biomedical Engineering*, **2011**, *39*, 1335-1348.
[494] S. Iwaki, K. Hanaoka, W. Piao, T. Komatsu, T. Ueno, T. Terai, and T. Nagano, *Bioorganic and Medicinal Chemistry Letters*, **2012**, *22*, 2798-2802.
[495] M. P. Lowe, D. Parker, O. Reany, S. Aime, M. Botta, G. Castellano, E. Gianolio, and R. Pagliarin, *Journal of the American Chemical Society*, **2001**, *123*, 7601-7609.
[496] K. E. Lokling, S. L. Fossheim, R. Skurtveit, A. Bjornerud, and J. Klaveness, *Magnetic Resonance Imaging*, **2001**, *19*, 731-738.
[497] K. E. Løkling, R. Skurtveit, A. Bjørnerud, and S. L. Fossheim, *Magnetic Resonance in Medicine*, **2004**, *51*, 688-696.
[498] E. Tóth, R. D. Bolskar, A. Borel, G. González, L. Helm, A. E. Merbach, B. Sitharaman, and L. J. Wilson, *Journal of the American Chemical Society*, **2005**, *127*, 799-805.

[499] R. A. Moats, S. E. Fraser, and T. J. Meade, *Angewandte Chemie International Edition*, **1997**, *36*, 726-728.
[500] S. Figueiredo, J. N. Moreira, C. F. G. C. Geraldes, S. Aime, and E. Terreno, *Bioorganic and Medicinal Chemistry*, **2011**, *19*, 1131-1135.
[501] C. Tu and A. Y. Louie, *Chemical Communications*, **2007**, *13*, 1331-1333.
[502] C. Tu, E. A. Osborne, and A. Y. Louie, *Tetrahedron*, **2009**, *65*, 1241-1246.
[503] C. Tu, R. Nagao, and A. Y. Louie, *Angewandte Chemie International Edition*, **2009**, *48*, 6547-6551.
[504] B. Jagadish, G. P. Guntle, D. Zhao, V. Gokhale, T. J. Ozumerzifon, A. M. Ahad, E. A. Mash, and N. Raghunand, *Journal of Medicinal Chemistry*, **2012**, *55*, 10378-10386.
[505] N. Raghunand, B. Jagadish, T. P. Trouard, J. P. Galons, R. J. Gillies, and E. A. Mash, *Magnetic Resonance in Medicine*, **2006**, *55*, 1272-1280.
[506] S. Aime, A. Barge, M. Botta, J. A. K. Howard, R. Kataky, M. P. Lowe, J. M. Moloney, D. Parker, and A. S. De Sousa, *Chemical Communications*, **1999**, *11*, 1047-1048.
[507] S. Bauhuber, C. Hozsa, M. Breunig, and A. Göpferich, *Advanced Materials*, **2009**, *21*, 3286-3306.
[508] D. Giustarini, I. Dalle-Donne, D. Tsikas, and R. Rossi, *Critical Reviews in Clinical Laboratory Sciences*, **2009**, *46*, 241-281.
[509] K. J. Barnham, C. L. Masters, and A. I. Bush, *Nature Reviews Drug Discovery*, **2004**, *3*, 205-214.
[510] W. Dröge, Physiological Reviews, **2002**, *82*, 47-95.
[511] F. Meng, W. E. Hennink, and Z. Zhong, *Biomaterials*, **2009**, *30*, 2180-2198.
[512] E. Fleige, M. A. Quadir, and R. Haag, *Advanced Drug Delivery Reviews*, **2012**, *64*, 866-884.
[513] S. Ganta, H. Devalapally, A. Shahiwala, and M. Amiji, *Journal of Controlled Release*, **2008**, *126*, 187-204.
[514] M. Reid and F. Jahoor, *Current Opinion in Clinical Nutrition and Metabolic Care*, **2000**, *3*, 385-390.
[515] P. O. Kiratli, H. Kiratli, F. Bozkurt, M. T. Ercan, and S. Bilgiç, *Nuclear Medicine Communication*, **2001**, *22*, 197-201.
[516] J. M. Macdonald, O. Schmidlin, and T. L. James, *Magnetic Resonance in Medicine*, **2002**, *48*, 430-439.
[517] P. E. Thelwall, A. Y. Yemin, T. L. Gillian, N. E. Simpson, M. S. Kasibhatla, Z. N. Rabbani, J. M. Macdonald, S. J. Blackband, and M. P. Gamcsik, *Cancer Research*, **2005**, *65*, 10149-10153.
[518] I. Dalle-Donne, R. Rossi, R. Colombo, D. Giustarini, and A. Milzani, *Clinical Chemistry*, **2006**, *52*, 601-623.
[519] R. Weissleder and V. Ntziachristos, *Nature Medicine*, **2003**, *9*, 123-128.
[520] V. Ntziachristos, *Annual Review of Biomedical Engineering*, **2006**, *8*, 1-33.
[521] R. Weissleder and M. J. Pittet, *Nature*, **2008**, *452*, 580-589.
[522] N. Kosaka, M. Ogawa, P. L. Choyke, and H. Kobayashi, *Future Oncology*, **2009**, *5*, 1501-1511.
[523] Y. Urano, D. Asanuma, Y. Hama, Y. Koyama, T. Barrett, M. Kamiya, T. Nagano, T. Watanabe, A. Hasegawa, P. L. Choyke, and H. Kobayashi, *Nature Medicine*, **2009**, *15*, 104-109.
[524] Z. Zhang and S. Achilefu, *Chemical Communications*, **2005**, *47*, 5887-5889.
[525] M. Ogawa, N. Kosaka, P. L. Choyke, and H. Kobayashi, *Cancer Research*, **2009**, *69*, 1268-1272.
[526] M. Kamiya, H. Kobayashi, Y. Hama, Y. Koyama, M. Bernardo, T. Nagano, P. L. Choyke, and Y. Urano, *Journal of the American Chemical Society*, **2007**, *129*, 3918-3929.
[527] B. Law, A. Curino, T. H. Bugge, R. Weissleder, and C. H. Tung, *Chemistry and Biology*, **2004**, *11*, 99-106.

[528] K. Kiyose, H. Kojima, Y. Urano, and T. Nagano, *Journal of the American Chemical Society*, **2006**, *128*, 6548-6549.
[529] X. a. Zhang, K. S. Lovejoy, A. Jasanoff, and S. J. Lippard, *Proceedings of the National Academy of Sciences of the United States of America*, **2007**, *104*, 10780-10785.
[530] I. Texier, J. Razkin, V. Ã. Josserand, D. Boturyn, P. Dumy, J. L. Coll, and P. Rizo, *Nuclear Instruments and Methods in Physics Research Section A: Accelerators, Spectrometers, Detectors and Associated Equipment*, **2007**, *571*, 165-168.
[531] F. Yu, P. Li, B. Wang, and K. Han, *Journal of the American Chemical Society*, **2013**, *135*, 7674-7680.
[532] J. Razkin, V. Ã. Josserand, D. Boturyn, Z. h. Jin, P. Dumy, M. Favrot, J. L. Coll, and I. Texier, *ChemMedChem*, **2006**, *1*, 1069-1072.
[533] M. Wei, P. Yin, Y. Shen, L. Zhang, J. Deng, S. Xue, H. Li, B. Guo, Y. Zhang, and S. Yao, *Chemical Communications*, **2013**, *49*, 4640-4642.
[534] D. Zhai, S. C. Lee, S. W. Yun, and Y. T. Chang, *Chemical Communications*, **2013**, *49*, 7207-7209.
[535] Y. Urano, *Current Opinion in Chemical Biology*, **2012**, *16*, 602-608.
[536] K. Licha and U. Resch-Genger, *Drug Discovery Today: Technologies*, **2011**, *8*, 87-94.
[537] J. Rao, A. Dragulescu-Andrasi, and H. Yao, *Current Opinion in Biotechnology*, **2007**, *18*, 17-25.
[538] H. Kobayashi and P. L. Choyke, *Accounts of Chemical Research*, **2011**, *44*, 83-90.
[539] J. Condeelis and J. E. Segall, *Nature Reviews Cancer*, **2003**, *3*, 921-930.
[540] Y. Hong, J. W. Y. Lam, and B. Z. Tang, *Chemical Communications*, **2009**, *29*, 4332-4353.
[541] Y. Hong, J. W. Y. Lam, and B. Z. Tang, *Chemical Society Reviews*, **2011**, *40*, 5361-5388.
[542] K. Li, D. Ding, Q. Zhao, J. Sun, B. Z. Tang, and B. Liu, *Scientia China Chemical*, **2013**, *56*, 1228-1233.
[543] Y. Lee, H. Mo, H. Koo, J. Y. Park, M. Y. Cho, G. w. Jin, and J. S. Park, *Bioconjugate Chemistry*, **2006**, *18*, 13-18.
[544] Y. Liu, Y. Yu, J. W. Y. Lam, Y. Hong, M. Faisal, W. Z. Yuan, and B. Z. Tang, *Chemistry - A European Journal*, **2010**, *16*, 8433-8438.
[545] Z. Tao, G. Hong, C. Shinji, C. Chen, S. Diao, A. L. Antaris, B. Zhang, Y. Zou, H. Dai, *Angewandte Chemie International Edition*,**2013**, *125*, 13240.
[546] D. Wang, T. Imae, and M. Miki, *Journal of Colloid and Interface Science*, **2007**, *306*, 222-227.
[547] D. C. Wu, Y. Liu, C. B. He, and S. H. Goh, *Macromolecules*, **2005**, *38*, 9906-9909.